

Sea-level reconstruction for Turonian sediments from Tanzania based on integration of sedimentology, microfacies, geochemistry and micropaleontology



Ines Wendler ^{a,*}, Jens E. Wendler ^a, Leon J. Clarke ^b

^a Department of Geosciences, Bremen University, P.O. Box 330440, 28334 Bremen, Germany

^b School of Science and the Environment, Faculty of Science and Engineering, Manchester Metropolitan University, Chester Street, Manchester M1 5GD, UK

ARTICLE INFO

Article history:

Received 3 March 2015

Received in revised form 9 July 2015

Accepted 12 August 2015

Available online 20 August 2015

Keywords:

Sea level

Cretaceous

Grain size

Foraminifera

Stable isotope

Sequence stratigraphy

ABSTRACT

Despite many advances in sea-level research, the nature of cyclic eustatic sea-level fluctuations during warm periods without, or with much reduced, polar ice remains enigmatic. Recently published $\delta^{18}\text{O}$ records from extremely well-preserved Turonian microfossils from Tanzania do not support the contentious idea of glacio-eustatic control of global sea-level changes during the warmest period of the Cretaceous. For the same locality (site TDP 31) we reconstruct relative sea-level changes based on sequence stratigraphy and integration of sedimentology, microfacies, geochemistry, and micropaleontology. Four local sequence boundaries (SBs TuTz1–4) are recognized: at the base, middle, and top of the *Helvetoglobotruncana helvetica* Zone and in the Late Turonian. The lowstands are characterized by increased grain size, enhanced organic carbon flux, faunal assemblage changes, and bulk $\delta^{13}\text{C}_{\text{org}}$ and foraminiferal $\delta^{13}\text{C}_f$ and $\delta^{18}\text{O}_f$ minima. Strong benthic and planktic foraminiferal turnovers above the top Middle Turonian SB TuTz3 probably reflect shallowing (from upper slope to outer shelf) and/or eutrophication.

The TDP 31 age model is refined through inter-regional comparison of planktic foraminiferal ranges and $\delta^{13}\text{C}$ records from three other South-Tethyan localities (ODP Holes 762C and 763B, Exmouth Plateau, and the Guru section, Tibet). This age model enables correlation of the regressive events at a global scale and suggests that, within stratigraphic uncertainty, the TDP 31 depositional sequences are synchronous with the global Turonian third-order sequences and are likely driven by eustasy. These correlations, together with recent astrochronological and radiometric dating, indicate a considerably younger age (91.17 ± 0.52 Ma) for the top *H. helvetica* Zone than currently assumed, resulting in zonal duration of 2.35 ± 0.52 myr. Foraminiferal stable-isotope data from TDP 31 indicate slight surface- and bottom-water warming during the regressions and possibly a minor surface-water salinity decrease, which is inconsistent with glacio-eustatic forcing of Turonian third-order sea-level cycles and is more in line with the model of aquifer-eustasy.

© 2015 Elsevier B.V. All rights reserved.

1. Introduction

In the light of current climate change and melting polar ice sheets, attempts to understand better the complex processes and feedback mechanisms that influenced global sea level over geologic time have gained momentum in recent years. Despite many advances in sea-level research, the nature of cyclic eustatic sea-level fluctuations during past warm periods without, or with much reduced, polar ice remains enigmatic. Solid earth dynamics that are unrelated to glacial cycles can explain first and second order sea-level cycles (Conrad, 2013), but not the third-order cycles that are evident from sequence stratigraphy (Haq, 2014).

Looking from the perspective of an icehouse world, it is hard to envision processes other than the waxing and waning of ice sheets as the main driver of these third-order eustatic sea-level fluctuations. Even for the Cenomanian and Turonian, the warmest period of the Cretaceous greenhouse climate (e.g. Huber et al., 2002; Friedrich et al., 2012), operation of glacio-eustasy remains an ongoing controversy (Miller et al., 2003, 2004; Moriya et al., 2007; Bornemann et al., 2008; Ando et al., 2009; MacLeod et al., 2013). Some modeling results for the Late Cretaceous suggest the possibility of the build-up and decay of Antarctic ice sheets on time-scales of 20–80 kyr under certain boundary conditions (Flögel et al., 2011). However, while theoretically possible, sedimentological evidence for glacial episodes during the mid-Cretaceous is missing. Geochemical arguments for a short (~200 kyr) glacial period in the Middle Turonian (Bornemann et al., 2008), or for explanation of relatively long-term (myr-scale) regressive cycles during the Cenomanian to

* Corresponding author. Tel.: +49 421 21865137; fax: +49 421 21865159.

E-mail address: flatter@uni-bremen.de (I. Wendler).

Coniacian (Galeotti et al., 2009), have been called into question (e.g. MacLeod et al., 2013; Uličný et al., 2014; Wendler and Wendler, 2016). Although the existence of sporadic, short-duration glacial episodes may be possible under greenhouse climate conditions, they do not seem to offer a convincing explanation for the repeated/cyclic third-order eustatic sea-level fluctuations that are evident during the mid-Cretaceous.

If past warm greenhouse climate conditions did not allow for substantial amounts of water to accumulate on land in a solid state (as ice in the cryosphere), then the focus for an explanation of eustatic sea-level cycles during these periods should probably be shifted from the solid to the liquid aspect of the hydrological cycle. Such alternative concepts for eustatic sea-level change might involve steric effects (ocean water volume in relation to temperature) and groundwater storage. The latter concept was first proposed by Hay and Leslie (1990), but has been considered in very few studies (Jacobs and Sahagian, 1993) and is only recently gaining more attention (Föllmi, 2012; Wagreich et al., 2014; Wendler et al., 2014; Wendler and Wendler, 2016; Wendler et al., 2011c; Wendler et al., 2016).

Key to understanding the eustatic component in sea-level oscillations is evaluation and comparison of the timing and magnitude of reconstructed relative sea-level changes from individual sections. This approach requires sufficiently precise stratigraphic correlation and correct interpretation of paleobathymetric proxies. Traditionally, biostratigraphy forms the basis for correlating sedimentary sequences, and additional methods such as magnetostratigraphy, astrochronology, and chemostratigraphy are increasingly used to: (1) improve the resolution of age models, (2) test for biostratigraphic synchronicity of marker species, and (3) more precisely relate different biostratigraphic schemes (e.g. Laurin et al., 2015; Sageman et al., 2014; Voigt et al., 2012; Wendler, 2013).

The combination of these correlative methods, together with the increasing number of published high-resolution records (e.g. Uličný et al., 2014), and availability of new, well-preserved Cretaceous material, e.g. from the Fossillagerstätte in Tanzania (Wendler and Bown, 2013; Wendler et al., 2013a; Wendler et al., 2013b), offer new chances, as well as challenges, for research on understanding the drivers of past greenhouse world eustasy. A recent compilation of Late Cretaceous $\delta^{13}\text{C}_{\text{carb}}$ records and biostratigraphic and magnetostratigraphic data (Wendler, 2013) provides the means for global correlation at increased temporal resolution for this geologic period and confirms synchronicity for some of the foraminiferal marker species. The study also points out discrepancies (i.e. species occurrence diachroneity) that challenge traditional biostratigraphic concepts and that need to be solved in order to improve stratigraphic correlations. The exceptionally well-preserved microfossils recovered in the Cretaceous sediments from Tanzania onshore drilling provide unprecedented structural detail for taxonomic and biostratigraphic studies (Falzoni et al., 2013, 2014; Haynes et al., 2015; Huber and Petrizzo, 2014; Petrizzo et al., 2011; Wendler et al., 2011a; Wendler et al., 2013b), as well as minimal alteration of geochemical parameters for palaeoclimate proxy development (Wendler et al., 2013a) and for testing the greenhouse glacier hypothesis (MacLeod et al., 2013). The wealth of detail preserved in these sediments challenges existing taxonomic concepts and ideas of proxy interpretation and, at the same time, offers a great chance for refinement of these concepts.

The mid-Cretaceous “Super-Greenhouse” is perfectly suited for studies on greenhouse climate eustasy and is well-represented in the Tanzanian sediments. In the present paper we summarize sedimentological, geochemical, and microfossil data from a Turonian drill site from Tanzania (TDP 31) and discuss their interpretation in terms of local sea-level history and the possible relation to global sequence stratigraphic cycles. The study presents one of the few open marine sections that combine microfossil biozones with sequence stratigraphy and chemostratigraphic interpretation for the Turonian. Additionally, the presence of exceptionally well-preserved microfossils in these

sediments allows comparison of patterns in stable isotope records, derived from translucent foraminifera, with the local sequence stratigraphic model. Grain-size and stable-isotope data from site TDP 31 are regionally compared to records from two other Turonian TDP sites (TDP 22 and TDP 36). For wider correlative purposes and for development of an age model for TDP 31, we also compare Turonian $\delta^{13}\text{C}$ records (bulk carbonate/bulk organic/foraminiferal) and stratigraphic ranges of planktic foraminiferal key species from four sections that were all located in the southern Tethys Ocean (Fig. 1), but on three different tectonic plates: site TDP 31 (Tanzania, Africa; new and published data), ODP Holes 762C and 763B (Exmouth Plateau, Australia; previously unpublished data), and Guru section (Tibet, Greater India; published data).

2. Materials and sampling

During the Tanzania Drilling Project (TDP), marine hemipelagic Cretaceous sediments were recovered at eighteen land-based drill sites near the Tanzanian coast during three field seasons from 2007 to 2009. Turonian sediments were cored in 10 of these sites, of which site TDP 31 ($10^{\circ}1'49.80''\text{S}$, $39^{\circ}38'44.00''\text{E}$) yielded the longest and most complete Turonian succession. For an initial attempt of local lithostratigraphic correlation, we also present grain-size and geochemical data for sites TDP 22 and TDP 36. For details on the location of these three sites, regional geology, and on initial sedimentologic, biostratigraphic, and geochemical results (bulk sediment: wt% carbonate and TOC, $\delta^{13}\text{C}_{\text{org}}$, $\delta^{13}\text{C}_{\text{carb}}$, and $\delta^{18}\text{O}_{\text{carb}}$) see Jiménez Berrocoso et al. (2015, 2012, 2010).

Site TDP 31 recovered 64 cores from a 115-m thick Lower Turonian to Coniacian interval of clay-rich and carbonate-poor siltstone. The Lower and Middle Turonian sediments below ~42 m depth are dark gray, finely bedded to laminated with minor signs of bioturbation (i.e. pyritized burrows in washed samples). The Upper Turonian sediments above ~42 m depth are lighter greenish-gray and largely bioturbated, with thicker and less distinct bedding. Core photographs for TDP 31 are provided in Appendix 1A–F. Successions of 130 m and 110 m thickness of Lower and Middle Turonian carbonate-poor sandy siltstones to silty claystones were drilled at sites TDP 22 and TDP 36, respectively. The cores were photographed, described, and sampled on site. Color variations in the core photographs due to the varying position of the sun were electronically normalized using the color of a wooden ruler for reference. For core numbering and sample abbreviation format see Jiménez Berrocoso et al. (2010).

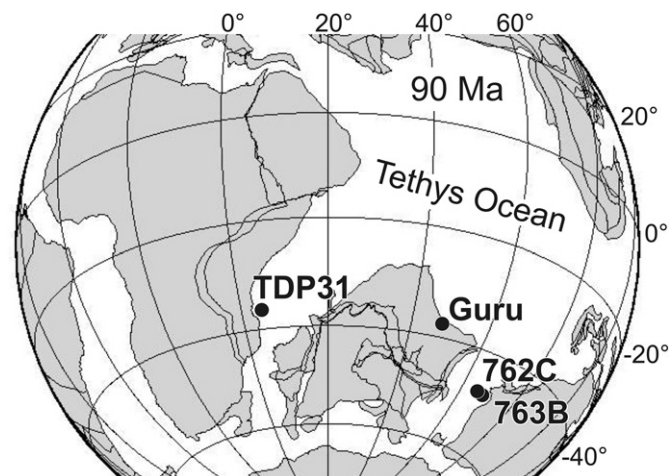


Fig. 1. Paleogeographic map for the late Turonian (~90 Ma) and the position of the four sections from the southern Tethys Ocean discussed in this study.

For TDP 31, a total of 206 bulk sediment samples of ~2 cm length were taken about every half meter (except from recovery gaps), resulting in temporal resolution of $\sim 16 \pm 3$ kyr (for age model see Section 6.5). These samples were used for grain-size analysis and determination of total organic carbon (TOC), wt% carbonate, $\delta^{13}\text{C}_{\text{carb}}$, $\delta^{18}\text{O}_{\text{carb}}$, $\delta^{13}\text{C}_{\text{org}}$, and for calcareous dinoflagellate cyst analysis. For nannofossil studies, 243 samples of 1–2 cm length were taken at least every half meter. At a sample spacing of ~1 m, one 20-cm long sample (total 116) and one 10-cm long sample (total 107) were taken for foraminiferal assemblage and isotope studies. The samples were disaggregated and screen-washed with tap water and, the residues ($>63\text{-}\mu\text{m}$ fraction) were air-dried. Sampling intervals for both bulk sediments and foraminifera in TDP 22 and TDP 36 were similar to those in TDP 31.

3. Geological setting and sequence stratigraphic approach

The benthic foraminiferal assemblage in TDP 31 indicates an outer shelf to upper slope paleobathymetry, which is supported by abundant and diverse planktic foraminifera and the fine grain size of the sediments (Jiménez Berrocoso et al., 2012). Grain-size variations between clay- and silt-rich intervals can reflect shifts in sedimentary patterns related to relative sea-level fluctuations and/or changes in the supply of clastic sediments driven by continental hydrology or oceanic currents. Most sequence stratigraphic interpretations are performed for sections from shallow-water or platform settings because of clearly developed sequence boundaries (SBs) and more dramatic depositional changes. By comparison, in deeper-water environments, where depositional changes are more subtle, sedimentation is usually continuous, and identification of SBs can be challenging. At several hundred meters water depth, changes in relative sea level would be reflected by slope mudstones and thin sandstones intercalated with coarser slope fan deposits. The latter are separated by correlative conformities that are equivalent to erosive SBs in shallower settings.

For an outer shelf to upper slope position, as inferred for TDP 31, the most appropriate sequence model appears to be that of Posamentier and Vail (1988) and Haq et al. (1987), as summarized and developed further in Catuneanu (2006). In this model, the correlative conformity marks the onset of the base-level fall and is positioned at the base of the early lowstand fan deposits, marking the onset of a falling-stage to lowstand package. Accumulation of clastic sediments in deep-water settings is controlled by four major processes: 1) progradation of shelf edge deltaic sediments following base-level fall, 2) gravity flows, 3) contour currents, and 4) pelagic sedimentation as a continuous background process (Catuneanu, 2006).

Changes in relative sea level can be modeled on the basis of timing and nature of both the shelf edge delta progradation and of the gravity flows. Both processes are the main suppliers of sediment to the deeper basin and are generally responsible for the input of coarser material. The composition of siliciclastic material retained in the shelf edge deltaic sediments is relevant for observations at the upper slope (as in TDP 31), while high-density turbidity flows would be responsible for sediment transport to the deeper slope and into the basin. Numerical modeling suggests that during greenhouse climate periods, progradation of deltas across the shelf, to deliver sediment to the outer shelf and slope, was promoted by low shelf accommodation space due to shallow shelf angles and low eustatic sea-level change amplitudes. Such effective sediment delivery to the outer shelf may even have involved sea-level highstands, thereby probably rendering the difference between highstand and lowstand deposits to be subtle (Sømmen et al., 2009), as observed in TDP 31.

Following the above-described sequence stratigraphic concept, the correlative conformity of a potential SB at TDP 31 would generally lie at the base of a coarser-grained interval. The interpreted grain-size shifts are subtle, but about four times larger than measurement

uncertainties (see Section 4.1). The most clay-rich intervals (below the SBs) then would have been deposited during transgression and highest relative sea level, while the coarser intervals above the SBs would reflect relative sea-level fall, during which two units are typically deposited. At the upper slope to outer shelf these intervals (lowstand packages in the view of Posamentier and Vail, 1988) consist of a forced-regressive lower part, retaining little sand, because it is exported further into the basin, and a normal regressive upper part that is coarser due to the trapping of sand on the upper slope to outer shelf. In turn, in deeper basinal positions, a lowstand fan (coarser) and a subsequent lowstand wedge (finer) typically form the two units of lowstand deposits.

Without basin-scale three-dimensional datasets obtained from seismic measurements or numerous drill sites, it is difficult to differentiate between supply-driven grain-size variations, e.g. due to climatic changes that can affect continental weathering, drainage (run-off amount and pathways), and oceanic circulation (distribution of water masses, flow patterns, and sediment routing), from those that were driven by relative sea-level fluctuations. Each of these processes can variably influence the different environmental parameters, but it can be expected that relative sea-level changes have the most profound and simultaneous spatial influence on sedimentation/erosion and on surface- and bottom-water properties, such as turbidity, temperature, salinity, stratification, nutrients, and oxygenation, and hence on faunal composition and geochemical proxy parameters. The synchronizing effect of relative sea-level fluctuations on the various proxies can be tested by comparing grain-size variations with faunal, geochemical, and microfacies data, that should exhibit concurrent shifts if controlled by the same forcing.

In our first approach, we follow the hypothesis that those bases of coarser-grained sedimentary intervals (potentially representing falling-stage and lowstand deposits) that coincide with changes in microfacies, faunal assemblages, and geochemical proxies likely represent SBs and reflect a drop in local base level. Of course, it can be expected that climatic and oceanographic factors unrelated to sea-level changes additionally influenced the sedimentary record, but without such encompassing synchronization of the various proxies. In our second approach, we further test sequence stratigraphic predictions by comparing the stratigraphic position of these local SBs with those of independently proposed Turonian sequences that are thought to have a eustatic character. A similar stratigraphic position would: (1) support the local sequence stratigraphic model and (2) indicate these local sea-level shifts have a significant eustatic component.

4. Methods

4.1. Grain-size analysis and sediment color

We measured grain size in 198 samples from TDP 31, in 118 samples from TDP 22 and in 200 samples from TDP36. Samples were oven-dried and disaggregated in water. The bleaching agent "Chlorox" was added (one drop) to prevent clotting of clay and organic particles during measurement. Grain-size analyses were done with a Beckman Coulter Inc. LS200 particle analyzer. Under automatic control of the required opacity within the measuring unit, slurry sample material was inserted into the water-filled analysis-container using a spatula. Consistency of the sample slurry was not too liquid, in order to prevent under-representation of the coarse size fraction due to rapid settling. Each sample was measured in triplicate, with 3 min integration time and application of 1 min of ultrasonication between runs. The plotted data show the averaged values from these triplicate measurements.

The data output of the particle-size analyzer gives the Gaussian grain-size distribution for the interval 0.4–2000 μm . Definitions used

for individual size fractions are: clay = 0.4–4 μm ; silt = >4–63 μm ; sand = >63–2000 μm . Percentages of the three size fractions were calculated using the areas of the Gaussian distribution curve within the respective size classifications. Standard deviations (SD) for the calculated mode, mean, and median values within the measurement triplets are 0–4 μm (mean SD is 0.5 μm). Duplicate measurements for 15 samples to test reproducibility of the grain-size fraction calculations revealed average variability of 4.4% (minimum 0%; maximum outlier 7.5%) for clay, 4.7% (min. 1.5%; max. 6%) for silt, and 3.4% (min. 0.25%; max. 7%) for sand. Ultrasound treatment profoundly affects the results, particularly for the sand fraction, because of the presence of grain aggregates in some samples, such that a strict ultrasound protocol had to be followed. Measurement of coarse grain sizes were verified, in terms of distinguishing coarse grains from aggregates, via microfacies analysis of the washed sample residues (see Section 4.2).

The grain-size mode illustrates shifts in the dominant grain size, and the ratio $S = (\text{silt} + \text{sand})/\text{clay}$ is used as a measure to integrate the three size fractions (Figs. 2 and 3). A 3-point running average (with a 0.5 m sampling interval thus averaging 1.5 m of section) was found appropriate to identify major coarse–fine units with thicknesses around 5–10 m. Based on a minimum of 5 measurements per potential lithological unit, the present study can resolve sedimentological cycles with a minimal thickness of >2.5 m ($\sim 80 \pm 18$ kyr; for age model see Section 6.5).

Sediment color analysis was performed parallel to the grain-size measurements by visually determining the color of the wet disaggregated sample-slurry using the Munsell color scheme.

4.2. Foraminifera, calcareous dinoflagellate cysts and microfacies analysis

Micro-splits of the >125- μm fraction from 130 washed samples were completely picked for benthic and planktic foraminifera with the goal of at least 300 specimens for each of these groups. Count data of biserial planktic foraminifera from Haynes et al. (2015; 92 samples) are complemented with new data for 38 additional samples. The washed samples were also used for microfacies analysis. Qualitative (presence/absence) and semi-quantitative data (rare/common/frequent/abundant) for additional microfossils, macrofossil fragments, and detrital components were collected using light microscope observations of the >63- μm fraction of the washed samples. The relative lightness of the dry residues was estimated on a scale from 1 (light) to 4 (dark), in order to support observations on color changes across the section. Mineralogical identification of detrital grains was supported by energy dispersive X-ray spectroscopy (EDX) and qualitative micro X-ray diffraction analysis (XRD).

Calcareous dinoflagellate cysts were picked for 15 (bulk) samples from ~2 mg of the 20–75- μm fraction (about 30–50 picking-tray fields) using an eyelash mounted on a pen. The picking time for this amount of material was ~6 h per sample, yielding between 50 and 120 specimens, except in the upper samples where the abundance of dinoflagellate cysts was very low. All dinoflagellate cyst specimens were mounted on a stub and identified with an SEM. The specimen counts were normalized to the number of tray-fields picked in order to provide a semi-quantitative measure of calcareous dinoflagellate cyst abundance

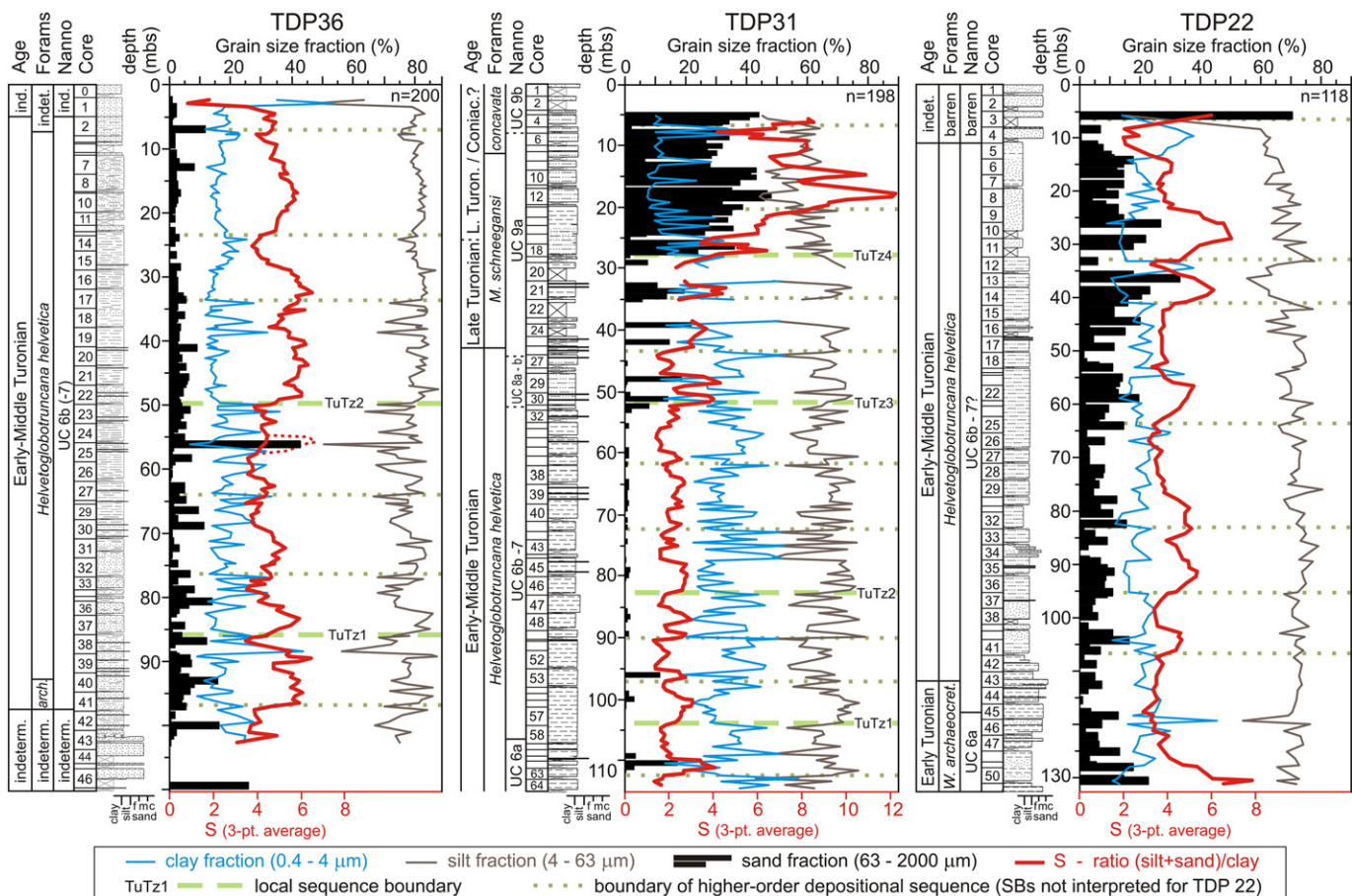


Fig. 2. Grain-size data and ratio $S = (\text{silt} + \text{sand})/\text{clay}$ obtained from three onshore drill sites in Tanzania. Lithological logs and biostratigraphy from Jiménez Berrocoso et al. (2010, 2012, 2015). Number (n) of measured samples given in upper right corner of the respective diagrams. Dotted and dashed lines mark the base of coarser-grained intervals that are interpreted as sequence boundaries (SBs dashed, TuTz = local sequence boundary; not interpreted for TDP 22), based on co-occurring faunal and geochemical shifts as explained in Section 3, or as higher-order depositional sequences (dotted).

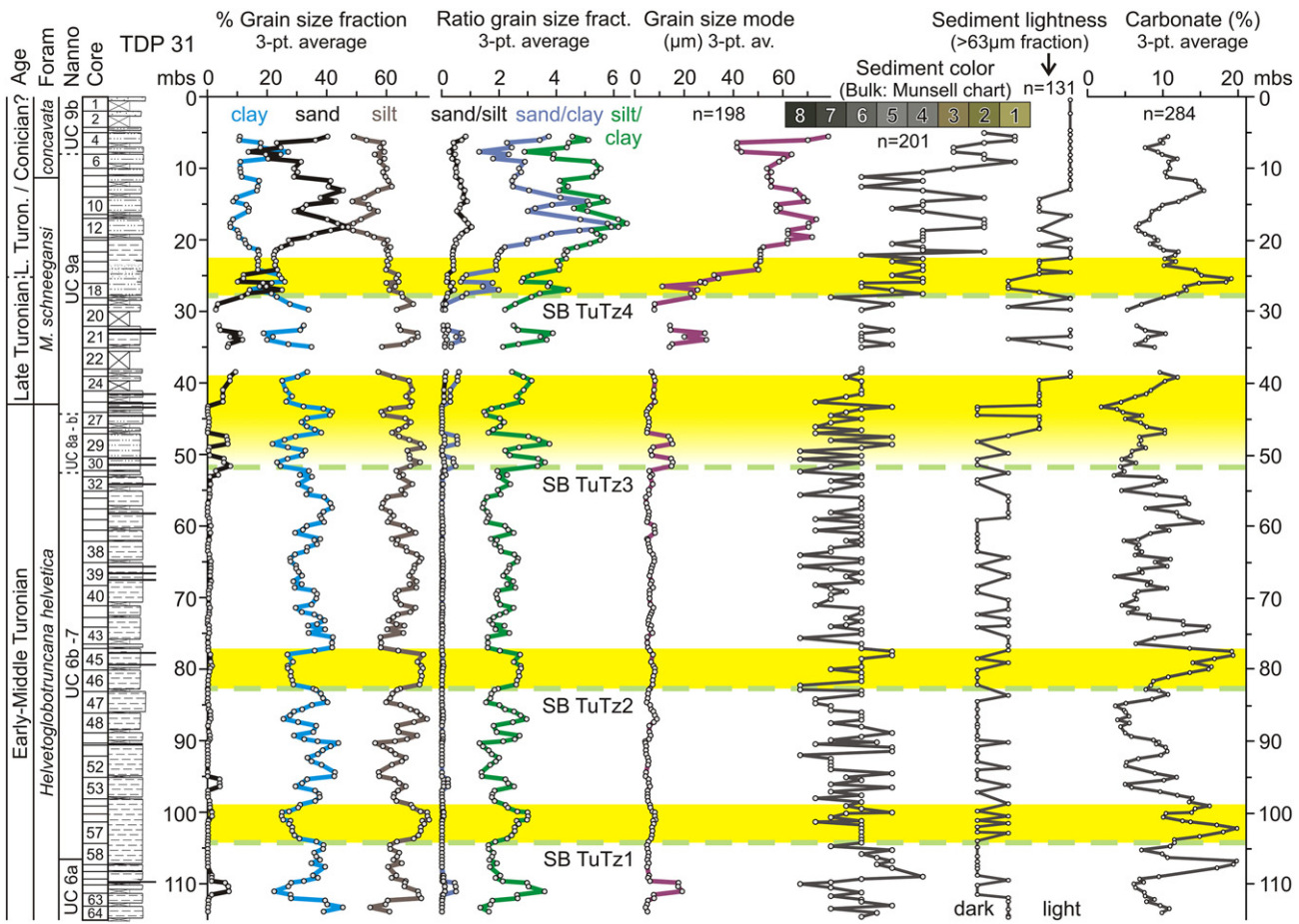


Fig. 3. Grain-size parameters, sediment color and lightness, and carbonate content for TDP 31. Sediment lightness (4 grades) derived from dry >63- μm fraction of washed samples and sediment color (Munsell chart) obtained from wet bulk samples: 1–3 light greenish-gray, 4–5 middle gray, 6–8 dark gray (for color codes see Table S3). Number (n) of measured samples is given above the respective curves. Carbonate percentage curve combines data from Jiménez Berrocoso et al. (2012) and this study (see Fig. 4). Dashed lines mark local sequence boundaries (SBs TuTz1 to 4). Shaded intervals above the SBs are characterized by sedimentological, faunal, and geochemical shifts that occurred during the falling stages and lowstands, as shown in this and the subsequent figures (see Section 3 for further explanation).

per sample. Diversity expresses the number of species observed in a sample with the above-described method.

Microfacies data on abundance, size, and roundness of detrital grains provide important information to complement the grain-size measurements obtained from the particle-size analyzer: (1) These observations verify if an increase in grain size indeed reflects larger detrital components (e.g. quartz grains), or more abundant foraminifera, or the presence of aggregated particles; (2) They provide information on grain sizes >2 mm that cannot be detected with the particle-size analyzer; (3) They increase the precision for recording larger grain sizes at low abundance because of the much larger sample volume studied, compared to the small amount of sample measured with the particle-size analyzer.

4.3. Geochemical analyses

The geochemical data for bulk sediments from TDP 31 in Jiménez Berrocoso et al. (2012; number of samples for TOC and bulk $\delta^{13}\text{C}_{\text{org}}$ = 58, for wt% carbonate = 96, and for $\delta^{13}\text{C}_{\text{carb}}$ and $\delta^{18}\text{O}_{\text{carb}}$ = 128) are complemented with new data for TOC and wt% carbonate (155 samples), and for $\delta^{13}\text{C}_{\text{carb}}$ and $\delta^{18}\text{O}_{\text{carb}}$ (69 samples). These additional measurements were performed at Bremen University (Germany). Carbonate content and TOC were determined with a Leco CS 200. Stable-isotope ratios were measured on a Finnigan MAT 251 gas source isotope-ratio mass spectrometer connected to

a Kiel III automated carbonate preparation device. The instrument was calibrated against an in-house laboratory standard (ground Solnhofen limestone), which in turn is calibrated against the NBS 19 international standard reference material. Over the measurement period, the analytical precisions for measurement of the in-house standard were 0.03‰ for $\delta^{13}\text{C}_{\text{carb}}$ and 0.05‰ for $\delta^{18}\text{O}_{\text{carb}}$. Isotope-ratio data are reported in standard δ -notation on the Vienna PDB (VPDB) scale.

Some bulk sample measurements were repeated to verify comparability of the data measured in Bremen with the published data for TDP site 31 that were originally determined at University of Missouri (USA): 13 samples for TOC (average difference 0.1%, maximum difference 0.35%), 51 samples for wt% carbonate (av. 7.2%, max. 26.5%), 10 samples for $\delta^{13}\text{C}_{\text{carb}}$ and $\delta^{18}\text{O}_{\text{carb}}$ (av. 0.47‰ and 0.23‰, respectively, max. 1.54‰ and 0.75‰, respectively). The data are illustrated with separate colors for the two laboratories. Systematic offsets were not observed for TOC and $\delta^{13}\text{C}_{\text{carb}}$. The average trends in $\delta^{18}\text{O}_{\text{carb}}$ values and wt% carbonate from samples measured in Bremen are systematically lower (by ~0.4‰ and 5%, respectively) than from samples measured in Missouri. Variability in replicate carbonate measurements at Missouri was 1.6% on average (max. 5.5%). The relatively large difference in carbonate values of replicate measurements (including sample preparation) between laboratories might in part reflect sample heterogeneity in combination with the generally low carbonate content of the sediments studied: carbonate from

un-recognized micro-veins or shell fragments would have a large influence on the values if variably present in the sub-samples. Minor variations in carbonate content and bulk $\delta^{18}\text{O}_{\text{Carb}}$ across the section are, therefore, not interpreted.

Bulk sediment isotope-ratio analyses for ODP Holes 762C and 763B were undertaken in the Department of Earth Sciences, University of Oxford (Clarke, 2002). The samples were wet-sieved through a 63- μm screen. The <63- μm fine-fraction portion was subject to isotope-ratio analyses, using a VG PRISM mass spectrometer with common acid bath. Analytical precision was better than 0.1‰ for determination of $\delta^{13}\text{C}_{\text{Carb}}$ values. Raw data for $\delta^{13}\text{C}_{\text{Carb}}$ values from ODP Holes 762C and 763B are provided in the supplementary materials (S3).

Methods for single species stable-isotope ratio analysis of foraminifera from TDP 22 and TDP 31 are described in MacLeod et al. (2013) and Wendler et al. (2013a). Each species was measured separately, but in order to simplify the patterns and to increase stratigraphic resolution and robustness of the signal, results for species with similar isotopic signatures have been grouped as described in Wendler et al. (2013a). The following groups are distinguished for benthic foraminifera: *Lenticulina* spp. Group, *Epistomina* spp. Group, *Berthelina berthelini* Group (*B. berthelini*, *Lingulogavelinella convexa*, *Lingulogavelinella globosa*, *Oridorsalis umbonatus*), and for planktic foraminifera: *Helvetoglobotruncana helvetica* Group (*H. helvetica*, *Helvetoglobotruncana praehelvetica*, *Whiteinella aprica*, *Whiteinella brittonensis*) and *Dicarinella hagni* Group (*D. hagni*, *Praeglobotruncana stephani*, *Praeglobotruncana gibba*, *Marginotruncana renzi*). The isotope-ratio values plotted for each group represent the average of all measurements per sample level from the different species included in each group (these were measured separately for each species) and include replicate measurements per species and sample. The total number of measurements represented in a curve is indicated in some of the figures, because this number is usually much larger than apparent from the number of plotted data points (sample levels). Typically, several specimens were used per measurement, such that the number of measurements does not denote the number of measured specimens.

4.4. X-ray diffraction analysis (XRD)

For 25 samples from TDP31, we performed XRD measurements for qualitative assessment of the total mineral assemblage using a Rigaku D/Max Rapid micro-X-ray diffractometer at the Department of Mineral Sciences, Smithsonian Institution (USA). Whole rock ground powder was glued to the tip of a thin glass fiber and exposed to an X-ray beam for 5 min. The following conditions were used for XRD measurements: U = 50 kV, I = 40 mA, collimator 0.3 mm and resolution 1000 \times 1000 μm . Diffraction patterns for Theta (deg) 0–35 were studied using the software package AreaMax™. The XRD measurements were performed on TDP 31 samples at sample spacing of 3–10 m. Samples from depths <12 m were not studied, because late-diagenetic influences from surface weathering were suspected.

The XRD diffractograms and an example peak determination are shown in Figs. S1 and S2. Raw data for grain size, sediment color, and geochemical measurements are provided in the supplementary materials (S3).

5. Results

5.1. Grain size and sediment color

The grain-size analyses for TDP 31, TDP 22, and TDP 36 indicate silt-dominated (centered around a mode of 10 μm) sediments throughout the measured sections (Fig. 2). Slight differences in apparent grain size between lithologic columns and grain-size measurements result from a combination of differences in sampling intervals and method of

grain-size identification: not all minor sand layers observed in the field were sampled and measured, and not all subtle grain-size differences measured in the laboratory are detectable during core description in the field. The grain-size measurements reflect stratigraphic trends, not the smaller bedding-scale variations. Grain-size alternations occur between more or less silty intervals within principally fine-grained successions. An exception is the upper 27 m of TDP 31 where the sand fraction increases to 30–40%, dominated by grains of 60–100 μm .

Differences in grain size between the sections become apparent when comparing the ratio $S = (\text{silt} + \text{sand})/\text{clay}$ (Fig. 2). The lowest S values, mainly between 2 and 3, are found for TDP 31, except in the upper part where S values are between 6 and 12. The TDP 22 sediments generally are coarser, with S values mainly between 3 and 5. The coarsest signature is observed for TDP 36, where S values are mainly between 4 and 6. In contrast, the contribution of the sand fraction is higher in TDP 22 than in TDP 36. Medium-scale stratigraphic variations in S values, with recurrence intervals of 5–10 m, are evident in all three sections. These changes, from more clay-rich to coarser (more silty) intervals, are used to distinguish sedimentological units. Following the concept explained in Section 3, the bases of these coarser-grained intervals represent potential SBs and are marked with dotted and dashed lines in Fig. 2, whereby the dashed levels coincide with changes in other proxies (see Sections 3 and 5.2–5.6) and are, therefore, considered to represent the boundaries of the main depositional sequences (base of falling-stage and lowstand deposits). The grain-size cycles separated by the dotted lines may represent higher-order depositional sequences or variations in clastic sediment flux that are unrelated to sea level.

In TDP 36, the average clay content is higher and more variable in the lower part of the *H. helvetica* Zone than in the higher part of the zone. This change occurs at ~50 m and marks the top of a subtle long-term finding upward trend in S values (by ~1 units). The interval above this level not only shows lower and less variable values in clay content but also less variability in silt and sand content. This pattern is not observed in TDP 22 and TDP 31, although a slight decrease in the average clay content across the *H. helvetica* Zone is also detectable in both records. The coarser interval in the upper part of TDP 31 occurs above the *H. helvetica* Zone; this stratigraphic level was not recovered at TDP 22 and TDP 36. The sandy part in the upper 10 m of TDP 22 is barren of microfossils and thus cannot be dated.

Plots of the 3-point moving average for the grain-size fractions, their ratios, and the grain-size mode for TDP 31 in Fig. 3 show the coarser-grained intervals more clearly than the detailed plots in Fig. 2, i.e. between 98–104 m, 77–82 m, 47–52 m, and above 27 m. Their bases (dashed lines in Fig. 3 and subsequent figures) are defined as local SBs TuTz1 to TuTz4. The shaded intervals above the SBs mark a succession of shifts in faunal composition and geochemical parameters that follow the initial change towards coarser sediments at the SBs, as described in the following sections.

Beside some small-scale (cm to dm) color variation between lighter and darker beds, the general sediment color in TDP 31 shifts at SB TuTz3 from dark gray to medium gray (at ~42 m) and at SB TuTz4 to lighter greenish-gray (at ~27 m, Fig. 3), which also is visible in the core photographs (Appendix 1A–F). The data for grain size and sediment color are given in the supplementary materials (S3).

5.2. TDP 31 – Geochemical data from bulk sediments

A compilation of the published (Jiménez Berrocoso et al., 2012) and new geochemical data for TDP 31 is given in Fig. 4. The carbonate content varies mainly between 5–15%. The lowest values were measured below 42 m, and they are slightly elevated, on average, above 27 m. Total organic carbon (TOC) below 42 m depth fluctuates between 0.5–2.0% with an average of ~1.0%. An up-section drop in TOC at 42 m is followed by a steady decrease (average between 42–27 m is 0.6%) and by another drop at 27 m to values below 0.4% (averaging 0.2%).

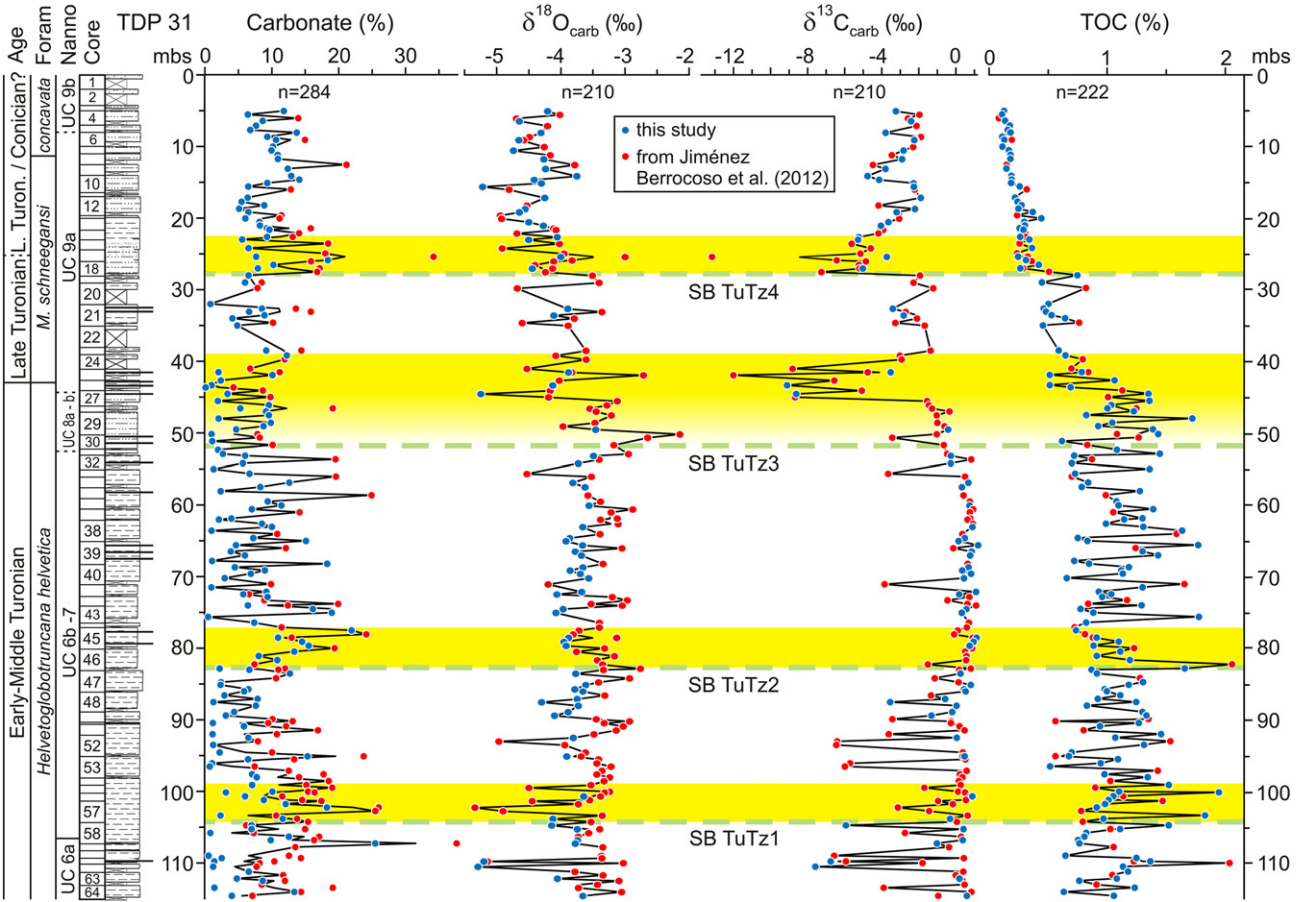


Fig. 4. Percent carbonate and TOC, and $\delta^{18}\text{O}_{\text{carb}}$ and $\delta^{13}\text{C}_{\text{carb}}$ values for bulk sediment samples from TDP 31. Number (n) of measured samples is given above the respective curves. Red dots: data from Jiménez Berrocoso et al. (2012), blue dots: data from this study. Black line marks the average for those samples with replicate measurements. Dashed lines and shaded intervals as in Fig. 3.

The carbonate content of 14 samples was too low for bulk sample isotope-ratio measurements. The $\delta^{18}\text{O}_{\text{carb}}$ values below 42 m fluctuate around an average of $-3.6\text{\textperthousand}$. Between 42–27 m, a trend towards lower $\delta^{18}\text{O}_{\text{carb}}$ values is observed, falling on average from $\sim -3.6\text{\textperthousand}$ to $\sim -4.0\text{\textperthousand}$, and then further decreasing to an average of $-4.4\text{\textperthousand}$ above 27 m. A slight positive shift in $\delta^{18}\text{O}_{\text{carb}}$ values is found at ~ 14 m. The $\delta^{13}\text{C}_{\text{carb}}$ values below 52 m mostly vary around $\sim -0.6\text{\textperthousand}$, but below 82 m a number of samples gave very low $\delta^{13}\text{C}_{\text{carb}}$ values (down to $-7.6\text{\textperthousand}$). Much less variability (except for 2 data points) in $\delta^{13}\text{C}_{\text{carb}}$ values is evident between 82–52 m. Between 52–45 m, the average $\delta^{13}\text{C}_{\text{carb}}$ values decrease to $\sim -1.0\text{\textperthousand}$, followed by a 4 m-thick interval with values consistently below $-4.0\text{\textperthousand}$ and averaging at about $-8.0\text{\textperthousand}$. From 40 m to 28 m depth the $\delta^{13}\text{C}_{\text{carb}}$ values vary around $-2.3\text{\textperthousand}$. Another interval of 6 m thickness with $\delta^{13}\text{C}_{\text{carb}}$ values below $-4.0\text{\textperthousand}$ is followed by higher $\delta^{13}\text{C}_{\text{carb}}$ values that average at $\sim -3.0\text{\textperthousand}$. A negative $\delta^{13}\text{C}_{\text{carb}}$ shift (by $\sim -3.0\text{\textperthousand}$) at ~ 14 m approximately parallels the positive shift in $\delta^{18}\text{O}_{\text{carb}}$.

5.3. TDP 31 – Planktic and benthic foraminiferal turnovers

The top of the *H. helvetica* Zone in TDP 31 marks an important faunal turnover in planktic foraminiferal species (Huber and Petrizzo, 2014) that is part of a series of changes associated with SB TuTz3. Another important shift in planktic foraminifera occurs shortly above SB TuTz4, where the relative and absolute abundance of biserial planktic foraminifera increases dramatically (Fig. 5; Haynes et al., 2015 and this study). Elevated abundance of biserial planktics also

is observed slightly above SBs TuTz1 and TuTz2. These two levels are also characterized by peak abundances of the benthic foraminifera *Tappanina laciniosa* that otherwise occurs in very low numbers throughout the section (Fig. 5).

Benthic foraminifera in TDP 31 can be grouped into two distinct assemblages, denoted A and B. Assemblage A dominates below 42 m, while assemblage B dominates above 27 m (Fig. 5). The interval between 42–27 m is characterized by species from both assemblages. The shift from assemblage A to B is not gradual but occurs in two drastic turnovers in species composition: 1) at ~ 45 m, as part of the shifts associated with SB TuTz3 and positioned slightly below the faunal turnover in planktic foraminifera, and 2) at ~ 27 m, synchronous with the increase in biserial planktics. Important species of assemblage A belong to the genera *Epistomina*, *Colomia*, *Ceratobulimina*, *Pseudopatellinella*, *Lingulogavelinella*, *Berthelina*, *Ammodiscus*, *Gloospira*, and also include abundant trochamminids. Assemblage B comprises species of the genera *Quadrrimorphina*, *Allomorphina*, *Stensioeina*, *Gavelinella*, *Gyroidinoides*, *Reussella*, *Frondicularia*, *Ramulina*, *Gaudryina*, *Spiroplectammina*, *Dorothia*, and abundant calcareous uniserial forms such as *Dentalina*, *Pleurostomella*, and *Nodosaria*. The uniserial benthics show a similar pattern as the biserial planktics, with a strong increase in relative abundance just above SB TuTz4 and slightly elevated abundance just above SBs TuTz1 and TuTz2, which also is expressed as minor peaks in the relative abundance of assemblage B species at these levels (Fig. 5).

While all foraminifera are cement infilled above ~ 27 m in TDP 31, preservation of most microfossils is excellent below that level. However,

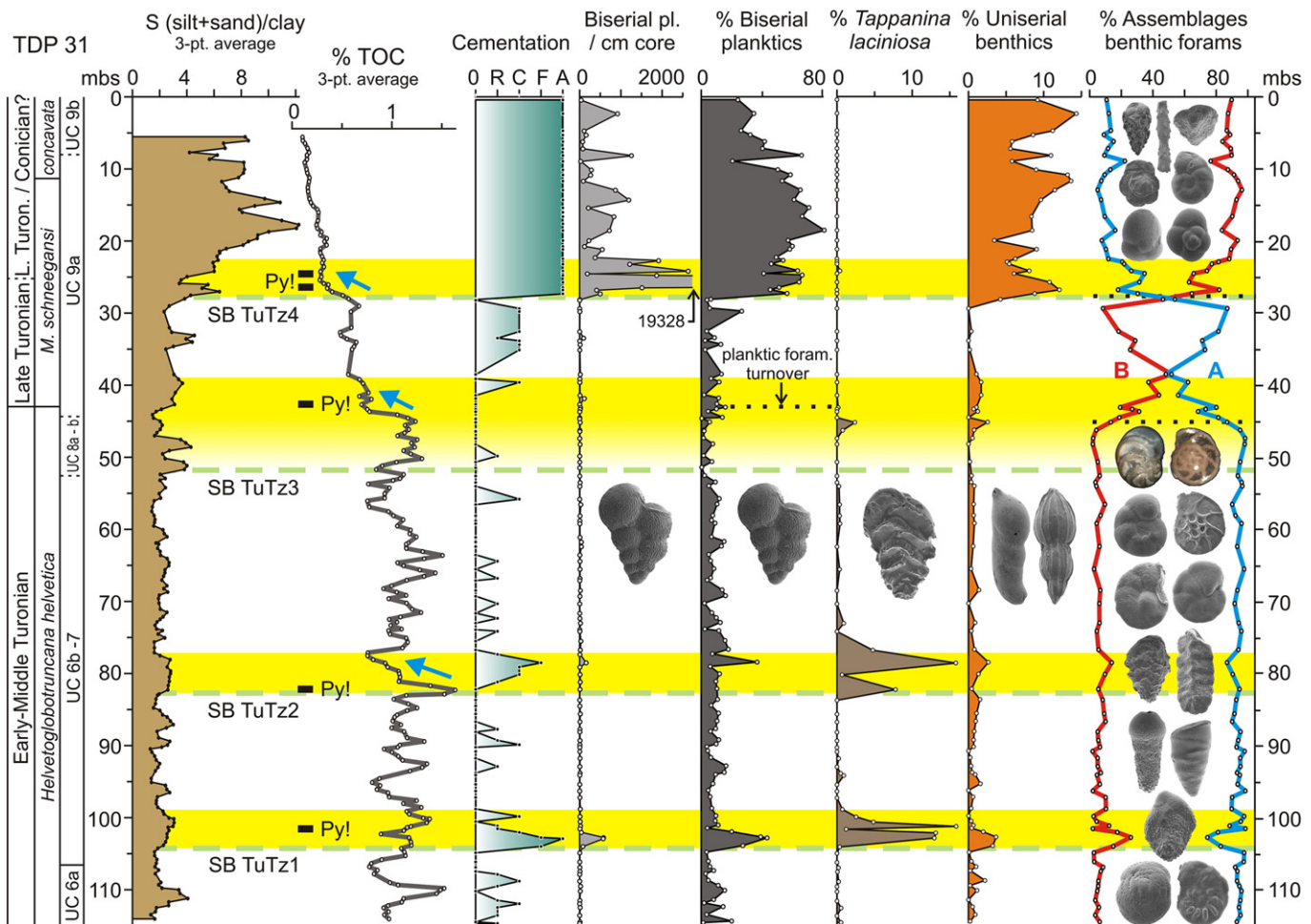


Fig. 5. Comparison of faunal shifts with changes in grain size, TOC percentage, and cementation in TDP 31. The TOC curve combines data from Jiménez Berrocoso et al. (2012) and this study (see Fig. 4). Biserial planktics are combined data from Haynes et al. (2015) and this study. Note faunal turnovers (black dotted lines) in benthic (this study) and planktic foraminifera (Huber and Petrizzi, 2014) and a drop in TOC percentage (arrows) in the lowstands above SBs TuTz3 and 4. Benthic foraminifera show a two-step shift from assemblage A (blue) to assemblage B (red). A dramatic increase in absolute, and relative, abundance of biserial planktic foraminifera and cementation of tests is found above SB TuTz4, together with a strong increase in grain size. The lowstands above SBs TuTz1 and 2 show abundance peaks of *T. laciniosa* and elevated abundance of biserial planktic foraminifera, benthic foraminiferal species of assemblage B, and cemented tests. Black bars with “Py!” indicate samples with very abundant pyrite. Dashed lines and shaded intervals as in Fig. 3.

rare cement-filled foraminifera can also be found in some samples below 27 m. It is interesting to note that, similar to the abundance of biserial planktic foraminifera and benthic foraminifera of assemblage B, slightly elevated abundance of cemented foraminifera tests is observed just above SBs TuTz1 and TuTz2 (Fig. 5).

5.4. TDP 31 – Foraminiferal carbon- and oxygen-isotope ratios

Carbon and oxygen isotope data of foraminifera (MacLeod et al., 2013; Wendler et al., 2013a) and bulk sediment (Jiménez Berrocoso et al., 2012) from TDP 31 are compared in Figs. 6 and 7. The $\delta^{13}\text{C}_{\text{org}}$ record shows four distinct minima that occur just above the four SBs (Fig. 6). While the upper two minima are paralleled by very low $\delta^{13}\text{C}_{\text{carb}}$ values, the lower two are not expressed in the $\delta^{13}\text{C}_{\text{carb}}$ record.

Isotope-ratio data from well-preserved, translucent foraminifera ($\delta^{18}\text{O}_{\text{f}}$ and $\delta^{13}\text{C}_{\text{f}}$) were obtained in the interval below ~34 m (MacLeod et al., 2013; Wendler et al., 2013a). The 3-point running average curves are illustrated for three benthic and two planktic groups (Figs. 6 and 7), following Wendler et al. (2013a). The two lower minima in the $\delta^{13}\text{C}_{\text{org}}$ record (above SBs TuTz1 and 2) are paralleled by the $\delta^{13}\text{C}_{\text{f}}$

curves of all planktic and benthic groups except the aragonitic *Epistomina* Group (Fig. 6). These two levels are further characterized by minima in $\delta^{18}\text{O}_{\text{f}}$ of all benthic and planktic groups (Fig. 7), whereby the minima in the planktics (at the lower minimum only the shallow living group) slightly postdate that of the benthics. Minor $\delta^{13}\text{C}_{\text{f}}$ and $\delta^{18}\text{O}_{\text{f}}$ minima in the records of most groups occur at ~62 m and ~90 m (compare to dotted lines in Fig. 2).

Starting at ~52 m (SB TuTz3), the $\delta^{13}\text{C}_{\text{f}}$ values of all planktic and benthic groups decrease strongly by ~1.5–2.0‰ across a stratigraphic interval of ~10 m thickness, first paralleled by the $\delta^{13}\text{C}_{\text{org}}$ and then by the $\delta^{13}\text{C}_{\text{carb}}$ records. A drop in $\delta^{18}\text{O}_{\text{f}}$ is observed for all groups within this interval, followed by another $\delta^{18}\text{O}_{\text{f}}$ decrease above 42 m. Similar to the foraminiferal data, the bulk sediment $\delta^{18}\text{O}_{\text{carb}}$ values decrease above SB TuTz3 and above SB TuTz4. Except for the large negative $\delta^{13}\text{C}_{\text{f}}$ shift above SB TuTz3, the trends in the $\delta^{13}\text{C}_{\text{f}}$ record of *Epistomina* differs from those of the calcitic benthic groups, possibly related to a temperature effect on carbon isotopic fractionation during biogenic aragonite formation (Grossman and Ku, 1986). The $\delta^{13}\text{C}_{\text{f}}$ values for *Lenticulina* are very low with large fluctuations that are thought to be related to strong vital effects and possibly an infaunal mode of life (Wendler et al., 2013a), and they are shown to a different scale (Fig. 6).

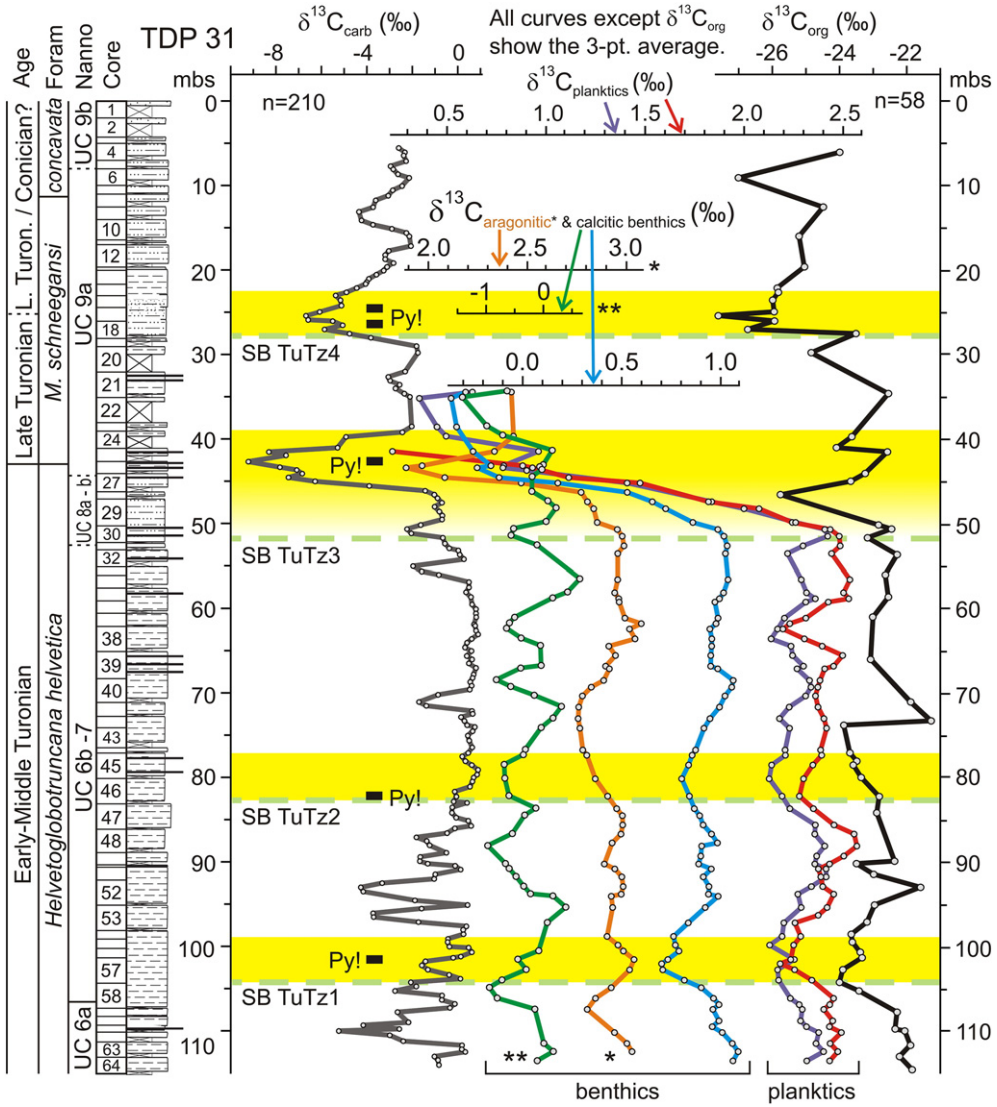


Fig. 6. Comparison of $\delta^{13}\text{C}$ data from bulk sediment carbonate (gray) and organic matter (black) and from benthic and planktic foraminifera for TDP 31. The $\delta^{13}\text{C}_{\text{carb}}$ curve combines data from Jiménez Berrocoso et al. (2012) and this study (see Fig. 4). The $\delta^{13}\text{C}_{\text{org}}$ data are from Jiménez Berrocoso et al. (2012) and $\delta^{13}\text{C}_f$ data for benthic and planktic foraminifera from MacLeod et al. (2013) and Wendler et al. (2013a). Lowstand intervals above the four SBs show minima in $\delta^{13}\text{C}_{\text{org}}$ and in $\delta^{13}\text{C}_f$ for all foraminiferal groups except the aragonitic group (*). Note different scale for Lenticulina Group (**). Dashed lines and shaded intervals are as in Fig. 3. For legend and n of $\delta^{13}\text{C}_f$ curves see Fig. 7.

Vertical gradients in $\delta^{13}\text{C}_f$ and $\delta^{18}\text{O}_f$ between the surface, thermocline, and bottom waters can be estimated from $\Delta\delta^{13}\text{C}_f$ and $\Delta\delta^{18}\text{O}_f$ values between the *H. helvetica* group, *D. hagni* group, and *B. berthelini* group, respectively (Fig. 8). Most changes in these gradients are small (<0.4‰), but they: (1) are comparable to some of the minor $\delta^{13}\text{C}_{\text{carb}}$ shifts that are globally correlated, (2) are an order of magnitude larger than analytical uncertainties, and (3) show some consistency in the $\Delta\delta^{13}\text{C}_f$ and $\Delta\delta^{18}\text{O}_f$ patterns relative to the SBs, suggesting that these shifts might be meaningful. At the SBs, and partly at the boundaries of higher-order depositional sequences, the surface–thermocline $\delta^{13}\text{C}_f$ gradient is reduced by 0.2–0.3‰, and surface–thermocline $\delta^{18}\text{O}_f$ gradients rise from low values at these boundaries to higher values above them. Increasing trends above the SBs are also observed for surface–bottom $\delta^{18}\text{O}_f$ gradients. The thermocline–bottom $\delta^{18}\text{O}_f$ gradient appears to reflect two long-term cycles of slowly decreasing values, separated by a more rapid rise at SB TuTz2. A similar rise is found above SB TuTz3, starting at the level of the most drastic faunal shifts at ~42 m. Surface–bottom and thermocline–bottom $\delta^{13}\text{C}_f$ gradients do not show a consistent pattern, but both decrease by 0.7–0.9‰ above SB TuTz3 and show minima

at the boundaries of higher-order depositional sequences at ~62 m and ~72 m.

5.5. TDP 22 – Foraminiferal carbon- and oxygen-isotope ratios

The foraminiferal stable-isotope records from TDP 22 are noisier and have a lower temporal resolution than those from TDP 31 (MacLeod et al., 2013). Two distinct minima in $\delta^{13}\text{C}_{\text{org}}$ (Jiménez Berrocoso et al., 2010) within the *H. helvetica* Zone are partly paralleled by minima in $\delta^{13}\text{C}_f$ of benthic foraminifera (Fig. S4). These trends are comparable to those in the lower half of the *H. helvetica* Zone at TDP 31. The isotope data from TDP 22 are described in more detail in the supplementary materials (S5).

5.6. TDP 31 – Microfacies analysis

Apart from foraminifera, the microfossil content in TDP 31 includes calcareous dinoflagellate cysts, radiolaria, and ostracods. The calcareous dinoflagellate cysts in the sediments from Tanzania are exceptionally

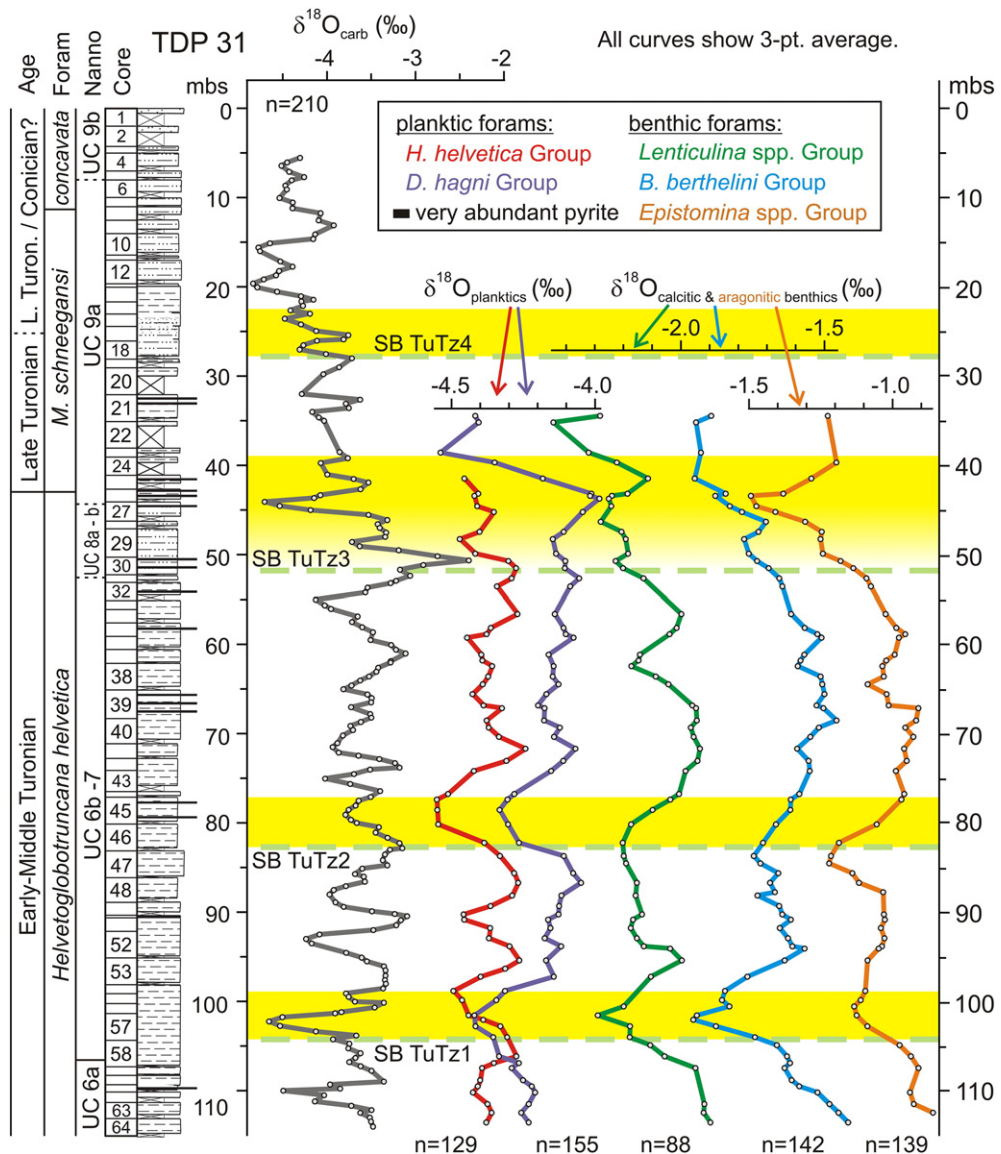


Fig. 7. Comparison of $\delta^{18}\text{O}$ data from bulk sediment carbonate (gray) and from benthic and planktic foraminifera for TDP 31. The $\delta^{18}\text{O}_{\text{carb}}$ curve combines data from Jiménez Berrocoso et al. (2012) and this study (see Fig. 4). $\delta^{18}\text{O}_f$ data for benthic and planktic foraminifera are from MacLeod et al. (2013) and Wendler et al. (2013a). Lowstand intervals above the four SBs show minima in $\delta^{18}\text{O}_f$ for all foraminiferal groups. Dashed lines and shaded intervals are as in Fig. 3. Data points show the average of replicate measurements and n indicates the number of total measurements represented by the respective curve.

well-preserved (Wendler and Bown, 2013; Wendler et al., 2013b). A semi-quantitative study of calcareous dinoflagellate cysts from TDP 31 shows that both absolute abundance and number of species are highest between ~70–90 m and decrease to very low values above 60 m (Fig. 9). Elevated abundance of radiolaria was observed above the four SBs: at ~102 m, ~82 m, ~44 m, and ~27 m (Fig. 10). Ostracods are more abundant just above SB TuTz1 and above ~45 m, especially between 27–18 m. Macrofossils in the studied material are represented by juvenile specimens, fragments, or small parts of their skeletal structures. They include fish, ammonites, scaphopods, gastropods, bivalves, echinoids, ophiuroids, holothurians, and rare crinoids (Figs. 11, 12).

Terrestrial components are represented by fragments of wood, tar, and rarely coal, pyritized seeds, spores, stems, and other plant remains (Fig. 13). Highest abundances of wood fragments are found between 22–48 m and in the top of the coarser intervals above SBs TuTz1 and 2, and they are less commonly observed in the upper

22 m of the section (Fig. 10). Pyritized, striated and stem-like plant remains (Fig. 13.3–4) occur in several samples with rare to common abundance between 42–45 m and are absent from the rest of the section. The tar fragments occur as clasts and can be chert-like, massive, or frothy, but also spherules, droplets, and string-like (sometimes twisted) shapes or other subaerial flow structures were observed (Fig. 13.12–16). In rare cases they bear patterned imprints of plant remains (Fig. 13.8–10), sometimes preserving detailed structures of stems such as cells and hair (Fig. 13.11). The distribution of the microfossils, macrofossil remains, and terrestrial components is summarized in Fig. 10; their characteristics are described in more detail in the supplementary materials (S5).

Results for the detrital components and secondary minerals (pyrite, sulfates, and glauconite) are summarized in Fig. 14. Elevated abundance of pyrite was observed near the four SBs, especially between 23–27 m (lowstand above SB TuTz4) and 38–47 m (lowstand above SB TuTz3). Glauconite was frequent only in one sample at 43 m (lowstand above

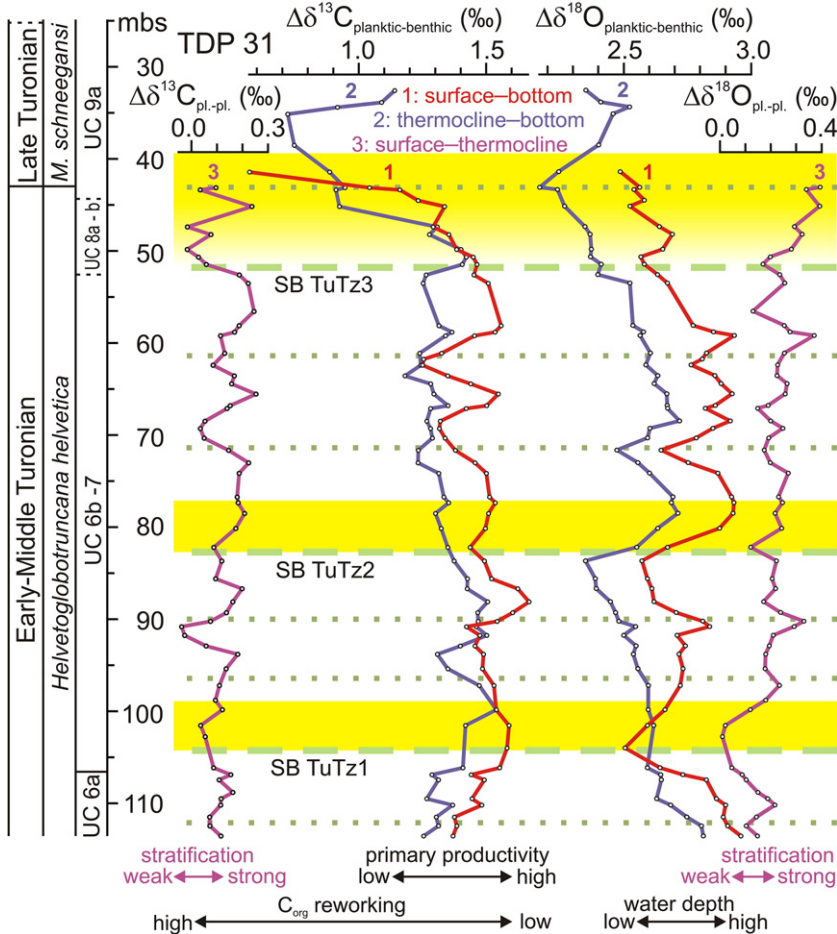


Fig. 8. Gradients in $\delta^{13}\text{C}_f$ and $\delta^{18}\text{O}_f$ between benthic and planktic foraminifera and among the two planktic groups for TDP 31. 1 = surface-bottom gradient (*H. helvetica* Group–*B. berthelini* Group); 2 = thermocline–bottom gradient (*D. hagni* Group–*B. berthelini* Group); 3 = surface–thermocline gradient (*H. helvetica* Group–*D. hagni* Group). The $\delta^{13}\text{C}_f$ and $\delta^{18}\text{O}_f$ data for benthic and planktic foraminifera are from MacLeod et al. (2013) and Wendler et al. (2013a). Note increase in planktic–benthic $\Delta\delta^{18}\text{O}_f$ above the SBs (and partly above the boundaries of higher order depositional sequences) and minima in surface–thermocline $\Delta\delta^{13}\text{C}_f$ at the SBs. See Section 6.2.2. for explanation. Dashed lines and shaded intervals are as in Fig. 3, dotted lines: boundaries of higher order depositional sequences as in Fig. 2.

SB TuTz3). The main detrital components are quartz, mica, heavy minerals (mainly garnet and ilmenite), and feldspar. The quartz grains are mostly angular to sub-angular and suggest a predominantly fluvial source, but some samples additionally contain well-rounded, typically larger, grains with a pitted (“frosted”) surface that appear to be of eolian origin. These rounded grains always occur in subordinate quantity but are slightly more common in the intervals above the SBs (Fig. 14). The XRD data indicate a fairly uniform mineralogical composition of the sediments throughout TDP 31. These results are described in the supplementary materials (S5) and illustrated Figs. S1 and S2.

6. Discussion

6.1. TDP 31 – Long-term trends in relative sea level

Beside a general paleobathymetric position at the upper slope to outer shelf, that is inferred for TDP 31 from benthic foraminifera and calcareous dinoflagellate cysts (see below), a long-term trend in relative sea level through the section is indicated. The stratigraphic record of TDP 31 can be subdivided into two parts based on sedimentological, faunal, and microfacies trends, with the main shift occurring near 42 m. Another strong shift in the various proxies is found within the upper part at ~27 m. The characteristics of the

upper and lower part of the section are summarized in Table 1 and apparently indicate a major change in palaeo-environmental conditions that might involve a change in water depth and/or trophic levels.

The transition from dark gray, fine-grained and finely bedded to laminated sediments in the stratigraphic section below ~42 m, to lighter, coarser-grained and bioturbated sediments without lamination in the interval above ~42 m indicates enhanced ventilation and could reflect a general shallowing trend upwards in the section. Supportive of such an interpretation are the observed elevated abundance of heavy minerals, coarse quartz grains, ostracods, and gastropods in the upper part of the section, because these would be expected to increase landwards from slope to the shelf. Alternatively, a change in magnitude of fluvial influx might be responsible for the observed change in clastic components. However, additional oceanographic changes would be required in order to explain the co-occurring faunal shifts. Furthermore, the largely invariant mineralogical composition of the sediments throughout the section (see S5 and Figs. S1 and S2) indicates that the source area and fluvial flow patterns did not change significantly during the studied period.

The conspicuous presence of juvenile ammonites above 40 m in the section, and especially above 27 m, also would be consistent with a shallowing if those juveniles lived at shallower water depths than adults

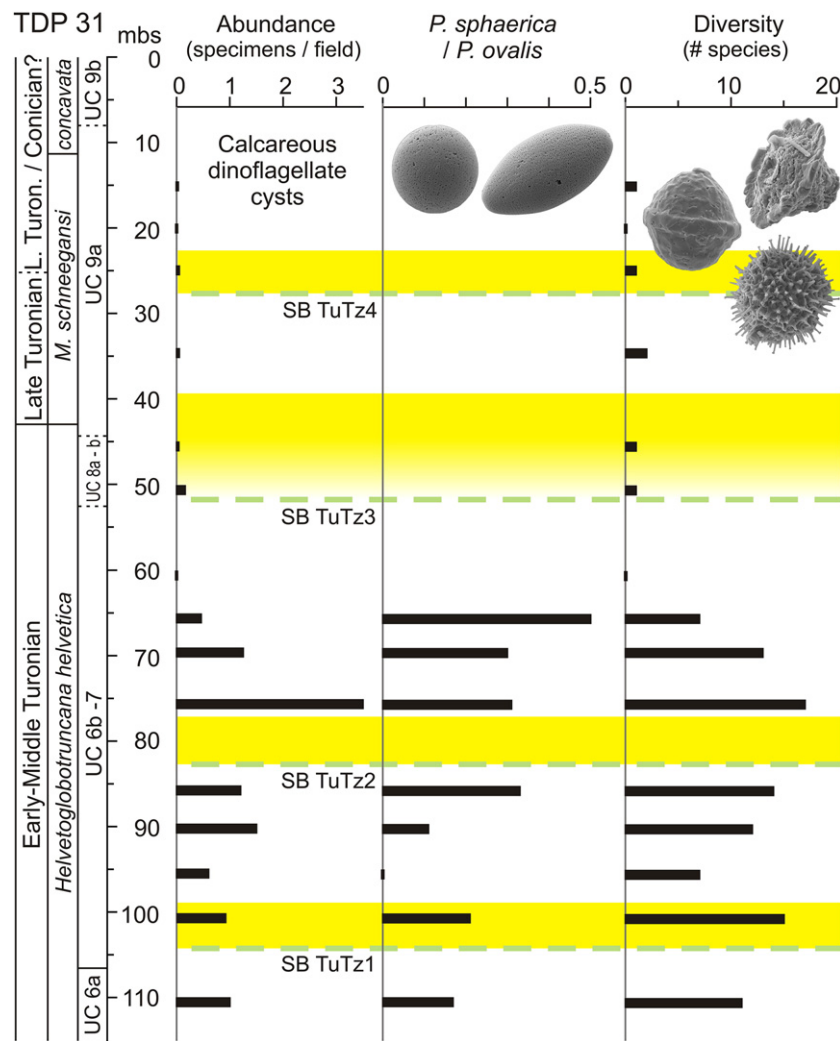


Fig. 9. Quantitative data for calcareous dinoflagellate cysts in TDP 31. Note strong drop in cyst abundance and diversity between 70–60 m that is interpreted to reflect an increase in turbidity. The generally low *P. sphaerica*/*P. ovalis* (Ps/Po) ratio indicates an outer shelf position. Dashed lines and shaded intervals are as in Fig. 3.

and would be representative of shelf environment. Such a pattern is known from a number of modern organisms, but it is not clear whether the same applies to ammonites. Ifrim et al. (2011) suggest a near-surface habitat for the larval stages of ammonites based on a study of Lower Turonian sediments, but whether that means juvenile ammonites were more abundant on the shelf than in the open ocean is not certain. In contrast to juvenile ammonites, scaphopods are absent from the upper part of the section. Today, these organisms live in a wide range of water depth in preferably muddy substrate, so their absence above 42 m and in the more silty lowstands, above SBs TuTz1 and 2, appears to mainly reflect the coarser substrate (Fig. 10).

The benthic foraminifera in the upper 27 m of the section (assemblage B) do not comprise species that are clearly indicative of shallow water/inner neritic habitats. Miliolids are present in low abundance throughout the section. Although the shift from faunal assemblage A to assemblage B is dramatic, there is no clear indication for a change in water depth based on the current knowledge of the depth ranges of the individual species. If there was a general shallowing then it probably shifted from an upper slope position to an outer shelf position. A more comprehensive analysis of the benthic foraminiferal assemblages in TDP 31 is beyond the scope of this paper and will be published elsewhere. Besides water depth,

an increase in nutrient availability appears to be indicated from species of assemblage B (e.g. higher abundance of infaunal species such as buliminids and uniserial forms, Fig. 5) and might also be responsible for the faunal shifts.

The abundance of infaunal benthic foraminifera such as buliminids is generally low in TDP 31, indicating mostly low to moderate nutrient levels. The relatively high TOC content, of typically more than 1.0% in the interval below ~43 m, appears to mainly reflect high abundance of tar fragments and other terrigenous organic material, such as coal and wood fragments (Fig. 10). High abundance of terrestrial organic matter implies that the organic compounds did not represent a good food source for the benthos, which explains the low abundance of infaunal species. Apart from the lowstands above SBs TuTz3 and 4, pyrite is generally more abundant in the lower part of the section, indicating periods of reduced ventilation in line with the presence of lamination and reduced bioturbation in this interval (Appendix 1).

The ratio of *Pithonella sphaerica* to *Pithonella ovalis* (Ps/Po) in TDP 31 is below 0.5, reflecting dominance of the latter species (Fig. 9). *Pithonella sphaerica* has been reported to be distributed throughout shelf settings, being most opportunistic and tolerant to varying nutrient and salinity levels (Dias-Brito, 2000), while *P. ovalis* shows preference for the outer shelf. A low Ps/Po ratio, therefore, indicates

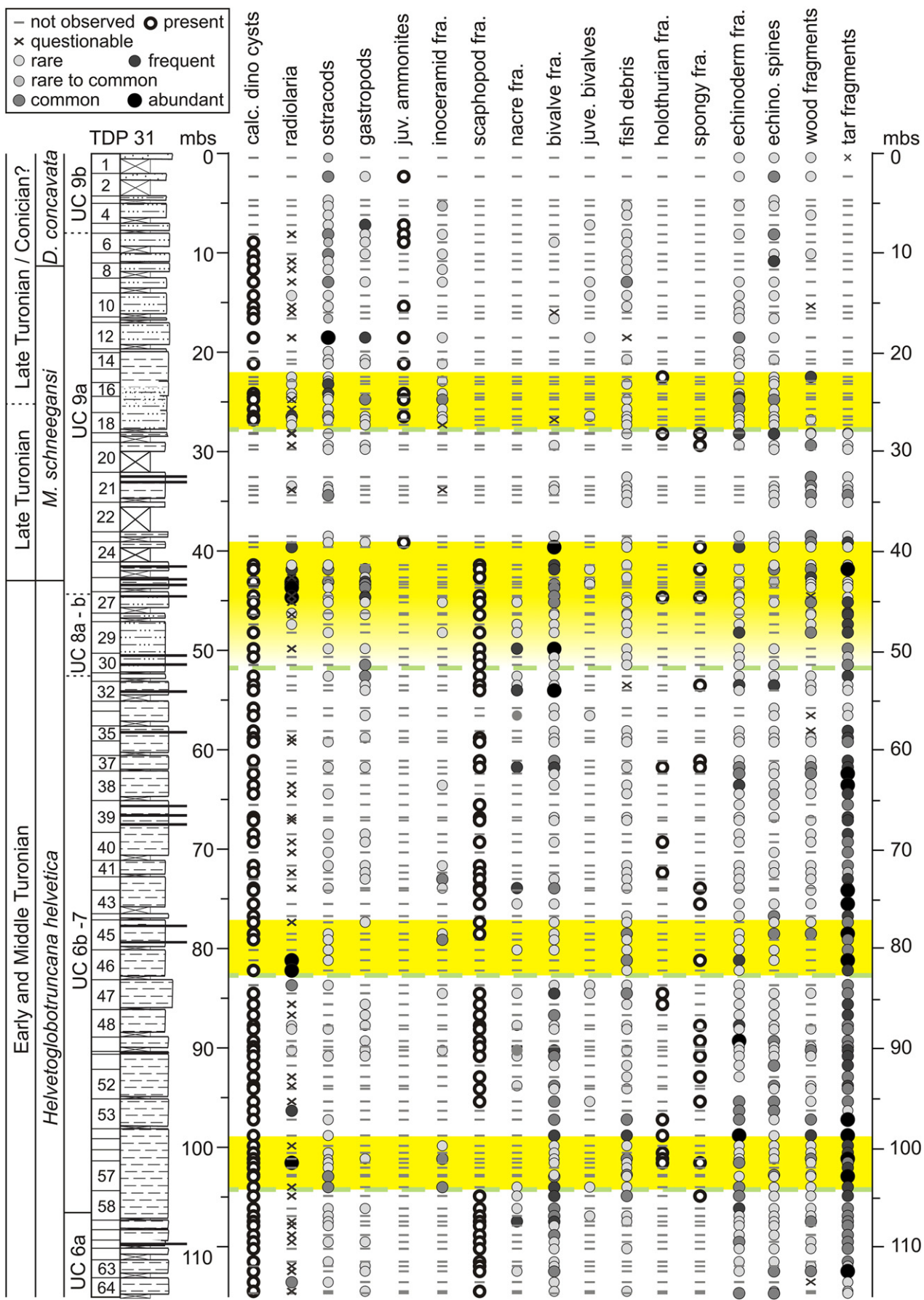


Fig. 10. Microfacies analysis results for TDP 31 – fossils. Qualitative and semi-quantitative data for microfossils and fragments of macrofossils from washed sample residues >63 µm. Abbreviations: calc. = calcareous, fra. = fragments, juve. = juvenile, echino. = echinoderm. Dashed lines and shaded intervals are as in Fig. 3.

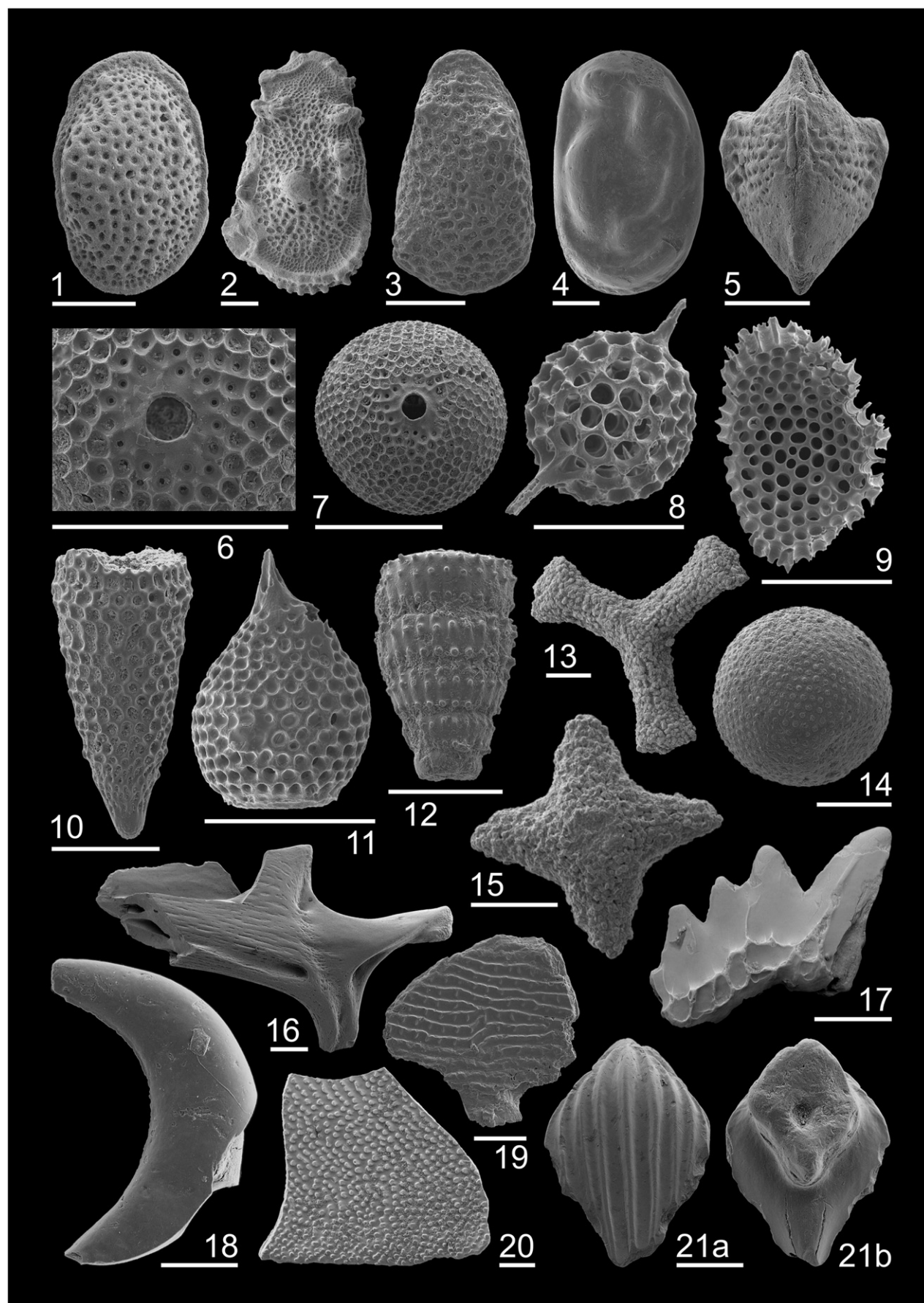


Fig. 11. Scanning electron microscope images of microfossils from TDP 31. 1–5: Ostracods. 6–11: Radiolaria (siliceous preservation). 12–15: Pyritized radiolaria. 16–21: Fish debris; 16: bone fragment; 17–18: teeth; 19–21: scales. All scale bars = 100 µm.

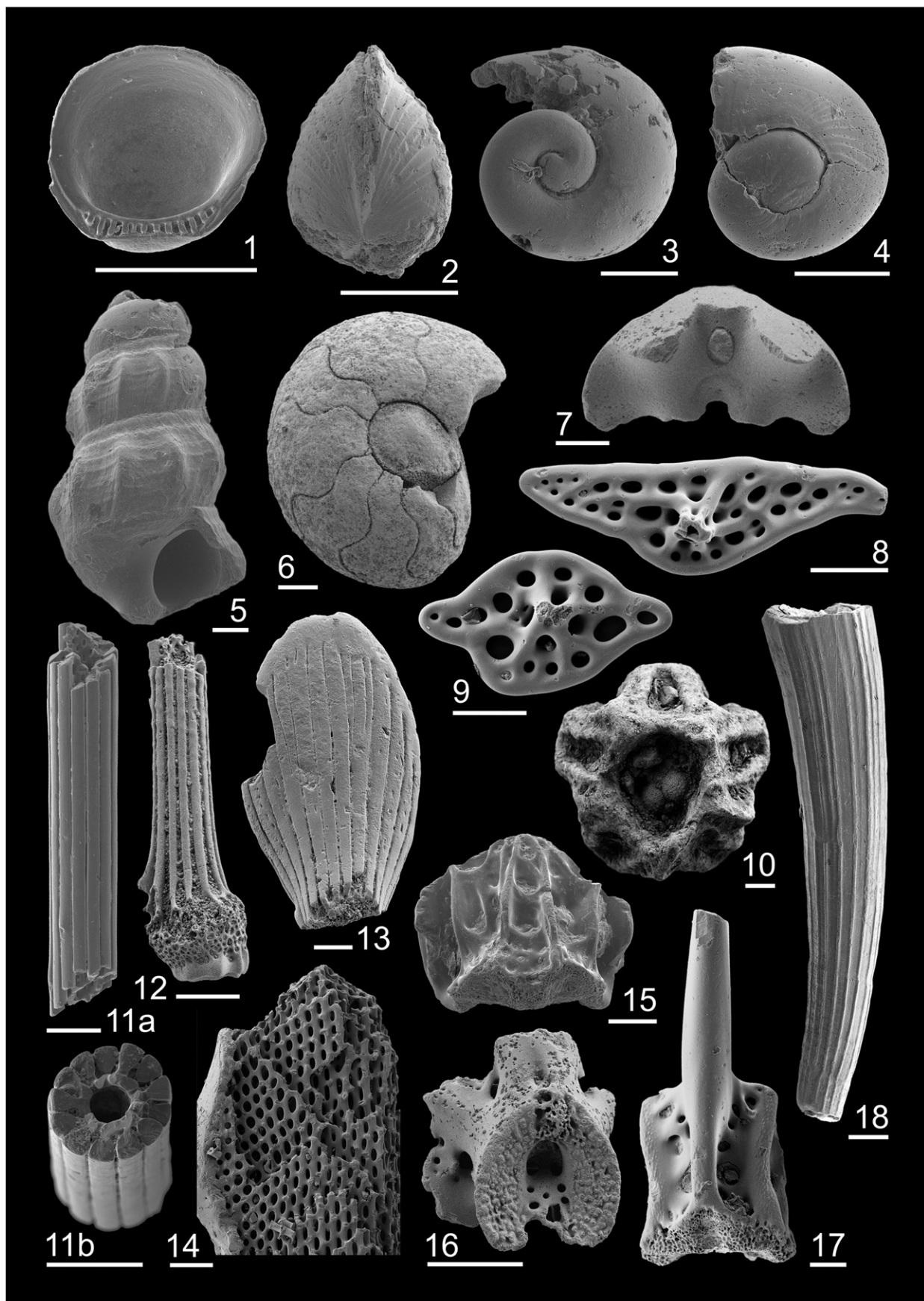


Fig. 12. Scanning electron microscope images of macrofossils and their fragments from TDP 31. 1–2: Juvenile bivalves. 3–5: Gastropods. 6–7: Fragments of juvenile ammonites. 8–9: Holothurian skin ossicles (translucent preservation). 10: Crinoid fragment. 11–13: Echinoid spines. 14–17: Echinoderm fragments. 18: Scaphopod. All scale bars = 100 µm except in 15 and 18 where they are 200 µm.

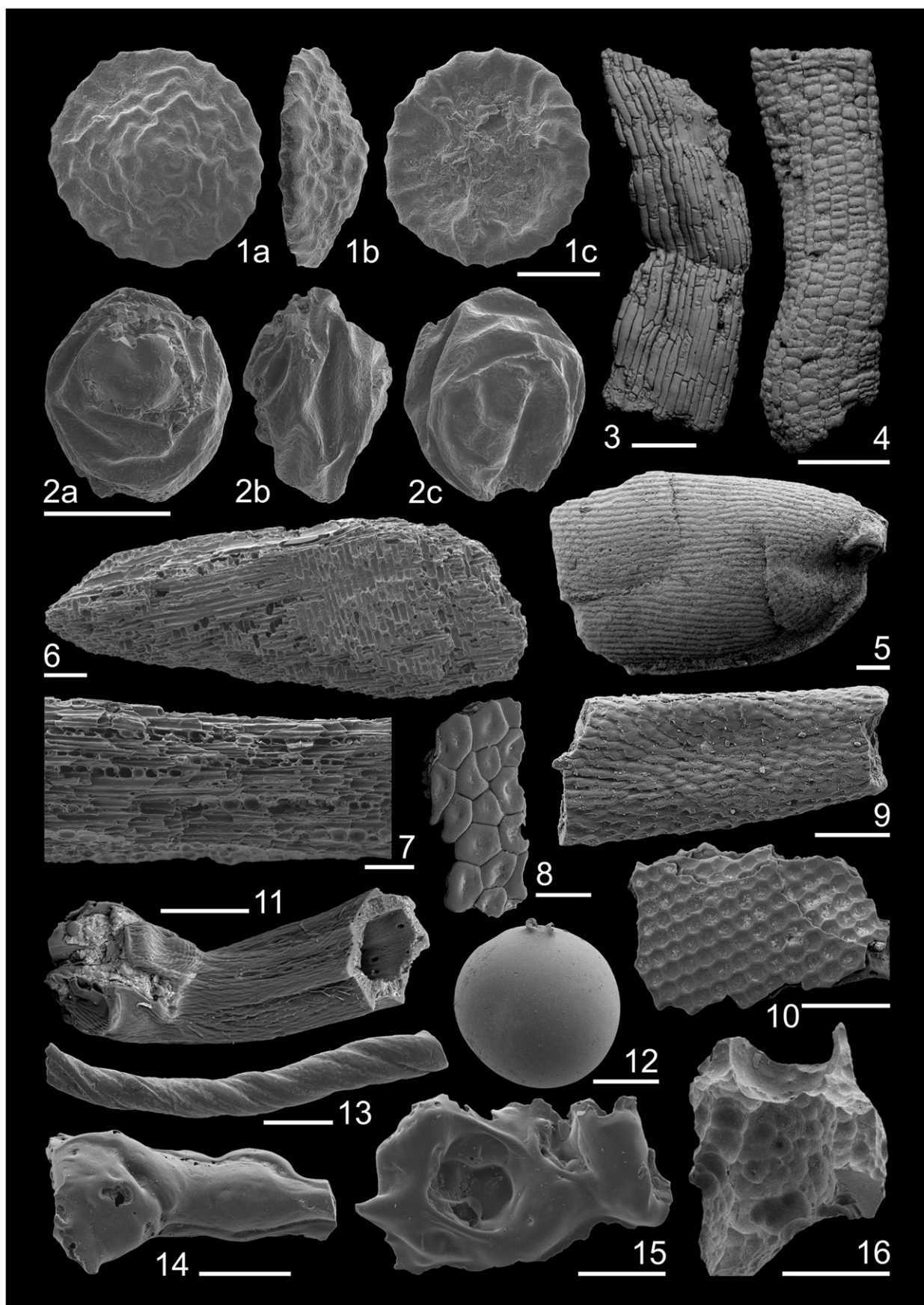


Fig. 13. Scanning electron microscope images of plant remains and tar fragments from TDP 31. 1–2: Spores, possibly of hornwort plants (S. Warny, personal communication). 3–4: Stem fragments (pyritized) with preserved cell structures. 5: Seed? 6–7: Fragments of fossil wood. 8–10: Plant imprints on tar. 11: Stem fragment with detailed cell structures (tar). 12–16: Tar fragments in various shapes: drop, string-like flow structures, and frothy clast. All scale bars = 100 µm.

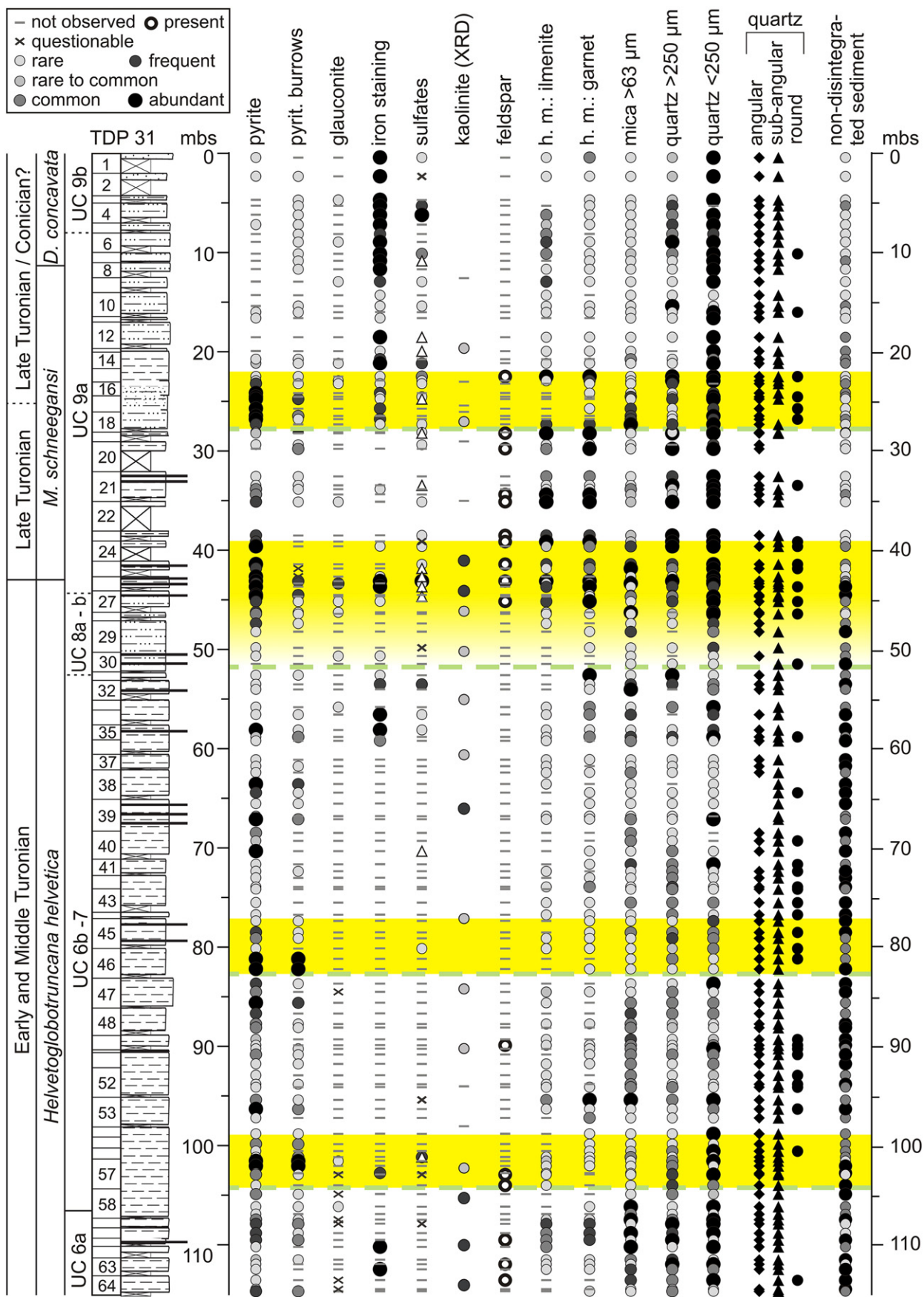


Fig. 14. Microfacies analysis results for TDP 31 – clastic components/minerals. Qualitative and semi-quantitative data for detrital grains and secondary minerals from washed sample residues and mico-XRD analysis results for kaolinite. Abbreviations: h. m. = heavy minerals, pyrit. = pyritized. Translucent sulfates (dots) are distinguished from white sulfates (triangles, qualitative only). Roundness of quartz grains is indicated with different symbols (qualitative only). Dashed lines and shaded intervals as in Fig. 3.

Table 1

Summary of characteristics in the stratigraphic intervals below and above ~42 m depth within TDP 31. A deeper (upper slope) environment is interpreted for the lower part of the sedimentary record, compared to the upper part (outer shelf).

Characteristics	Interval below ~42 m	Interval above ~42 m
Sediment lightness	Darker	Lighter
Sediment color	Gray	Greenish
Laminated intervals	Present	Absent
Grain size	Finer	Coarser
Heavy minerals	Lower abundance	Higher abundance
Disintegration	Not fully disintegrated	Very well
Bulk sediment $\delta^{18}\text{O}$	Higher	Lower
$\delta^{13}\text{C}_{\text{org}}$	Higher	Lower
TOC content	Higher	Lower
Tar fragments	Higher abundance	Lower abundance
Benthic foraminifera	Assemblage A	Assemblage B
Calcareous dinoflagellate cysts	Abundant, diverse	Low abundance to absent
Ostracods	Lower abundance	Higher abundance
Gastropods	Lower abundance	Higher abundance
Juvenile ammonites	Absent	Present
Scaphopods	Present	Absent
Bivalve fragments and nacre	Higher abundance	Lower abundance

an outer shelf to upper slope position and is in line with the paleobathymetry inferred from benthic foraminifera. An increasing Ps/Po ratio thus suggests a shift to more proximal conditions due to falling sea level (Wendler et al., 2002a,b; Zügel, 1994). A general shallowing trend might therefore be suspected from the rising Ps/Po ratio in the interval below ~65 m, but this interpretation is inconsistent with interpretation of other microfacies and geochemical proxy data. Accordingly, the distribution of calcareous dinoflagellate cysts in TDP 31 probably reflects a change in factors other than sea level as discussed below.

The low abundance and diversity of calcareous dinoflagellate cysts in the upper 60 m is very conspicuous (Fig. 9). It might be suspected that they are diluted by enhanced clastic influx above 42 m, where the grain size and quartz content increase, but cyst abundance already decreases between 65–60 m and foraminifera are very abundant in the sandy interval. As typical organisms of shelf environments, the abundance of calcareous dinoflagellate cysts should increase with a change from upper slope to outer shelf conditions (apparently contradicting depth interpretations for TDP 31). However, these observations were made in sediments from carbonate-dominated, meso- to oligotrophic shelf areas. The depositional setting at TDP 31 was dominated by siliciclastic influx, and higher turbidity can be expected with decreasing distance from the coast. All modern dinoflagellates that form calcareous cysts live autotrophically and prefer environments with low turbidity. The fact that calcareous dinoflagellate cysts were very abundant in the Cretaceous Chalk Sea suggests they had similar ecological preferences during the Cretaceous, which would explain their low abundance in the shallower and supposedly more turbid environment that is inferred for the upper part of TDP 31.

The highest long-term relative sea level in TDP 31 is inferred for the interval between ~60–95 m, culminating at ~60–70 m and interrupted by a regression near 80 m. This interpretation is based on several lines of evidence. (1) The most clay-rich parts within TDP 31 occur between ~76–72 m and ~60–56 m (Figs. 2 and 3), bracketing an interval with the most distinct lamination in the section (especially 68–65 m, Appendix 1D). (2) Quiet and stable sedimentary conditions are indicated by the highest values, and lowest fluctuations, in bulk sediment $\delta^{13}\text{C}_{\text{carb}}$ between ~56–81 m (Fig. 4). (3) Highest $\delta^{18}\text{O}_f$ values of the benthic foraminifera and highest planktic–benthic $\delta^{18}\text{O}_f$ gradients are observed between ~60–95 m (peaks between ~58–70 m), suggestive of the lowest bottom-water temperatures and deepest water (Figs. 7 and 8). (4) Microfacies analysis (Fig. 14) shows lowest abundance of quartz (~60–95 m, minimum at ~60–70 m) and heavy minerals

Table 2

Summary of characteristics in the coarser-grained intervals (falling-stage and lowstand deposits) above the four sequence boundaries (SBs) in TDP 31. Note that SBs TuTz1 and 2 have a different character than SBs TuTz3 and 4. Data sources: 1 = this study; 2 = Jiménez Berrocoso et al. (2012); 3 = MacLeod et al. (2013) and Wendler et al. (2013a); 4 = Haynes et al. (2015); 5 = Huber and Petrizzo (2014). Abbreviations: n.d. = no data.

Characteristics in coarser-grained interval above SB	Data source	Data shown in Fig.	SB TuTz1 (~104 m)	SB TuTz2 (~82 m)	SB TuTz3 (~52 m)	SB TuTz4 (~28 m)
Increased grain size	1	2, 3	X	X	X	X
Absence of scaphopod fragments	1	10	X	X	X	X
Very high abundance of pyrite	1	5, 14	X	X	X	X
Increased abundance of radiolaria	1	10	X	X	X	X
Minimum in $\delta^{13}\text{C}_{\text{org}}$	2	6	X	X	X	X
Minimum in $\delta^{13}\text{C}$ of benthic Foraminifera	3	6	X	X	X	n.d.
Minimum in $\delta^{13}\text{C}$ of planktic foraminifera	3	6	X	X	X	n.d.
Minimum in $\delta^{18}\text{O}$ of benthic foraminifera	3	7	X	X	X	n.d.
Minimum in $\delta^{18}\text{O}$ of planktic foraminifera	3	7	X	X	X	n.d.
Rising carbonate content	1 & 2	3	X	X	X	X
Increase in abundance of benthic assemblage B species	1	5	X	X	X	X
Increase in abundance of biserial planktic foraminifera	1 & 4	5	X	X		X
Increase in abundance of cemented foraminifera	1	5	X	X		X
Increased abundance of <i>T. Laciniosa</i>	1	5	X	X	(X)	
Low $\Delta\delta^{13}\text{C}$ surface – thermocline	1 & 3	8	(X)	(X)	X	n.d.
Rising $\Delta\delta^{18}\text{O}$ surface – thermocline	1 & 3	8	X	X	X	n.d.
Rising $\Delta\delta^{18}\text{O}$ thermocline – bottom	1 & 3	8	X	X	(X)	n.d.
Lower abundance of mica >63 μm	1	14	X	X		
drop in TOC	1 & 2	5		X	X	X
Increase in sand fraction	1	2, 3		X	X	X
Change in sediment color	1	3		X	X	X
Strong faunal turnover in benthic foraminifera	1	5		X	X	X
Strong faunal turnover in planktic foraminifera	4 & 5	5			X	X
Very low bulk sediment $\delta^{13}\text{C}_{\text{carb}}$	1 & 2	6			X	X
Sand fraction >20%	1	2, 3				X
Dominance of benthic assemblage B species	1	5				X
Planktic foraminifera dominated by biserial species	1, 4	5				X
All foraminiferal tests cement-filled	1, 2	5				X
Presence of juvenile ammonites	1	10				X

(~60–95 m) and absence of microscopically detectable glauconite and feldspar (~60–90 m), as would be expected for the most distal position. (5) If calcareous dinoflagellate cyst abundance in this siliciclastic depositional environment was mainly controlled by turbidity, as discussed above, their abundance maximum between ~70–90 m (Fig. 9) would indicate lowest turbidity and greatest distance from the coast. Another interval of high relative sea level might be suspected for the base of the TDP 31 stratigraphic section where clay contents, benthic $\delta^{18}\text{O}_f$ values, and planktic–benthic $\delta^{18}\text{O}_f$ gradients are also high, but this interpretation is not supported by microfacies data.

6.2. TDP 31 – Sea level and environmental changes at the sequence boundaries

The four coarser-grained intervals that are associated with changes in foraminiferal assemblages (Fig. 5), shifts in geochemical proxies (Figs. 6 to 8) and microfacies (Figs. 10 and 14) are interpreted to represent falling-stage and lowstand deposits, in a fan setting of the upper slope with a local SB at their base (see Section 3), termed SB TuTz1–4. A summary of the changes concurrent with various other proxies is given in Table 2. The other coarse–fine intervals in the section would represent higher-order depositional sequences that may be related to relative sea level change or to other factors that influenced the supply of clastic material. A mainly fluvial source of the latter can be inferred from the predominantly angular to sub-angular shape of the quartz grains. Minor abundance of rounded grains, of typically larger size and with a “frosted” surface, indicate subordinate eolian contribution, especially during late lowstand and transgression, which is in line with a more proximal position as inferred for these intervals (Fig. 14). Rounded grains are absent from the clay-rich intervals below the SBs, consistent with a more distal position during high relative sea level. In the following sections we discuss the sequence stratigraphic interpretation with respect to the faunal, microfacies, and geochemical data from TDP 31.

6.2.1. Organic carbon flux, nutrients, and productivity

Despite a generally high abundance of terrestrial organic matter within the sediments of TDP 31, there is indication for enhanced nutrient availability and flux of labile (marine) organic matter during the regressive phases based on increased abundance of infaunal benthic foraminifera, radiolaria, and pyrite (Figs. 5 and 10) and minima in $\delta^{13}\text{C}_{\text{org}}$ (Jiménez Berrocoso et al., 2012) and in $\delta^{13}\text{C}_f$ of benthic and planktic foraminifera (MacLeod et al., 2013; Wendler et al., 2013a; Fig. 6). Some allochthonous contribution to these parameters from shallower and potentially more productive areas (lateral C_{org} flux) is possible, because re-deposition can be expected, especially during lowstands. Sedimentary evidence for reworking (disturbed bedding) exists above SB TuTz1 (at ~101 m) and above SB TuTz3 (at ~45 m, see Appendix 1). Whatever the source, these indicators for enhanced organic matter flux are consistently observed above the four SBs, in both cases supporting the sequence stratigraphic interpretation. Most of the organic carbon obviously was re-mineralized, because TOC is slightly elevated only at the base of the lowstand intervals and then decreases, except in the lowstand above SB TuTz1 where TOC remains elevated, perhaps indicating better preservation of the organic matter in the aftermath of oceanic anoxic event 2 (Fig. 5).

That organic matter flux (vertical and/or lateral) was enhanced during the lowstands is further suggested by the conspicuous peaks in abundance of the benthic foraminifera *T. laciniosa*, especially in the lowstands above SBs TuTz1 and 2, together with a slightly elevated abundance of uniserial benthic species that, similar to *T. laciniosa*, are considered to have lived infaunally (Fig. 5). Increased abundance of *T. laciniosa* was described repeatedly from environments with high organic matter flux and reduced oxygenation (Gustafsson et al., 2003; Holbourn and Kuhnt, 2002; Kuhnt and Wiedmann, 1995; Tronchetti

and Grosheny, 1991). Thus, the peaks in abundance of *T. laciniosa* can be used to indicate periods of enhanced primary production, in settings where organic carbon is not well-preserved. Similar abundance peaks of *T. laciniosa* were described from a Lower to Middle Turonian section in the Northern Calcareous Alps in Austria, and they were related to orbitally-driven productivity cycles (Wendler et al., 2009). The lower amplitude of the *T. laciniosa*-peak above SB TuTz3, and its absence at SB TuTz4, is consistent with the idea of a general shallowing upwards through the stratigraphic section, because this species is typically observed in upper bathyal environments (Arenillas et al., 2000; Sliter and Baker, 1972).

Elevated abundance of biserial planktic foraminifera above SBs TuTz1 and 2, and especially their dramatic increase at SB TuTz4 (Fig. 5; Haynes et al., 2015 and this study), also is consistent with shallowing, increased nutrient availability and/or sediment redistribution during the postulated relative sea-level falls. Biserial planktic foraminifera were repeatedly interpreted as typical for epicontinental seas (Leckie, 1987) and as opportunists in eutrophic environments, based on their distribution patterns and isotopic signature with lower $\delta^{13}\text{C}_f$ values than co-occurring planktic species (Bornemann and Norris, 2007; Haynes et al., 2015; MacLeod et al., 2001; Wendler et al., 2013a). The latter observation indicates disequilibrium carbon-isotope fractionation and possibly incorporation of respiratory CO_2 during fast growth, as is typical for an opportunistic life style (Wendler et al., 2013a). Such a life style also would be consistent with a relatively large temperature tolerance that is indeed indicated from the regionally variable $\delta^{18}\text{O}_f$ patterns of biserial planktic foraminifera, relative to other planktic species (Haynes et al., 2015).

The interval between 26.5–22.7 m above SB TuTz4 is characterized by very high relative and absolute abundance of biserial planktic foraminifera (Haynes et al., 2015 and this study), partly overlapping with an interval of relatively high carbonate content, of 15–20%, between 27.5–23.5 m. In one sample (at 25.72 m), from a light gray, homogenous interval with ~20% carbonate (Appendix 1B), biserial planktic foraminifera make up almost the entire residue, and their absolute abundance is an order of magnitude higher than in the other samples of this interval (Fig. 5). The residue of the next higher sample at 24.75 m consists almost entirely of pyrite, followed by a sudden drop in the abundance of biserial planktic foraminifera at 24.52 m. This low abundance suggests dissolution of the calcitic tests in acidic pore waters due to organic matter degradation, as is observed in oceanic regions with high organic carbon fluxes (Wendler et al., 2002a). Similar sudden drops also are observed in the abundance peaks of *T. laciniosa* in the lowstands above SBs TuTz1 and 2, and one of these drops (at 101.54 m) also coincides with very high abundance of pyrite and radiolaria and a decrease in calcitic benthic foraminifera.

The high abundance of biserial planktic foraminifera above SB TuTz4 (Haynes et al., 2015 and this study) certainly contributes significantly to the elevated carbonate content in this interval. A rise in carbonate content also is observed above the other three SBs (Fig. 3), either reflecting elevated productivity of carbonate producing organisms and/or redeposition of relatively carbonate-rich shallow-water sediments. Similar fluctuations might have occurred at the higher-order depositional sequences, as indicated from their relation to higher frequency variability in carbonate content through the section.

The relative abundance of biserial planktic foraminifera remains high in the upper 27 m (Haynes et al., 2015 and this study), suggesting continuously high nutrient levels and/or shallower water depth. Alternatively, a constant lateral surface–water influx from shallower areas may be considered. However, the increased abundance of infaunal uniserial benthic foraminifera across this interval (Fig. 5) also points to elevated nutrient availability. A possible nutrient source could be high fluvial influx, as supported by abundant quartz in the upper 27 m of the section. Enhanced fluvial influx also seems possible for the lowstands above the other three SBs, as explained in the following section.

6.2.2. Stable-isotope data and vertical isotope gradients

The observed long-term up-section decrease in planktic–benthic $\delta^{18}\text{O}_f$ gradients is consistent with rising bottom-water temperatures, due to a general shallowing through the section. However, this argument cannot explain the short-term rises in the $\delta^{18}\text{O}_f$ gradients across the lowstands (Fig. 8). Instead, this pattern either reflects stronger warming of surface, compared to bottom, waters and/or elevated freshwater influx, whereby salinities did not drop below the tolerance level of planktic foraminifera. Both effects would be consistent with the minima in $\delta^{18}\text{O}_f$ of benthic and planktic foraminifera above the SBs (Fig. 7). The decrease in $\delta^{18}\text{O}_f$ values of the planktic species might be caused by decreased surface-water salinity and/or warming of the surface waters, whereas the lower $\delta^{18}\text{O}_f$ values of the benthic species most likely reflect warmer bottom waters during shallower sea level.

It is interesting to note that the $\delta^{18}\text{O}_f$ minima occurred slightly later for planktic, compared to benthic species, perhaps initially reflecting surface-water warming and later the combined effect of warming and a minor surface-water salinity decrease that would not affect the benthic fauna. Enhancement of surface-water stratification during the lowstands also is suggested by rising surface–thermocline $\delta^{18}\text{O}_f$ and $\delta^{13}\text{C}_f$ gradients above the SBs (Fig. 8). The observed $\delta^{18}\text{O}_f$ minima in benthic and planktic foraminifera, that indicate warming during the lowstands, argue against the contentious hypothesis of glacio-eustatic forcing of eustatic sea-level changes during the Turonian. Instead, the observations are consistent with the hypothesis of aquifer-eustasy (Hay and Leslie, 1990; Wagreich et al., 2014; Wendler et al., 2011c; Wendler et al., 2014, 2016) and with enhanced hydrological cycling during regressions (i.e. warmer temperatures, more seawater evaporation, and both increased fluvial runoff and filling of surface and subsurface aquifers).

The largest drop in benthic species $\delta^{18}\text{O}_f$ values occurs above SB TuTz3 (Fig. 7), where a shift from the upper slope to the outer shelf is proposed. Consistent with significant shallowing at this interval, enhanced stratification in the upper water layers and bottom-water warming are indicated by a rising surface–thermocline $\delta^{18}\text{O}_f$ gradient and a decreasing thermocline–bottom $\delta^{18}\text{O}_f$ gradient, respectively (Fig. 8). The surface–bottom $\delta^{18}\text{O}_f$ gradient above SB TuTz3 might reflect a combination of both processes, first dominated by increasing stratification at the surface and later by the decreasing surface–bottom temperature contrast as the regression proceeded.

Seawater $\delta^{13}\text{C}_{\text{DIC}}$ (DIC = dissolved inorganic carbon) values typically decrease from the surface to the sea floor due to ^{12}C -depletion in surface waters during primary production and ^{12}C -release at the sea floor during organic matter re-mineralization, whereby increased primary production leads to stronger vertical $\delta^{13}\text{C}_{\text{DIC}}$ gradients in the water column. This mechanism can explain the elevated planktic–benthic $\delta^{13}\text{C}_f$ gradients in the lowstand above SB TuTz1, for which elevated organic matter flux is indicated. However, the latter also is true for the lowstands above SB TuTz2 and 3, seemingly inconsistent with the planktic–benthic $\delta^{13}\text{C}_f$ gradients that show a minimum above SB TuTz2 and a strong decrease above SB TuTz3 (Fig. 8). Similarly, the bulk $\delta^{13}\text{C}_{\text{org}}$ values (Jiménez Berrocoso et al., 2012) and $\delta^{13}\text{C}_f$ values of both benthic and planktic foraminifera (MacLeod et al., 2013; Wendler et al., 2013a) decrease strongly above SB TuTz3 (Fig. 7). If enhanced primary production or lateral influx of C_{org} (as indicated from higher abundance of radiolaria and pyrite between 42–45 m) would be the only factors that influenced the $\delta^{13}\text{C}$ values of foraminifera and bulk organic matter, the drop in $\delta^{13}\text{C}$ values should be expressed only in the benthic fauna. The decrease in $\delta^{13}\text{C}_f$ of benthic and planktic foraminifera and in the planktic–benthic $\delta^{13}\text{C}_f$ gradients can be explained with ^{12}C -enrichment of surface waters caused by enhanced re-mineralization of organic material from exposed shelf areas during lower sea level. The low carbon-isotope ratios of the re-mineralized marine and terrestrial organic matter must have lowered the $\delta^{13}\text{C}_{\text{DIC}}$ in both surface and

bottom waters. Additionally, enhanced fluvial influx (low $\delta^{13}\text{C}_{\text{DIC}}$) of re-mineralized terrestrial organic matter (with typically low $\delta^{13}\text{C}_{\text{org}}$ values) might have added to the ^{12}C -enrichment of surface waters and lowered the surface to bottom $\delta^{13}\text{C}_{\text{DIC}}$ gradients. Elevated abundance of wood fragments especially above SB TuTz3 appears to support this hypothesis (Fig. 10).

The very low bulk carbonate $\delta^{13}\text{C}_{\text{carb}}$ values above SBs TuTz3 and 4 might also be influenced by enhanced fluvial influx of terrestrial carbon (supplying ^{12}C to DIC when re-mineralized), but the extremely low values from some samples indicate an additional contribution from diagenesis. The low carbonate content of the sediments provides little buffer capacity for pore fluids during organic matter degradation, enhancing the effects of early diagenesis. It has been suggested that the $\delta^{13}\text{C}_{\text{carb}}$ values should not be considered reliable if the ratio $\text{C}_{\text{carb}}/\text{C}_{\text{org}}$ is below 7:1 (Saltzman and Thomas, 2012; Scholle and Arthur, 1980). About 70% of the samples with a $\text{C}_{\text{carb}}/\text{C}_{\text{org}}$ ratio <7 have very low $\delta^{13}\text{C}_{\text{carb}}$ values. Some bulk $\delta^{13}\text{C}_{\text{carb}}$ values also may be influenced by cement-filled micro-veins (late diagenesis). The potential significance of tar fragments for the bulk $\delta^{13}\text{C}$ signal remains unclear. If there was any influence, it seems it cannot be the sole reason for the very low bulk $\delta^{13}\text{C}_{\text{carb}}$ values above SBs TuTz3 and 4, because tar fragments are abundant throughout the lower part of the section and absent from the interval above SB TuTz4, where the upper $\delta^{13}\text{C}_{\text{carb}}$ minimum occurs.

6.2.3. Faunal shifts and considerations on taphonomy and preservation

The interval below SB TuTz3 is characterized by a very consistent faunal composition of benthic and planktic foraminifera, with the only exception being the two lowstand intervals with abundance peaks of *T. laciniosa* (this study) and slightly increased abundance of biserial planktic foraminifera (Fig. 5; Haynes et al., 2015 and this study). This observation is consistent with a minor effect of regressive phases on the benthic fauna that can be expected for water depths >200 m at the upper slope, as is inferred for the interval below SB TuTz3. The interval above this SB is thought to represent shallower water depth, probably around 200 m, and contains two dramatic shifts in benthic and planktic faunas that are associated with SBs TuTz3 and 4. Comparison of these two shifts shows that they are quite different (Table 2).

The lower faunal turnover is part of a succession of events that follow above the base of the coarser interval at SB TuTz3:

- 1) at ~ 52 m the beginning of the strong up core decrease in $\delta^{13}\text{C}_f$ values of benthic and planktic foraminifera,
- 2) between 50–45 m a $\delta^{13}\text{C}_{\text{org}}$ minimum,
- 3) at ~ 48 m a first shift in sediment color and lightness,
- 4) at ~ 45 m an increase in quartz content,
- 5) at ~ 45 m a strong drop in bulk carbonate $\delta^{13}\text{C}_{\text{carb}}$ and $\delta^{18}\text{O}_{\text{carb}}$,
- 6) at ~ 45 m an increase in abundance of heavy minerals,
- 7) at ~ 46 –44 m a faunal turnover in benthic foraminifera,
- 8) at ~ 45 –42 m peak abundance of ostracods and gastropods,
- 9) ~ 45 –39 m peak abundance of pyrite and radiolaria,
- 10) at ~ 45 m beginning of microscopic evidence of feldspar,
- 11) at ~ 45 m last occurrence of nacre fragments,
- 12) at ~ 44 m a drop in TOC and carbonate,
- 13) at ~ 43 m a second shift in sediment color and lightness (including an iron-stained interval between 42.8–43.8 m, Appendix 1C),
- 14) at ~ 43 m a faunal turnover in planktic foraminifera,
- 15) at ~ 43 m a drop in surface–bottom $\delta^{13}\text{C}_f$ gradients,
- 16) at ~ 43 m elevated abundance of glauconite,
- 17) at ~ 42 m another increase in grain size,
- 18) at ~ 42 m last occurrence of scaphopods,
- 19) ~ 42 –39 m peak abundance of bivalve fragments,
- 20) at ~ 39 m drop in abundance of tar fragments.

The distribution of these changes across more than 10 m thickness of the section, and especially the notable difference of ~ 2 m between the faunal turnover in benthic and planktic foraminifera, indicate that, despite the strong changes in the foraminiferal

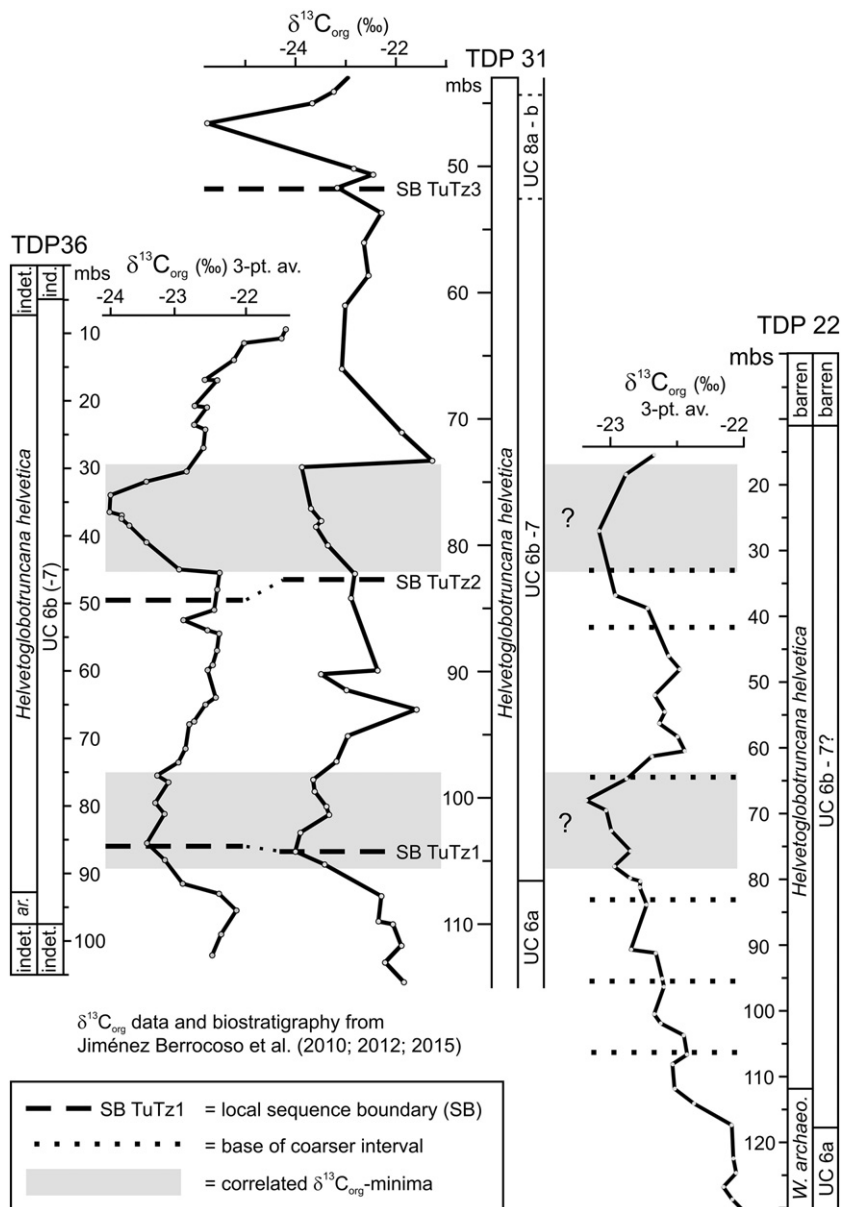


Fig. 15. Regional comparison of bulk $\delta^{13}\text{C}_{\text{org}}$ records from three drill sites in Tanzania. Shaded intervals mark correlated bulk $\delta^{13}\text{C}_{\text{org}}$ minima. Correlations with TDP 22 are uncertain (see supplementary materials S5).

assemblages, the event was gradual and is probably fully reflected in the sedimentary record without occurrence of a major hiatus. This assumption also is reflected in the benthic turnover itself that occurs somewhat gradually across several samples. While some benthic species show an abrupt drop, or increase, in their abundance, the transition is more gradual for other species. The turnover in the planktic species is more abrupt and coincides with the last occurrence of *H. helvetica* (Huber and Petrizzo, 2014). Some condensation of the sedimentary record might be indicated from the slightly elevated abundance of glauconite at ~43 m, although this could have been re-deposited from shallower areas.

The upper faunal turnover above SB TuTz4 is very abrupt, occurring between two samples at 28.11 m and 27.30 m. Here, the turnovers in benthic and planktic species occur together and coincide with: 1) a strong increase in % sand fraction, 2) the final shift towards benthic species of assemblage B, 3) a dramatic increase in absolute and relative abundance of biserial planktic foraminifera (Haynes et al., 2015 and

this study), 4) the base of a more continuous occurrence of juvenile ammonites, and 5) the base of the interval with 100% cement-filled foraminiferal tests. Additional changes at SB TuTz4, including minima in bulk $\delta^{13}\text{C}_{\text{org}}$ and $\delta^{13}\text{C}_{\text{carb}}$, are similar to the other SBs, as summarized in Table 2. The abruptness and co-occurrence in the benthic and planktic faunal turnovers indicate that this interval is condensed and may contain a hiatus between the base of core 18 and the top of core 19 (27.95–28.00 m; Appendix 1B).

According to the lower relative sea level and elevated C_{org} flux that are inferred for the interval above SB TuTz3, the benthic foraminiferal species of assemblage B apparently indicate shallower and/or nutrient-richer environments than species of assemblage A. This can explain the slightly elevated abundance of assemblage B species during the lowstands above SBs TuTz1 and 2 (Fig. 5), for which similar conditions are indicated. The same interpretation also applies for the somewhat elevated abundance of biserial planktic foraminifera within these intervals (Haynes et al., 2015 and this study). As

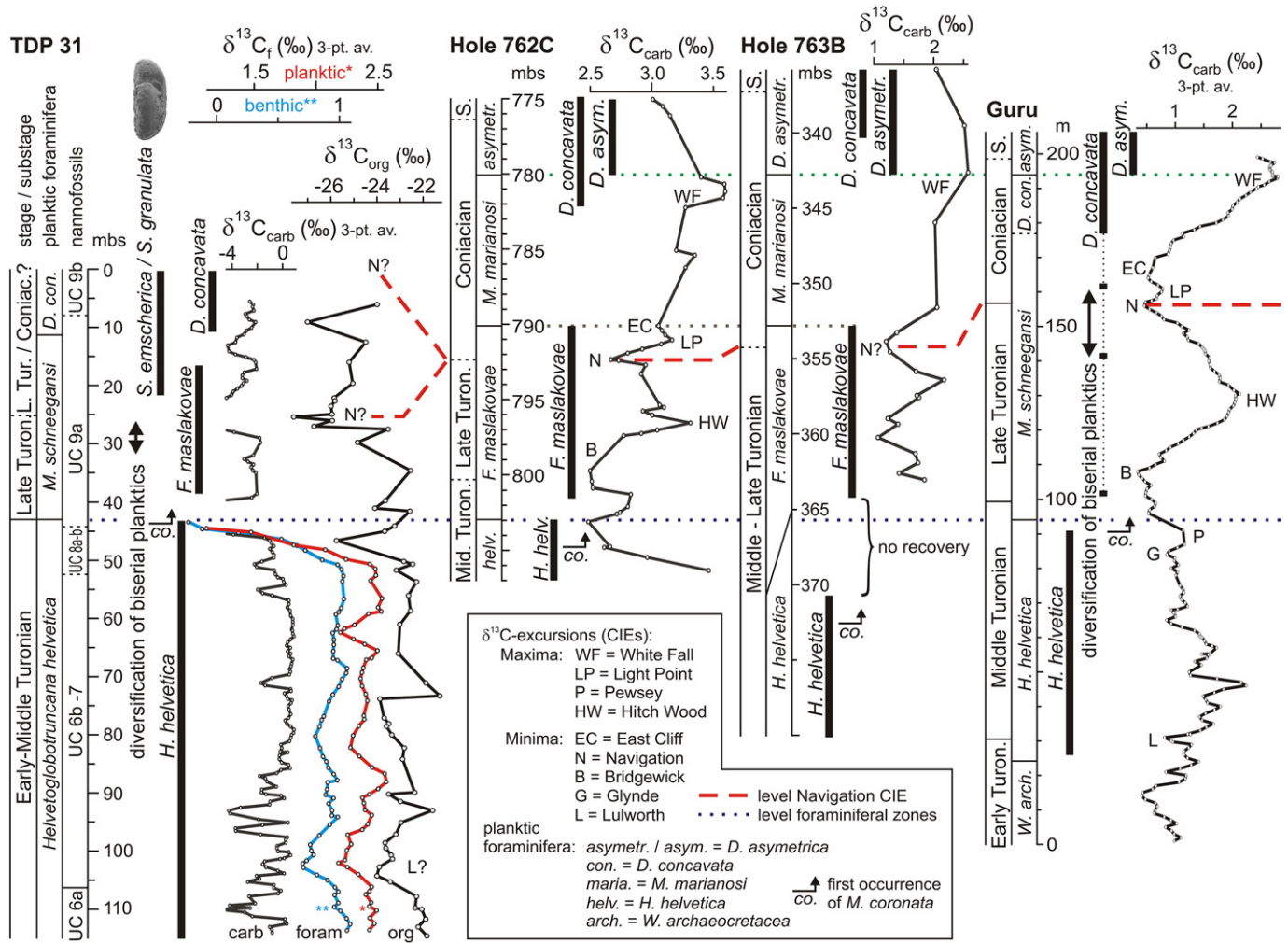


Fig. 16. Comparison of $\delta^{13}\text{C}$ records and foraminiferal ranges in four sections from the southern Tethys (for location see Fig. 1). The bulk $\delta^{13}\text{C}_{\text{carb}}$ curve for TDP 31 combines data from Jiménez Berrocoso et al. (2012) and this study (see Fig. 4); bulk $\delta^{13}\text{C}_{\text{org}}$ data for TDP 31 are from Jiménez Berrocoso et al. (2012); foraminiferal $\delta^{13}\text{C}_f$ data for TDP 31 are from MacLeod et al. (2013) and Wendler et al. (2013a); red*: *H. helvetica* Group, blue**: *B. berthelini* Group; bulk $\delta^{13}\text{C}_{\text{carb}}$ data for Guru (Tibet) from Wendler et al. (2011b). Biostatigraphy and planktic foraminiferal ranges for TDP 31 from Jiménez Berrocoso et al. (2012) and Huber and Petrizzi (2014), for Holes 762C and 783B (Exmouth Plateau, Australia) from Petrizzi (2000, 2002) and for Guru from Wendler et al. (2011b). Records are aligned along planktic foraminiferal zones (dotted lines). Correlated level of the Navigation CIE is marked with a dashed line, showing two alternative interpretations for TDP 31, either consistent with benthic and planktic foraminifera (lower position) or with nannofossils (higher position). Note position of the $\delta^{13}\text{C}_{\text{carb}}$ minimum of the Navigation CIE in the upper part of the range of *F. maslakovae* in Holes 762C and 763B and similar position of a bulk $\delta^{13}\text{C}_{\text{org}}$ minimum in TDP 31. An interval of diversification of biserial planktic foraminifera occurs just below this minimum in TDP 31 (after Haynes et al., 2015) and at a comparable stratigraphic interval in Guru (Wendler et al., 2011b).

mentioned above, both groups could also have been re-deposited from shallower areas, because enhanced down-slope transport of sediments can be expected at the upper slope during regressions. Some indication for re-deposition in the lowstands above SBs TuTz1 and 3 can be seen in the core photographs that show mottling and disturbed bedding at 100.5–101.5 m and at 44–46 m (Appendix 1C).

Accordingly, the elevated abundance of cement-filled foraminifera in the lowstand sediments above SBs TuTz1 and 2 merits further consideration. Cemented foraminiferal tests are absent from most samples below 27 m, and, where present, only a few specimens were observed. In some samples from the lowstand deposits, however, cemented tests are common to frequent (Fig. 5). It is interesting to note that specimens from assemblage B species are preferably cemented. This selective cementation cannot be explained by late-diagenetic cementation due to enhanced pore water flow in these slightly coarser sediments. Instead, it suggests early diagenetic cementation in presumably shallower water depth and re-deposition of the cement-filled specimens. This

does not exclude the possibility that, during regression, the preferred (shallower/nutrient-richer) habitat of assemblage B species may have expanded into the depositional setting of TDP 31. The relative contribution of primary (productivity) and secondary (taphonomic) signals is difficult to assess, but both point to a regression in support of the interpreted SBs. Unlike in the upper 27 m of the section, where all foraminiferal tests are cemented, some of the specimens of assemblage B in the lowstand deposits above SBs TuTz1 and 2 are well-preserved and not cemented, which excludes the possibility of down-hole contamination during coring of TDP 31.

For the upper 27 m of section TDP 31 it is not clear whether the strong cementation is of late-diagenetic origin, caused by groundwater flow in the coarser-grained and more porous sediments that are close to the modern surface, or if the cement was formed syndepositionally during the Cretaceous, or by a combination of the two. Similarly, the decreasing TOC contents towards the top of the section (Fig. 5) might reflect a combination of: (a) organic matter degradation due to late-diagenetic oxidative processes that increase towards the

present exposure surface and (b) increased oxygen exposure times for the sediments during the Cretaceous, caused by reduced accommodation space and lower sedimentation rates during the late lowstands. The latter process would explain the stepwise decrease in TOC at SBs TuTz3 and 4 and the TOC drop at SB TuTz2, despite indication for enhanced C_{org} flux. The changes in sediment color at SBs TuTz3 and 4 (Fig. 3, Appendix 1) also reflect the sedimentological changes at these SBs, i.e. a decrease in mica and TOC (that are darker), an increase in quartz content (lighter), and the higher oxidative state of iron minerals (greenish hues).

With respect to microfossil preservation, it is interesting to note that, despite a generally stable mineralogical composition throughout TDP 31, a change in presence of kaolinite can be observed, this clay mineral mostly being present below ~40 m and largely absent above this level (Figs. 14 and S1). Burial experiments have shown that secular changes in average clay mineralogy, particularly the kaolinite content, may have been significant factors for the opening and closing of the taphonomic window for exceptional preservation of Burgess Shale type carbonaceous fossils (Wilson and Butterfield, 2014). By analogy, clay mineralogy also may be important for calcareous microfossil preservation. For example, prevention of decomposition of the organic membrane of calcareous dinoflagellate cysts is probably critical to yield excellent preservation of these fossils. The absence of kaolinite above ~40 m might, in fact, be related to the higher abundance of cemented microfossils above ~40 m (Fig. 5) and a change from the glassy to "frosty" appearance of foraminifera shells above ~34 m. The main change in preservation, to complete cementation of the tests above ~27 m, does however seem to reflect predominantly early and/or late diagenetic cementation in relation to grain size and surface weathering processes as discussed above.

6.3. Regional comparison

There is no obvious similarity in the grain-size records of TDP 22, TDP 31, and TDP 36, from which the three sections could be correlated lithologically. The base of the *H. helvetica* Zone has been identified in TDP 22 and TDP 36, but the position of this boundary is less certain than the top of the zone, because the species is very rare at the base of its range (Huber and Petrizzo, 2014). In TDP 31, the base of the *H. helvetica* Zone was originally placed at 106.52 m (Jiménez Berrocoso et al., 2012), but the range of *H. helvetica* was later extended to the base of the section when rare specimens of the species were found down to the lowest sample (Huber and Petrizzo, 2014; MacLeod et al., 2013). Because the species is very rare in the lower 10 m of TDP 31, the base of the section can be assumed to be close to the base of the *H. helvetica* Zone, although the latter cannot be determined exactly. The top of the *H. helvetica* Zone was recovered only in TDP 31; therefore, the upper 43 m of TDP 31 cannot be compared to the other two Tanzanian sections.

Carbon-isotope stratigraphy is difficult in the studied sections because of the low carbonate content in the sediments and the low and variable bulk sediment $\delta^{13}C_{carb}$ values. The bulk $\delta^{13}C_{org}$ signal might be influenced by variable terrestrial organic matter supply, and it is not clear whether such a regional influence was stronger than the global component of the oceanic seawater DIC carbon-isotope signal. However, for regional correlation purposes the bulk $\delta^{13}C_{org}$ records of the three sites might be useful. There are two obvious bulk $\delta^{13}C_{org}$ minima evident in all three records (Jiménez Berrocoso et al., 2010, 2012, 2015) that potentially represent isochronous intervals (Fig. 15; cf. Haynes, 2012). In TDP 31 these minima occur in the lower and middle part of the *H. helvetica* Zone. In TDP 36 the lower bulk $\delta^{13}C_{org}$ minimum also is a few meters above the base of the *H. helvetica* Zone. The correlation of these two $\delta^{13}C_{org}$ minima between TDP 36 and TDP 31 seems to be supported by the similar position of the bases of two coarser intervals (potential SBs) relative to the interval of low bulk $\delta^{13}C_{org}$ values in both sections: the first (SB TuTz1 in TDP 31) at the base of the $\delta^{13}C_{org}$

minimum and the second (SB TuTz2 in TDP 31) slightly below the $\delta^{13}C_{org}$ minimum. These drill sites are less than two km apart, and similarity in their bulk $\delta^{13}C_{org}$ records is very likely.

The distance between site TDP 22 and the other two drill sites is slightly more than 5 km, and correlation of the bulk $\delta^{13}C_{org}$ minima is less certain, because a consistent pattern between grain-size data and isotopic signature is not obvious from this record (details are discussed in S5). Stratigraphic age assignment is further limited by absence of a second zonal boundary higher in the section. The differences observed between TDP 31 and TDP 22 could be related to water depth and associated sedimentary processes, i.e. local currents/sediment redistribution and completeness of the records.

The bulk $\delta^{13}C_{org}$ correlations in Fig. 15 indicate lower sedimentation rates and a deeper setting for TDP 31 than for the two other Tanzanian sections, consistent with the finer grain size in TDP 31. A shallower palaeo-water depth at TDP 22 compared to TDP 31 also is suggested by the comparison of isotope data from benthic and planktic foraminifera between the two sections. The magnitude in $\delta^{18}O_f$ shifts of the planktic foraminiferal groups is similar in both sections (Figs. 7 and S4), but the $\delta^{18}O_f$ shifts of the benthic groups are larger in TDP 22 than in TDP 31 (MacLeod et al., 2013; Wendler et al., 2013a), as would be expected from a shallower and less stable bottom-water environment at TDP 22. Furthermore, on average the absolute $\delta^{18}O_f$ values of the planktic and benthic groups are lower in TDP 22 than in TDP 31 (MacLeod et al., 2013), indicating higher seawater palaeotemperatures and thus a shallower setting for TDP 22. Because sediment reworking is more likely enhanced in shallower water depths, the sedimentary record of TDP 22 is possibly less complete than that of TDP 31, which might also explain the sedimentary differences between these two sites.

6.4. TDP 31 – A south Tethys comparison

Similar to correlations on a regional scale, the comparison of the sequence stratigraphic model for TDP 31 with sequence stratigraphic frameworks elsewhere cannot be based on the TDP 31 bulk sediment $\delta^{13}C_{carb}$ data. Nevertheless, the position of the local SBs, relative to the ranges of stratigraphically important planktic foraminiferal species and trends in $\delta^{13}C_f$, can give some clues for a potential correlation. The faunal turnover in planktic foraminifera related to SB TuTz3 in TDP 31 co-occurs with the last occurrence of *H. helvetica* (Huber and Petrizzo, 2014). It is possible that this level coincides with a change in oceanic circulation patterns during the transition from an upper slope to an outer shelf position at TDP 31. However, the apparently synchronous (at least Tethys Ocean wide) extinction of *H. helvetica* in conjunction with a major drop in $\delta^{13}C_{carb}$ on a global scale (Wendler, 2013), suggests that the changes in oceanographic conditions at SB TuTz3 in TDP 31 are not purely local phenomena, but may have a significant eustatic component, involving a eustatic sea-level drop and changes in the global carbon budget.

Isotope records and planktic foraminiferal ranges for four sections from the southern Tethys are compared in Fig. 16. While from the same oceanic province, between ~35°S–47°S in the southern Tethys, these sections represent marine sedimentation on three different tectonic plates: ODP Holes 762C and 763B from the Exmouth Plateau on the Australian Plate, the Guru section in southern Tibet on the Plate of Greater India, and TDP 31 in Tanzania on the African Plate. Three of these $\delta^{13}C$ records cover the top of the *H. helvetica* Zone and consistently display low $\delta^{13}C$ values in the top of the zone. In TDP 31, this minimum is reflected in the $\delta^{13}C_f$ data from glassy planktic and benthic foraminifera (MacLeod et al., 2013; Wendler et al., 2013a) and perhaps also in the bulk $\delta^{13}C_{org}$ record (Jiménez Berrocoso et al., 2012). This minimum coincides with an interval of very low $\delta^{13}C_{carb}$ values that appear to be diagenetically altered, likely in relation to the SB.

Following an interval of high $\delta^{13}C_{carb}$ values in the Upper Turonian (Hitch Wood Carbon Isotope Excursion – CIE), another $\delta^{13}C_{carb}$

Table 3

Summary of ages and references for carbon isotope excursions (CIEs) and stratigraphic levels near the local SBs in TDP 31. Ages marked in bold were used for calculating average sedimentation rates within TDP 31 (see section 6.5.); *uncertainty from Turonian/Coniacian boundary age (Sageman et al. 2014); **refers to CIEs, not to *H. helvetica* Zone in Eldrett et al. (2015a) because of their uncommon definition of the zone (first occurrence of *M. renzi* to last occurrence of *P. gibba*).

Local SB	Assumptions for age model in TDP 31 (see Section 6.5.)	$\delta^{13}\text{C}$ minimum above SB	Stratigraphic level	Reference	Age (Ma)	Uncertainty (Ma)	Reference	Anchored to absolute age	Reference
TuTz4	(A) The $\delta^{13}\text{C}_{\text{org}}$ minimum at 25.4 m is the Navigation CIE (consistent with foraminifera).	Navigation CIE?	Turonian /Coniacian boundary	Jarvis et al. (2006); Walaszczyk et al. (2010); Wendler (2013)	89.75	± 0.38	Sageman et al. (2014); Laurin et al. (2015) based on Wendler et al. (2014) and Laurin et al. (2015)	base Turonian (93.9 Ma ± 0.15)	Meyers et al. (2012)
					89.60	± 0.15			
TuTz3	(B) The $\delta^{13}\text{C}_{\text{org}}$ minimum at 25.4 m is in the Late Turonian (consistent with nannofossils).	$\delta^{13}\text{C}$ minimum below Hitch Wood 2 CIE? Bridgewick CIE?	regression in TUR 6 in Bch-1 core (Bohemian Basin) early Late Turonian	Uličný et al. (2014) Jarvis et al. (2006)	-90.6	n.d. (± 0.38)*	Uličný et al. (2014)	base Coniacian (89.75 Ma ± 0.38)	Sageman et al. (2014)
					91.11	± 0.14 (± 0.38)*	Laurin et al. (2015)	base Coniacian	Sageman et al. (2014)
TuTz1	The top <i>H. helvetica</i> Zone at 42.88 m is between the Pewsey and the Lower Southerham CIEs. The top <i>H. helvetica</i> Zone at 42.88 m is in the uppermost <i>C. woollgari</i> Zone. The minimum in $\delta^{13}\text{C}_{\text{f}}$ and $\delta^{13}\text{C}_{\text{org}}$ between 38–50 m is the interval of low $\delta^{13}\text{C}$ between the Pewsey and the Bridgewick CIEs (including the Middle / Late Turonian boundary). The $\delta^{13}\text{C}_{\text{org}}$ minimum at 104.25 m is the Lulworth CIE.	local signal? just after Pewsey CIE	between Pewsey and Lower Southerham CIEs	Wendler (2013)	-	-	-	-	-
					-91.7**	± 0.15	Eldrett et al. (2015a)	base Turonian (94.1 Ma ± 0.13)	Eldrett et al. (2015a)
		just after Pewsey CIE between Pewsey and Bridgewick CIEs	top <i>C. woollgari</i> Zone \approx base Late Turonian Bridgewick CIE Lower Southerham CIE Pewsey CIE	Jarvis et al. (2006); Wendler (2013)	-91.5	n.d. (± 0.38)*	Uličný et al. (2014)	base Coniacian	Sageman et al. (2014)
					91.31	± 0.07 (± 0.38)*	Laurin et al. (2014)	base Coniacan	Sageman et al. (2014)
					91.11	± 0.14 (± 0.38)*	Laurin et al. (2015)	base Coniacian	Sageman et al. (2014)
		top Lulworth CIE base Lulworth CIE	base <i>C. woollgari</i> Zone = base Middle Turonian late Early Turonian	Wendler (2013); Wendler et al. (2014); Wilmsen et al. (2014); Haq (2014) Jarvis et al. (2006); Wendler (2013); Uličný et al. (2014)	92.90	n.d.	Ogg et al. (2012)	not indicated	Meyers et al. (2012)
					92.90	± 0.15	Wendler et al. (2014)	base Turonian	Meyers et al. (2012)
		Lulworth CIE			93.10	± 0.15	Sageman et al. (2006); Wilmsen et al. (2014)	base Turonian	
					93.20	± 0.15	Wendler et al. (2014)	base Turonian (93.9 Ma ± 0.15)	Meyers et al. (2012)
					-93.3	± 0.13	Eldrett et al. (2015b)	base Turonian (94.1 Ma ± 0.13)	Eldrett et al. (2015b)
					-92.9	n.d. (± 0.38)*	Uličný et al. (2014)	base Coniacan	Sageman et al. (2014)

minimum is found in the sections from the Exmouth Plateau and Tibet, marking the Turonian/Coniacian boundary (Navigation CIE, Fig. 16). This boundary is difficult to define for TDP 31 because of inconsistent stratigraphic indication from nannofossils versus planktic foraminifera (Huber and Petrizzo, 2014; Jiménez Berrocoso et al., 2012) and benthic foraminifera (this study). In Tibet, an interval of diversification in biserial planktic foraminifera was recorded just below the Navigation CIE (Wendler et al., 2011b). A similar interval of diversification of biserial planktic foraminifera was observed below SB TuTz4 in TDP 31 (cf. Haynes et al., 2015), overlain by a distinct minimum in bulk $\delta^{13}\text{C}_{\text{org}}$ (Jiménez Berrocoso et al., 2012), again co-incident with very low, diagenetically altered, bulk sediment $\delta^{13}\text{C}_{\text{carb}}$ values above the SB. This $\delta^{13}\text{C}_{\text{org}}$ minimum might correspond to the Navigation CIE. Unfortunately, this interpretation cannot be tested with $\delta^{13}\text{C}_f$ data, because all foraminiferal tests are cement-filled in the upper 27 m of TDP 31.

Additional evidence for interpreting this bulk $\delta^{13}\text{C}_{\text{org}}$ minimum in TDP 31 as the Navigation CIE comes from its position in the upper part of the range of *Falsotruncana maslakovae* and the respective position of a $\delta^{13}\text{C}_{\text{carb}}$ minimum in Holes 762C and 763B, based on the ranges of planktic foraminifera from Huber and Petrizzo (2014) and Petrizzo (2000, 2002), respectively. *Falsotruncana maslakovae* has a relatively short stratigraphic range, and its extinction in the southern Tethys was observed close to the first occurrence of the nannofossil *Micula staurophora* (= *Micula decussata*) in the lower Middle Coniacian (Petrizzo, 2003). *Micula staurophora* was not observed in TDP 31, and the nannofossils indicate a Late Turonian age for the top of the section (Jiménez Berrocoso et al., 2012), in which case the Navigation CIE would lie above the TDP 31 stratigraphic section top. On the other hand, typical Coniacian benthic foraminiferal species of *Stensioeina* (*S. emscherica* and *S. granulata*) are abundant in the upper 22 m within TDP 31. The first occurrence of *S. emscherica* was during the Early Coniacian (Walaszczuk et al., 2013). *Stensioeina granulata* is thought to first occur during the Middle Coniacian (base *Volviceramus koeneni* Zone; Bailey, 1978; Dubicka and Peryt, 2014; Koch, 1977; Niebuhr et al., 1999), although Walaszczuk et al. (2004) reported *S. granulata* also from the Early Coniacian. The occurrence of these species in TDP 31 suggests a Coniacian age for the upper 22 m of the section, consistent with the age indicated from *F. maslakovae* and with the interpreted position of the Navigation CIE that suggests the position of the Turonian/Coniacian boundary near 25 m.

Above the two carbon-isotope minima of the Navigation and East Cliff CIEs there is a rise in $\delta^{13}\text{C}_{\text{carb}}$ towards high values between the White Fall and Kingsdown CIEs in the Upper Coniacian (Jarvis et al., 2006). The first occurrence of *Dicarinella asymmetrica* lies at this interval of high $\delta^{13}\text{C}_{\text{carb}}$ values in the sections from Tibet and from the Exmouth Plateau (Fig. 16), and it appears to be a globally synchronous event relative to $\delta^{13}\text{C}_{\text{carb}}$ stratigraphy (Wendler, 2013). The Coniacian/Santonian boundary for Holes 763B and 762C was positioned below the *D. asymmetrica* Zone in Petrizzo (2000), but the boundary should now be placed higher, because the species first occurs during the Late Coniacian, according to the current definition for the base Santonian (Lamolda et al., 2014). A more precise placement of the boundary based on $\delta^{13}\text{C}_{\text{carb}}$ stratigraphy currently is not possible because of the low resolution of the $\delta^{13}\text{C}_{\text{carb}}$ record throughout this stratigraphic interval. The section top of TDP 31 lies stratigraphically below the first occurrence of *D. asymmetrica* and above the first occurrence of *Dicarinella concavata* (Jiménez Berrocoso et al., 2012). The first occurrence of the latter species has been shown to be diachronous between the early Late Turonian and the Middle Coniacian (Wendler, 2013). Therefore, the first occurrence of *D. concavata* in TDP 31 would be consistent with both a Late Turonian (nannofossils) and a Coniacian (benthic foraminifera) age for the upper 27 m of the section.

The base of TDP 31 can be assumed to be close to the base of the *H. helvetica* Zone, based on the rarity of the species at this level (Huber and Petrizzo, 2014). There is evidence for diachroneity of the first occurrence of *H. helvetica* (Caron et al., 2006; Huber and

Petrizzo, 2014; Ifrim and Stinnesbeck, 2008), which is caused by several factors that include rarity of the species at the base of its range and differences in taxonomic concepts among workers with respect to the gradual evolution of *H. helvetica* from *Helvetoglobotruncana praehelvetica* (Huber and Petrizzo, 2014). The reported first occurrence of *H. helvetica* might often represent the interval where the species becomes more abundant and can be found easily within a sample, especially when the study is based on thin-sections. Comparison of the first occurrence of *H. helvetica* relative to carbon-isotope stratigraphy in six sections from both hemispheres indicates the base of the *H. helvetica* Zone lies between the Holywell and the Lulworth CIE, in most cases slightly below the latter (Wendler, 2013). Because the base of TDP 31 must be close to the base of the *H. helvetica* Zone, it is likely that the minimum in bulk $\delta^{13}\text{C}_{\text{org}}$ values (Jiménez Berrocoso et al., 2012) and in $\delta^{13}\text{C}_f$ of the benthic and planktic foraminifera (MacLeod et al., 2013; Wendler et al., 2013a) above SB TuTz1 corresponds to the $\delta^{13}\text{C}_{\text{carb}}$ minimum of the Lulworth CIE in the top Lower Turonian (Fig. 16).

6.5. TDP 31 – Age model and accumulation rates

An estimate of time constraint and accumulation rates in TDP 31 can be made based on the position of the top *H. helvetica* Total Range Zone and the interpretation of the $\delta^{13}\text{C}_f$ and $\delta^{13}\text{C}_{\text{org}}$ minima above SBs TuTz1, 3 and 4, provided these bio- and chemostratigraphic events are synchronous and their ages are known. Table 3 summarizes ages from the recent literature for various bio- and chemostratigraphic levels near the SBs.

The last occurrence of *H. helvetica* is marked by an abrupt drop from high abundance to absence of the species (Huber and Petrizzo, 2014). This level appears to be synchronous, at least across the Tethys Ocean (Wendler, 2013), and, in contrast to the first occurrence of the species, generally is thought to represent a good biostratigraphic level for correlation. Because *H. helvetica* typically is absent or rare in epicontinental and shallow-water sections that are dated with macrofossils, correlation between the *H. helvetica* Zone and macrofossil zonations remains uncertain. This uncertainty in correlation also results in uncertainty about the absolute age of the last occurrence of *H. helvetica* and, accordingly, about the duration of the *H. helvetica* Zone. The current ages assigned to the base and top of the zone in the Geological Time Scale (GTS) 2012 (Ogg et al., 2012) are 93.52 Ma and 92.99 Ma, respectively, resulting in a zonal duration of 0.53 myr. In earlier biostratigraphic schemes (Hardenbol et al., 1998) the top of the *H. helvetica* Zone was correlated to the middle *Collignoniceras woollgari* ammonite Zone of northern Europe and the top *C. woollgari* Zone of the Western Interior Seaway, with an age of 92.08 Ma in GTS 2012. The GTS 2004 age for the top *H. helvetica* Zone was 91.5 Ma (Gradstein et al., 2004), and some recent papers (e.g. Frijia et al., 2015; MacLeod et al., 2013) prefer to use the GTS 2004 instead of the GTS 2012 ages.

In TDP 31 the top of the *H. helvetica* Zone is close to the base UC9 nannofossil Zone that has an age of 91.78 Ma in GTS 2012. Based on carbon-isotope stratigraphy, the top of the *H. helvetica* Zone correlates to a level between the Pewsey CIE and the Lower Southerham CIE (Wendler, 2013), a level that occurs in the topmost *C. woollgari* Zone in the English Chalk (Jarvis et al., 2006), with an age of ~90.86 Ma in GTS 2012. The difference between the latter age and the one assigned to the top *H. helvetica* Zone in GTS 2012 is 2.66 myr, which is five times the duration of the zone in GTS 2012. This large magnitude of uncertainty significantly hampers correlation between micro- and macrofossil dated stratigraphic sections, as well as the inter-regional comparison of sequence boundaries and reconstructed relative sea-level shifts, if different biostratigraphic schemes are used.

An increasingly applied method to overcome these uncertainties in ages of biostratigraphic zones is the combination of bio-, chemo- and astrochronology, radiometric dating, and sequence stratigraphy (e.g. Jarvis et al., 2006; Joo and Sageman, 2014; Laurin et al., 2014,

2015; Meyers et al., 2012; Sageman et al., 2006; Sageman et al., 2014; Uličný et al., 2014; Walaszczyk et al., 2010; Wendler, 2013; Wendler et al., 2014; Wilmsen et al., 2014). The Lower Southerham CIE (just above the top of the *H. helvetica* Zone) has an age between 90.65 Ma and 91.69 Ma (astrochronologically calibrated ages including uncertainties from Joo and Sageman, 2014; Laurin et al., 2015; Wendler et al., 2014; see Table 3) and results in an average duration of 2.35 myr (± 0.52 myr) for the *H. helvetica* Zone, if applying the GTS 2012 age of 93.52 Ma for the base of the zone. This duration is more than four times longer than in the GTS 2012, about three times the minimal duration of 0.75 myr suggested from the range of *H. helvetica* in the Rock Canyon section (Huber and Petrizzo, 2014), and shorter than the maximal duration of 2.66 myr as calculated from the GTS 2012 age of 90.86 Ma for the base *Subproinocyclus neptuni* ammonite Zone that commences shortly above the top *H. helvetica* Zone based on chemostratigraphy (Wendler, 2013). The position of the Pewsey CIE just below the top of the *H. helvetica* Zone suggests an age of ~91.5 Ma for the last occurrence of *H. helvetica* and ~2 myr for the duration of the Zone, based on the new age model for the English Chalk $\delta^{13}\text{C}_{\text{carb}}$ reference curve (Uličný et al., 2014).

A recent astrochronological calibration (combined with U-Pb dating from bentonites) of the Iona-1 core from the Western Interior Seaway (Eldrett et al., 2015a) indicates a similar duration of ~2 myr for the *H. helvetica* Zone, based on their ages for the first occurrence of *H. helvetica* (their F17 bio-event, 93.21 Ma \pm 0.13) and the level just above the positive $\delta^{13}\text{C}$ excursion that they correlate to the Pewsey CIE (~91.7 Ma \pm 0.15). It should be noted that Eldrett et al. (2015a) define their *H. helvetica* Zone from the first occurrence of *Marginotruncana renzi* and *Marginotruncana schneegansi* to the last occurrence of *Praeglobotruncana gibba*, while *H. helvetica* is observed to the top of the Iona-1 core, including ~30 m of section that Eldrett et al. (2015a) interpret to be of Coniacian age. Through this stratigraphic interval *H. helvetica* occurs sporadically, but in several samples and partly with frequent abundance, without indication for reworking (J. Eldrett, personal communication). However, the possibility of allochthonous sediment contribution in the lower part of the Austin Chalk, that in some areas displays an unconformity at its base, also is supported from nannofossil evidence. The last occurrence of the nannofossil *Stoverius achylosus* lies within the Coniacian interval of the Iona-1 core (Eldrett et al., 2015a), much higher than typically observed (in UC9a: Burnett, 1998; Lees, 2008; and in UC7: Corbett et al., 2014). If these fossils were not reworked, this would indicate that the apparently synchronous last occurrence of *H. helvetica* in the Tethys Ocean does not reflect a global extinction event, but that the species survived until the Coniacian outside of the Tethys Ocean. If true, this could explain the unusually high last occurrence of *H. helvetica* within the Upper Turonian (above the level of the Hitch Wood CIE) that was reported from Japan (Takashima et al., 2010). For both cases it should be evaluated carefully whether or not the fossils are reworked. In any case, for the Tethys we assume a synchronous last occurrence of the species with an approximate age of ~91.5 Ma. For TDP 31, this age results in average sedimentation rates of 3.6 cm/kyr between SB TuTz1 (104.25 m, base Lulworth CIE) and the top of the *H. helvetica* Zone (42.88 m, above SB TuTz3; see bold marked ages in Table 3).

Sedimentation rates in the upper ~43 m of TDP 31 depend on interpretation of the bulk $\delta^{13}\text{C}_{\text{org}}$ minimum evident above SB TuTz4. It could represent: (A) the Navigation CIE – as indicated by benthic (and planktic) foraminifera, resulting in a sedimentation rate of at least 1.0 cm/kyr, or more, if a hiatus is present at SB TuTz4, or (B) a level in the Late Turonian, as indicated by nannofossils (Jiménez Berrocoso et al., 2012). A late Turonian negative $\delta^{13}\text{C}$ shift could either be (B1) the $\delta^{13}\text{C}$ minimum below the Hitch Wood 2 peak (Laurin et al., 2014; Uličný et al., 2014), or (B2) the Bridgewick CIE, both representing regressive intervals (Gale, 1996; Uličný et al., 2014). It is also possible that these two levels are amalgamated with a hiatus at

SB TuTz4, so that part of the lower Upper Turonian would be missing. Sedimentation rates within the upper part of TDP 31 for option (B) range between 1.9 cm/kyr (B1) and 4.4 cm/kyr (B2; for ages see Table 3). Alternatively, SB TuTz4 could be unrelated to eustasy and represent a local base-level drop that currently cannot be dated.

If interpretation (A) is correct, the three depositional sequences between the four SBs in TDP 31 have an average duration of ~1 myr. A similar cycle frequency has recently been calculated for a Cenomanian/Turonian $\delta^{13}\text{C}_{\text{carb}}$ record that is related to sea-level change by Wendler et al. (2014) and confirmed by Laurin et al. (2015), who show that this cyclicity is globally synchronous and pervasive throughout the Albian to Campanian.

6.6. TDP 31 – A global comparison

Lowery et al. (2014) report $\delta^{13}\text{C}_{\text{carb}}$ and foraminiferal abundance data for a section from the Western Interior Seaway (Bouldin Creek outcrop, Texas) that are very similar to the observations made at SBs TuTz3 and 4 in TDP 31: two distinct $\delta^{13}\text{C}_{\text{carb}}$ minima, the first in the top of the *H. helvetica* Zone, coinciding with increased abundance of benthic foraminifera and peak abundance of pyrite, and the second in the middle/upper *M. schneegansi* Zone, coinciding with a strong increase in biserial planktic foraminifera. The similarities with TDP 31 could be coincidental, but it is possible that both records reflect similar conditions that were related to eustatic sea-level changes. In the following, we compare the stratigraphic position of the four local SBs TuTz1–4 with stratigraphic positions of base-level falls reported elsewhere and that are thought to reflect a significant eustatic sea-level component.

6.6.1. SB TuTz1 – Uppermost Lower Turonian

The local SB TuTz1 within TDP 31 lies near the base of the *H. helvetica* Zone, somewhat below the Lower/Middle Turonian boundary (see Section 6.4). The overlaying $\delta^{13}\text{C}_{\text{org}}$ and $\delta^{13}\text{C}_f$ minima are thought to represent the Lulworth CIE in the uppermost Lower Turonian. The latter appears to be globally synchronous and is located in the uppermost *Mammites nodosoides* Zone, just below the base of the *C. woollgari* Zone that is commonly used to mark the Lower/Middle Turonian boundary (Jarvis et al., 2006; Joo and Sageman, 2014; Uličný et al., 2014; Wendler, 2013; Wendler et al., 2014; Wilmsen et al., 2014).

A SB is positioned just below the Lulworth CIE in many sections: in the English Chalk (Gale, 1996; Jarvis et al., 2006), in several regions in Germany (Niebuhr et al., 2011, 2014; Richardt and Wilmsen, 2012; Richardt et al., 2013; Wiese, 2009; Wilmsen and Nagm, 2013b; Wilmsen et al., 2014), in the Bohemian Basin (Uličný et al., 2014), in southern Italy (Frijia et al., 2015), in Jordan and Egypt (Bauer et al., 2003; Lüning et al., 1998; Schulze et al., 2003, 2005; Wendler et al., 2010, 2014; Wilmsen and Nagm, 2013a), and in the Western Interior Seaway (Joo and Sageman, 2014; Laurin and Sageman, 2007; Sageman, 1996; Sageman et al., 1997; White and Arthur, 2006). The stratigraphic level of the SBs below the Lulworth CIE in the uppermost *M. nodosoides* Zone and slightly above the base *H. helvetica* Zone appears to be equivalent to KTu2 of Haq (2014).

6.6.2. SB TuTz2 – Mid-Middle Turonian

The SB TuTz2 within TDP 31 occurs in the middle of the *H. helvetica* Zone and might correlate to a widely recognized and presumably synchronous SB in the Middle Turonian (middle *C. woollgari* Zone), as summarized in Wilmsen and Nagm (2013a; their figure 11). They describe this SB from four sections in Egypt and show that it occurs in the Sinai (Bauer et al., 2003), Jordan (TuJo 2; Schulze et al., 2003, 2005; Wendler et al., 2010), Israel (Buchbinder et al., 2000), Tunisia (Robaszynski et al., 1990), in several regions in Germany (SB Tu2; Niebuhr et al., 2011; Richardt and Wilmsen, 2012; Wiese, 2009), in the Anglo-Paris Basin (Gale, 1996), as well as being noted as Tu 2 in the sequence stratigraphic scheme developed for the European basins in Hardenbol et al. (1998). The apparently equivalent SB in the English

Chalk lies above the Round Down CIE and is overlain by the negative Glynde CIE in the subsequent lowstand (Gale, 1996). This regression seems to correspond to KTU3 in Haq (2014).

6.6.3. SB TuTz3 – Uppermost Middle Turonian

The most pronounced Turonian regression in the global sequence stratigraphic scheme in Haq (2014) is termed KTU4 and is placed within the uppermost *C. woollgari* Zone. It is a widely recognized SB near the Middle/Upper Turonian boundary (Bauer et al., 2003; Buchbinder et al., 2000; Frijia et al., 2015; Gale, 1996; Hardenbol et al., 1998; Niebuhr et al., 2011, 2014; Richardt and Wilmsen, 2012; Robaszynski et al., 1990; Sageman et al., 1997; Schulze et al., 2003, 2005; Uličný et al., 2014; Voigt and Hilbrecht, 1997; Walaszczyk et al., 2013; Wendler et al., 2010, 2014; Wiese, 2009; Wilmsen and Nagm, 2013a) that has been called Tu3 in most studies (an additional Turonian SB was added at the base of the Turonian in Haq, 2014).

The latest Middle Turonian, as defined by ammonites, correlates to the top of the *H. helvetica* Zone (Wendler, 2013) and is consistent with the position just above SB TuTz3 within TDP 31 and with a chemostratigraphic level above the Pewsey CIE and near the Lower Southerham CIE (Jarvis et al., 2006; Richardt and Wilmsen, 2012; Wendler, 2013; Wendler et al., 2014). The global sea-level reconstruction in Haq (2014) suggests that this was the longest and most pronounced regression during the Turonian. It coincides with a globally recognizable, expanded interval, with the lowest $\delta^{13}\text{C}_{\text{carb}}$ values throughout the Turonian, that is positioned between the Pewsey and the Bridgewick CIEs (“plateau” of Jarvis et al., 2006) and contains the Middle/Upper Turonian boundary. The largest drop in $\delta^{13}\text{C}_f$ values of planktic and benthic foraminifera in TDP 31 occurs at this level (top of the *H. helvetica* Zone, above SB TuTz3, Fig. 6). The subsequent transgressive surface in the Bohemian Basin slightly pre-dates the Caburn CIE and is recognized as the most prominent Turonian correlation level within that basin (basal TUR 5; Uličný et al., 2014).

6.6.4. SB TuTz4 – (Mid- or uppermost) Upper Turonian

The last Turonian globally recognized regression in Haq (2014) is placed slightly below the Turonian/Coniacian boundary that is characterized by the $\delta^{13}\text{C}_{\text{carb}}$ minimum of the Navigation CIE (Jarvis et al., 2006). A SB (or regression/hiatus) at this stratigraphic level was reported from Egypt (Bauer et al., 2003), Israel (Buchbinder et al., 2000), Tunisia (Robaszynski et al., 1990), several regions in Germany (Niebuhr et al., 2011; Richardt and Wilmsen, 2012; Voigt and Hilbrecht, 1997; Walaszczyk et al., 2010; Wiese, 2009), the English Chalk (Gale, 1996), France (Jarvis and Gale, 1984), and the Western Interior Seaway (e.g. Walaszczyk et al., 2014). A terminal Turonian short-term regression was also reported from the Bohemian Basin (Uličný et al., 2014).

Correlation of Upper Turonian SBs is complicated by additional SBs that were distinguished in some of the sections (Niebuhr et al., 2011; Wiese, 2009; Wiese et al., 2004) because of insufficient bio-, chemo-, and sequence stratigraphic resolution in most studies. In addition, these late Turonian SB's likely reflect the 400 kyr astronomical forcing of sea-level fluctuations, thus suggesting a particularly clear representation of this orbital cycle within this stratigraphic interval. Furthermore, the presence of a hiatus in the uppermost Turonian in many regions (e.g. Corbett et al., 2014; Gale, 1996; Joo and Sageman, 2014; Walaszczyk et al., 2014; Wilmsen and Nagm, 2013a) hampers exact dating of a SB and, especially in low-accommodation settings, might have amalgamated two or more SBs of the Upper Turonian 400 kyr-cycles (Buchbinder et al., 2000; Wilmsen and Nagm, 2013a). The presence of an Upper Turonian hiatus is also suspected for TDP 31, and correlation of SB TuTz4 is uncertain, as discussed in Section 6.5.

6.6.5. Sea level and $\delta^{13}\text{C}$ records

A relationship between presumed eustatic sea-level changes and globally recognizable shifts in bulk rock $\delta^{13}\text{C}_{\text{carb}}$ has been repeatedly

proposed (e.g. Arthur et al., 1987; Berger and Vincent, 1986; Fanton and Holmden, 2007; Jarvis et al., 2002, 2006; Jenkyns, 1996; Mitchell et al., 1996; Ripperdan et al., 1992; Scholle and Arthur, 1980; Voigt and Hilbrecht, 1997; Weissert et al., 1998; Wendler, 2013). The relationship between sea level, shelf-sea area, and global organic carbon burial/exhumation explains why carbon-isotope records are often related to sequence stratigraphy (e.g. Gale, 1996; Mitchell et al., 1996; Wendler et al., 2010, 2014; Wilmsen and Nagm, 2013a). Eustatic sea-level lowstands are typically characterized by distinct $\delta^{13}\text{C}_{\text{carb}}$ minima, because less organic carbon can be buried with shelf seas that are reduced in area, as well as via reworking of organic-rich sediments being enhanced on the exposed shelf, which continues into the subsequent transgressive phase.

However, such a relationship is not always straight forward and the pattern may reverse when large carbonate platforms are exposed and ^{13}C -rich carbonates are eroded, leading to positive $\delta^{13}\text{C}_{\text{carb}}$ shifts during the regression (Immenhauser et al., 2008). While the latter scenario was demonstrated for some of the Paleozoic CIEs, a positive correlation between global sea level and $\delta^{13}\text{C}$ values typically is observed for the Cretaceous. Despite this general relationship, detailed studies on global patterns in $\delta^{13}\text{C}_{\text{carb}}$ values and their relationship to sea level and orbital parameters have demonstrated a more complex picture (Laurin et al., 2015; Uličný et al., 2014), as may be expected from the multiple marine, terrestrial, and atmospheric feedback mechanisms involved in the global carbon cycle. For example, terrestrial sites of organic carbon burial, such as lakes, peats, and soils, represent efficient carbon sinks (e.g. Sobek et al., 2009), with the potential to influence the global carbon-isotope budget. If eustatic sea-level changes during greenhouse climate periods were controlled by the strength of the hydrological cycle that charged and discharged surface and subsurface groundwater storage (see Wendler and Wendler, 2016; Wendler et al., 2016), the associated changes in terrestrial organic matter burial may be significant enough to be reflected in the carbon-isotope records. Higher groundwater levels during global sea-level falls would favor terrestrial C_{org} burial, thereby rising exogenic $\delta^{13}\text{C}$ values and counteracting the effect of decreasing exogenic $\delta^{13}\text{C}$ values due to C_{org} reworking on exposed shelf areas.

Temporal differences between the various feedback mechanisms of the carbon cycle, as well as changes in their relative strength, may be responsible for positive or negative correlations between sea level and $\delta^{13}\text{C}$ values on different time scales, or cause lag-times between the two, making their phase relationship and interpretation of a causal link ambiguous. In a detailed study of relative sea-level changes and bulk $\delta^{13}\text{C}_{\text{org}}$ values in Turonian sediments from Bohemia, Uličný et al. (2014) stress the importance of high-resolution studies and the need to distinguish between long-term (third-order or longer) and intermediate- to short-term (400 kyr or shorter) $\delta^{13}\text{C}$ - and relative sea-level fluctuations, with respect to their correlation and interpretation. For example, it is possible that a short-term transgression during an intermediate-term regression adds to the reworking of organic material, rather than to allow for its accumulation, if the highstand duration is short relative to subsidence rates. In such a case, the transgressive pulse would correlate with a negative, rather than a positive, $\delta^{13}\text{C}$ shift, e.g. as observed for the Navigation CIE in the Bohemian Basin (Uličný et al., 2014).

Uličný et al. (2014) confirm a broad correlation between $\delta^{13}\text{C}$ values and “long-term” (myr-scale/third-order) eustatic sea-level changes and demonstrate absence of a clear correlation between $\delta^{13}\text{C}$ values and short- or intermediate-term (400 kyr or shorter) relative sea-level changes. Because of the relatively deep depositional setting at TDP 31 (outer shelf to upper slope) we expect that minor/short-term sea-level fluctuations are not reflected to the same extent (in the various proxies) as the third-order (myr-scale) sea-level changes and probably just influenced grain-size changes. However, these influences cannot easily be distinguished from changes in clastic sediment dynamics (supply or flow paths).

Some CIEs, such as the uppermost Middle Turonian positive shift of the Pewsey CIE, have been related to both eustatic sea-level high (Gale, 1996; Jarvis et al., 2006; Uličný et al., 2014; Wendler et al., 2014) and low stands (Bornemann et al., 2008; Takashima et al., 2010; Voigt and Wiese, 2000; Wiese and Voigt, 2002), which underlines the importance of stratigraphic uncertainties in global correlation for how isotopic records are interpreted, e.g. with respect to the question of glacio-eustasy versus aquifer-eustasy during greenhouse climate periods (for further discussion see Wendler and Wendler, 2016). Within the Bohemian Basin, the broad positive excursion of the Pewsey CIE (*sensu lato*) is characterized by a regression at the beginning of the CIE, a short-term transgression coinciding with highest $\delta^{13}\text{C}$ values and a regression at the declining limb of the CIE (Uličný et al., 2014). As progressively higher-resolution $\delta^{13}\text{C}$ - and relative sea-level records become available, we also need increasing bio- and chemostratigraphic precision for their robust inter-regional correlation, in order to understand better the causes and consequences of past and future eustatic sea-level change.

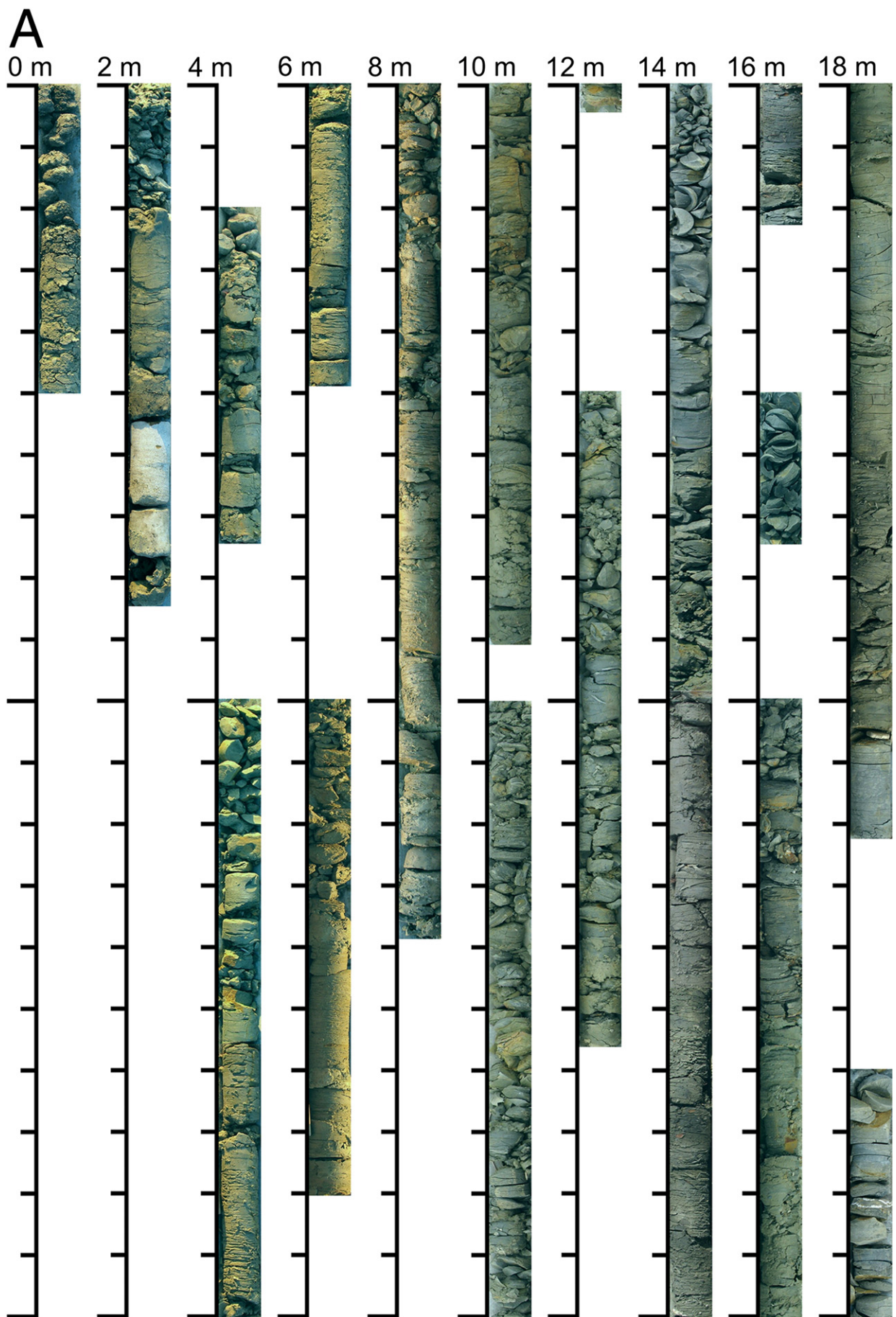
7. Conclusions

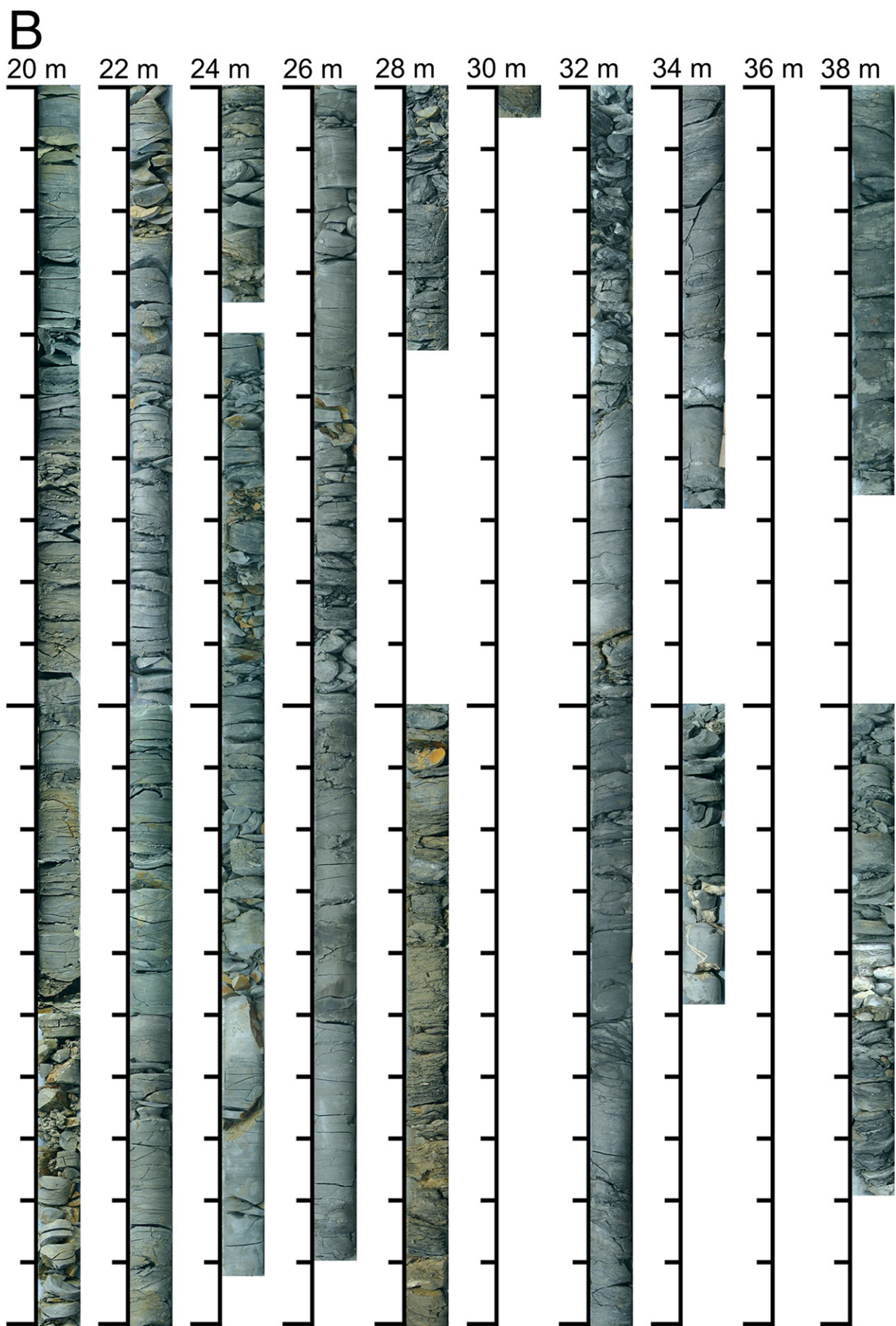
- 1) Four depositional sequences are identified in TDP 31 based on combined sedimentological, faunal, and geochemical constraints. The corresponding sequence boundaries (SBs) are positioned at the base, middle, and top of the *H. helvetica* planktic foraminiferal Zone and either in the middle(?) Upper Turonian or just below the Turonian/Coniacian boundary. The falling-stage and lowstand deposits are characterized by increased grain size, faunal changes, enhanced (largely terrestrial) organic matter flux, and $\delta^{13}\text{C}_{\text{org}}$ and $\delta^{13}\text{C}_f$ minima that are correlated to three other stratigraphic sections in the southern Tethys Ocean, based on ranges of planktic foraminiferal biostratigraphic marker species.
- 2) The combination of sequence stratigraphy, bio- and chemostratigraphy in the Tanzanian records and bio- and chemostratigraphic correlation with other sections from the south Tethys Ocean enables comparison with sequence stratigraphic schemes and relative sea-level records elsewhere. Similarity in the timing of third-order regressive events between many sections at a global scale suggests that, within the range of (bio- and chemo-) stratigraphic uncertainty, the compared Turonian sequences are synchronous and most likely driven by eustasy.
- 3) The local SBs TuTz1 and 2 evident in TDP 31 are also observed in TDP 36. They are overlain by bulk $\delta^{13}\text{C}_{\text{org}}$ minima that are interpreted to represent the Lulworth CIE at the Lower/Middle Turonian boundary and a $\delta^{13}\text{C}_{\text{carb}}$ minimum above the Round Down CIE in the Middle Turonian, respectively. These two SBs can be correlated to regressions KTU2 and KTU3 of Haq (2014).
- 4) The SB TuTz3 in the top of the *H. helvetica* Zone within TDP 31 coincides with a strong faunal turnover in benthic and planktic foraminifera, and it possibly marks a shallowing in the section from an upper slope to an outer shelf position and/or eutrophication. It correlates with the marked global SB in the top of the *C. woollgari* Zone (KTU4 of Haq, 2014) that occurs at the Middle/Upper Turonian boundary in many European, Western Interior Seaway, and Middle East sections. The Middle/Late Turonian shallowing trend interpreted for TDP 31 is consistent with the onset of eustatic long-term regression, following the highest Cretaceous global sea level during the Early Turonian (Haq, 2014).
- 5) The last occurrence of *H. helvetica* is observed just above the marked SB that represents a strong regression near the Middle/Late Turonian boundary and correlates to a level in the uppermost *C. woollgari* Zone, near the Lower Southerham CIE. This correlation means that the top of the *H. helvetica* Zone has a considerably younger age of $\sim 91.2 \pm 0.52$ Ma (based on recent radiometric dating and astrochronology) than indicated in GTS 2012 and in Haq (2014). Accordingly, the duration of the *H. helvetica* Zone is estimated at 2.35 myr (± 0.52 Ma), which is more than four times longer than presented in GTS 2012.
- 6) A second strong faunal turnover in benthic and planktic foraminifera within TDP 31 occurs at SB TuTz4 that can be correlated either to shortly below the Turonian/Coniacian boundary and to KTU5 of Haq (2014) or to a stratigraphic level in the middle(?) Upper Turonian. This SB is characterized by a $\delta^{13}\text{C}_{\text{org}}$ minimum (Navigation CIE?), a dramatic increase in abundance of biserial planktic foraminifera and a strong increase in sediment grain size. The abrupt sedimentological, geochemical, and faunal changes suggest the presence of a hiatus at this SB. The upper 25 m of the section are sand-rich and probably represent lowstand deposits of the first Coniacian sequence or the latest Turonian.
- 7) The proposed bio- and chemostratigraphic age model for the three sedimentary sequences in TDP 31 between SB TuTz1 (Lulworth CIE, ~ 93.2 Ma, slightly below the Lower/Middle Turonian boundary) and SB TuTz4 (if correctly interpreted as Navigation CIE, ~ 89.8 Ma, at the Turonian/Coniacian boundary) suggests an average cycle duration of ~ 1 myr, consistent with recent astrochronological constraints for the same time interval.
- 8) Minor negative $\delta^{18}\text{O}_f$ shifts in benthic and planktic foraminifera within the falling-stage and lowstand deposits in TDP 31 indicate bottom- and surface-water warming and/or slightly decreased surface-water salinity, an interpretation that can also explain the observed rising surface-bottom and surface-thermocline $\delta^{18}\text{O}_f$ gradients and a phase-shift in $\delta^{18}\text{O}_f$ minima between benthic and planktic foraminifera within the lowstands. These observations are inconsistent with a glacio-eustatic sea-level forcing during the Turonian and would be consistent with the model of aquifer-eustasy. The latter model predicts an enhanced hydrological cycle during warmer periods that caused both enhanced fluvial runoff (higher supply of freshwater, clastic sediments, and nutrients) and a net transfer of water from the oceans to terrestrial aquifers (surface and groundwater), leading to eustatic sea-level fall. Inversely, cooler temperatures are expected for periods with rising global sea level in the absence of significant polar ice sheets.

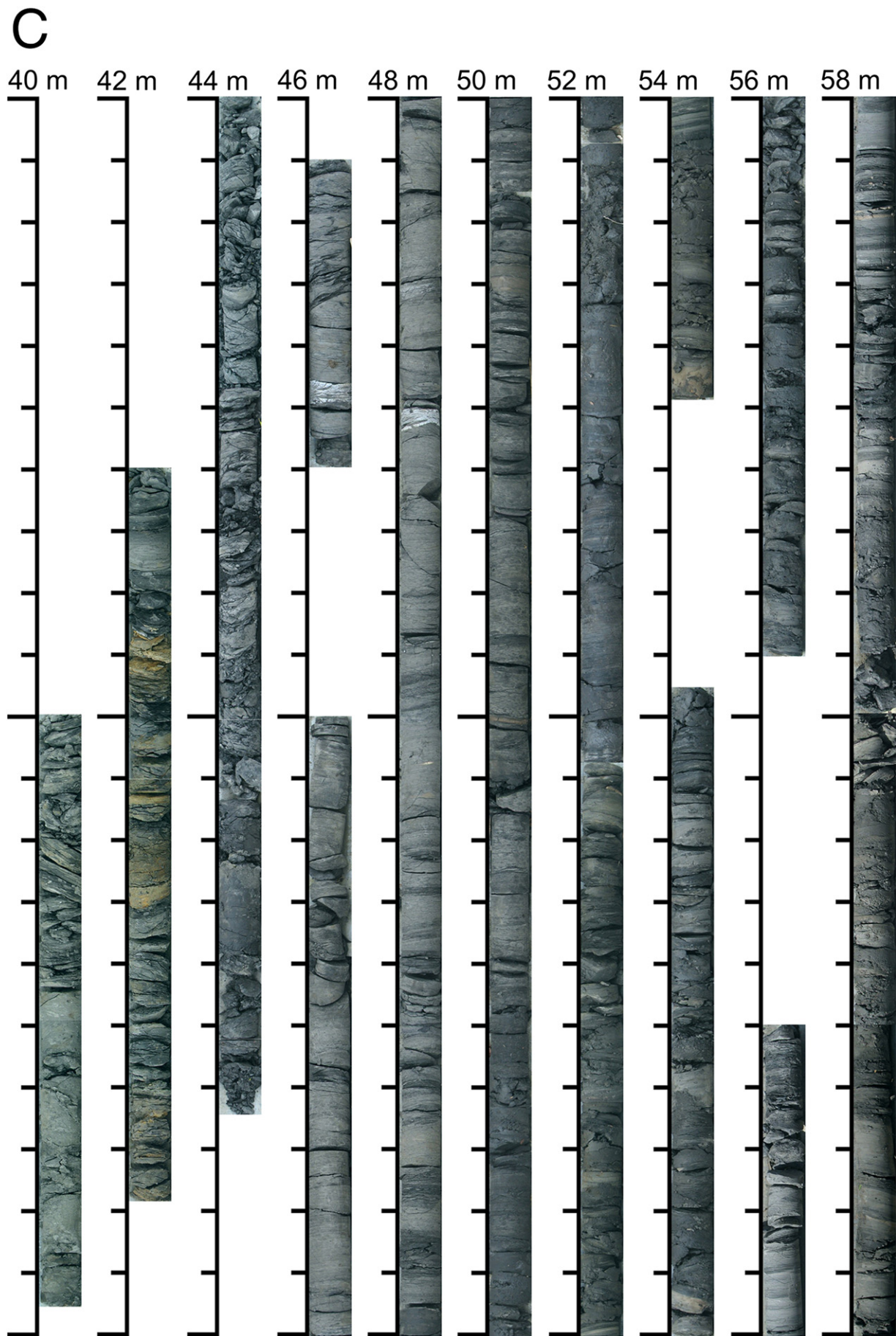
Supplementary data to this article can be found online at <http://dx.doi.org/10.1016/j.palaeo.2015.08.013>.

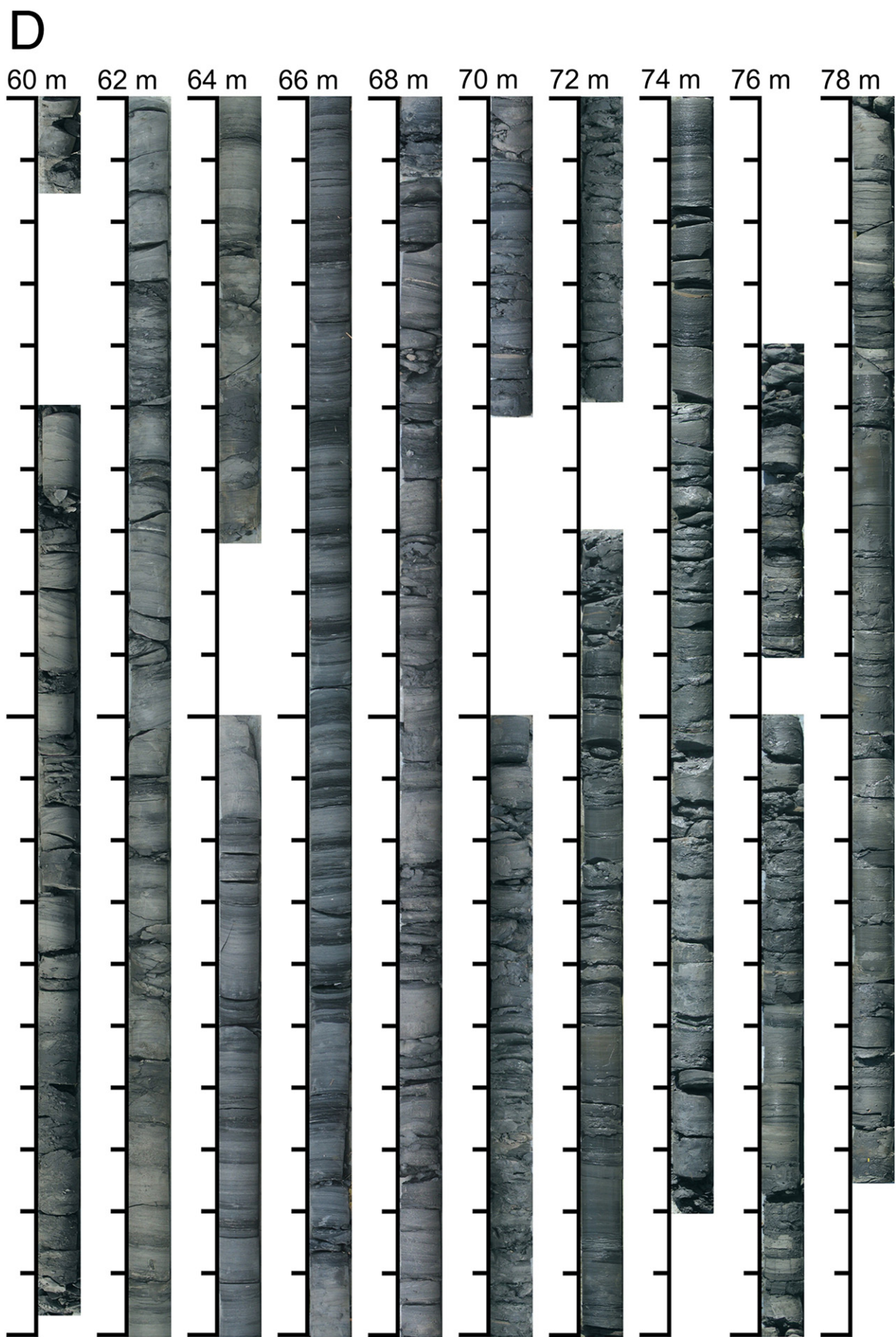
Acknowledgements

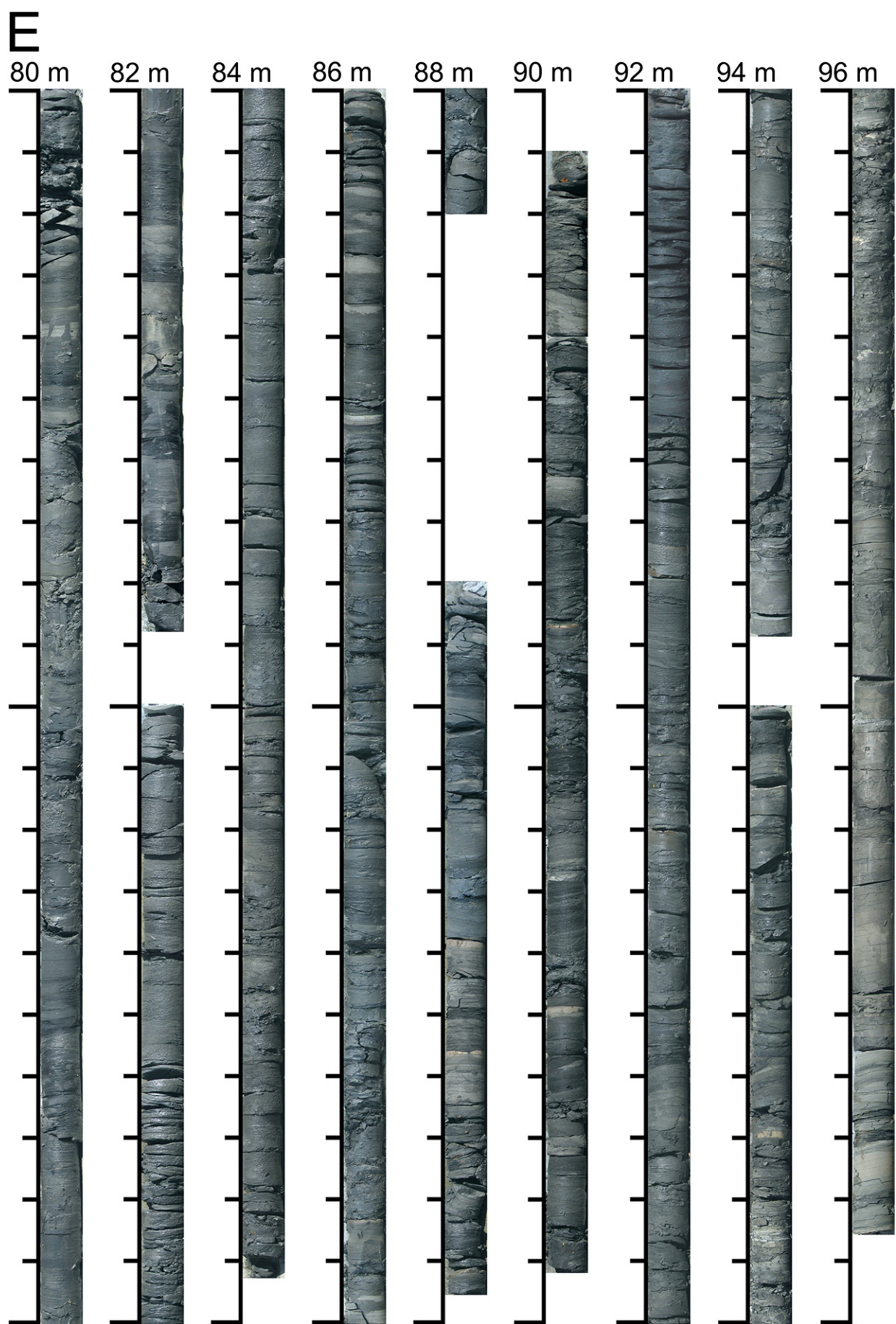
The study could not have been accomplished without the general support by B.T. Huber (Department of Paleobiology, Smithsonian Institution) and H. Willems (Department of Geosciences, Bremen University) and their efforts for funding through their institutions (to I.W.). We thank the TDP team for their co-operation during fieldwork in Tanzania and for subsequent discussion of the data. Assistance with foraminifer picking by L. Petruny and S. Haynes, as well as technical help with grain-size analyses by E. Jacobs and W. Boykins (Smithsonian Institution), are acknowledged gratefully. We are thankful to J. Post (Department of Mineral Sciences, Smithsonian Institution) for micro-XRD data processing and mineral determination, to P. Witte (Bremen University) and S. Whittaker (Smithsonian Institution) for assistance with EDX measurements and SEM work, and to H. Willems, M. Wilmsen, S. Warny, A. Sadekov, Z. Dubicka, C. Ifrim, and M. Reich for discussions and help with identification and interpretation of some of the macro- and microfossils. We thank K.G. MacLeod and two reviewers for constructive comments that helped to improve the manuscript. This research was funded by DFG grant WE 4587/1-1 (to J.W.), the Smithsonian Institution's Scholarly Studies Program and the University of Bremen (to I.W.). This paper is a contribution to UNESCO-IUGS IGCP project 609 "Climate-environmental deteriorations during greenhouse phases: Causes and consequences of short-term Cretaceous sea-level changes".

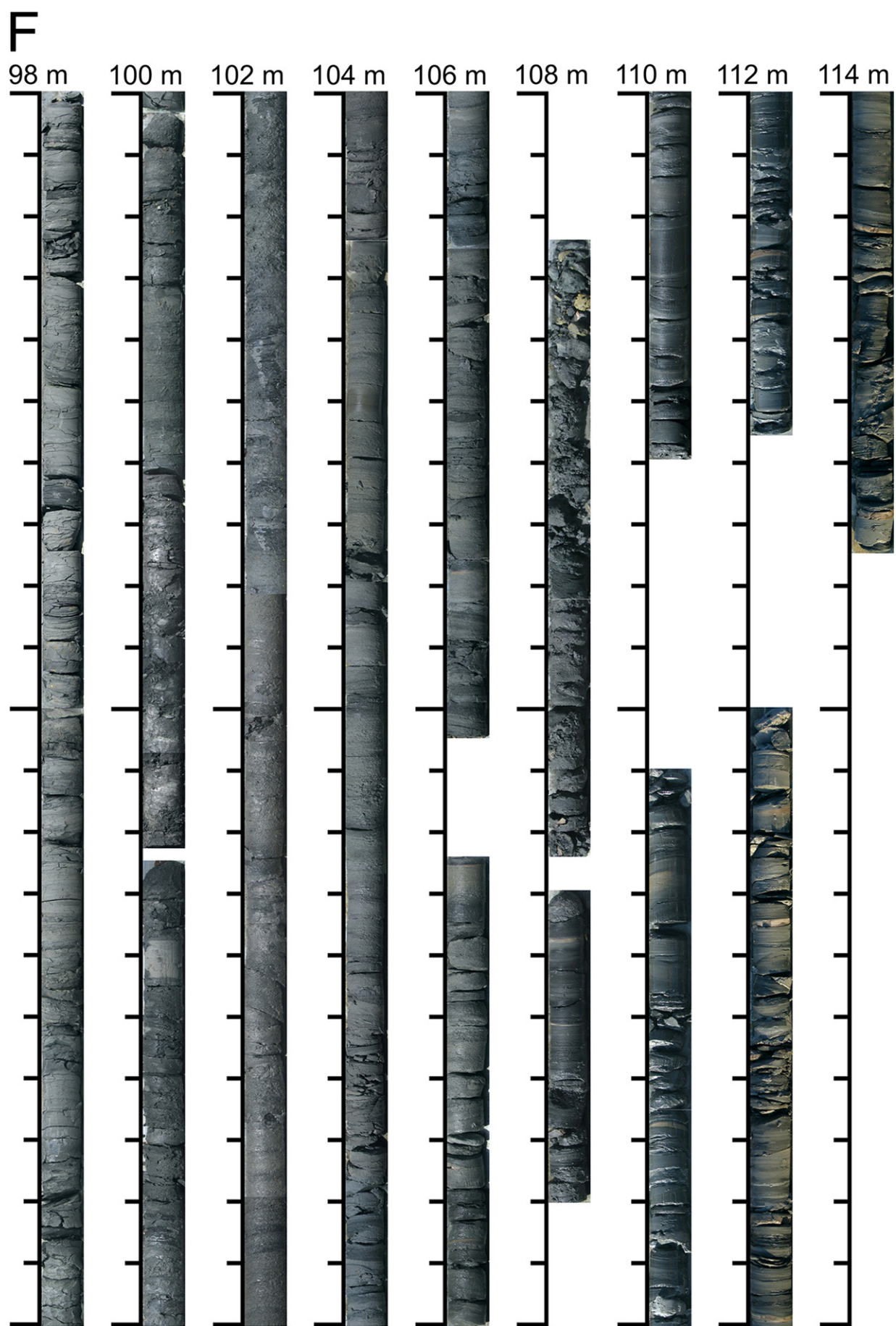
Appendix 1A–F. Core photographs from TDP 31.











References

- Ando, A., Huber, B.T., MacLeod, K.G., Ohta, T., Khim, B.-K., 2009. Blake Nose stable isotopic evidence against the mid-Cenomanian glaciation hypothesis. *Geology* 37, 451–454.
- Arenillas, I., Alegret, L., Arz, J.A., Molina, E., 2000. El uso didáctico de los foraminíferos en la enseñanza de ciencias de la tierra: su distribución paleoceanográfica en el transito Cretacio-Terciario. *Enseñanza de las Ciencias de la Tierra* 82, 108–118.
- Arthur, M.A., Schlanger, S.O., Jenkyns, H.C., 1987. The Cenomanian–Turonian oceanic anoxic event, II. Palaeoceanographic controls on organic-matter production and preservation. In: Brooks, J., Fleet, A.J. (Eds.), *Marine Petroleum Source Rocks*. Geological Society Special Publication, London, pp. 401–420.
- Bailey, H.W., 1978. A Foraminiferal Biostratigraphy of the Lower Senonian. University of Plymouth, p. 285.
- Bauer, J., Kuss, J., Steuber, T., 2003. Sequence architecture and carbonate platform configuration (Late Cenomanian–Santonian), Sinai, Egypt. *Sedimentology* 50, 387–414.
- Berger, W.H., Vincent, E., 1986. Deep-sea carbonates; reading the carbon-isotope signal. *Geol. Rundsch.* 75, 249–269.
- Bornemann, A., Norris, R.D., 2007. Size-related stable isotope changes in Late Cretaceous planktic foraminifera: implications for paleoecology and photosymbiosis. *Mar. Micropaleontol.* 65, 32–42.
- Bornemann, A., Norris, R.D., Friedrich, O., Beckmann, B., Schouten, S., Sinninghe Damsté, J.S., Vogel, J., Hofmann, P., Wagner, T., 2008. Isotopic evidence for glaciation during the Cretaceous supergreenhouse. *Science* 319, 189–193.
- Buchbinder, B., Benjamini, C., Lipson-Benitah, S., 2000. Sequence development of Late Cenomanian–Turonian carbonate ramps, platforms and basins in Israel. *Cretac. Res.* 21, 813–843.
- Burnett, J.A. (with contributions from LT. Gallagher, M.J. Hampton), 1998. Upper Cretaceous, in: Bown, P.R. (Ed.), *Calcareous Nannofossil Biostratigraphy*. British Micropalaeontological Society Series, Chapman and Hall/Kluwer Academic Publishers, London, pp. 132–199.
- Caron, M., Dall'Agnolo, S., Accarie, H., Barrera, E., Kauffman, E.G., Amédro, F., Robaszynski, F., 2006. High-resolution stratigraphy of the Cenomanian–Turonian boundary interval at Pueblo (USA) and wadi Bahloul (Tunisia): stable isotope and bio-events correlation. *Geobios* 39, 171–200.
- Catuneanu, O., 2006. *Principles of Sequence Stratigraphy*. Elsevier, Amsterdam.
- Clarke, L.J., 2002. *Stable-Isotopic Evidence for Long-Term Mid- to Late Cretaceous Oceanographic and Climatic Change*. University of Oxford, UK, p. 287.
- Conrad, C.P., 2013. The solid Earth's influence on sea level. *Geol. Soc. Am. Bull.* 125, 1027–1052.
- Corbett, M.J., Watkins, D.K., Pospichal, J.J., 2014. A quantitative analysis of calcareous nannofossil bioevents of the Late Cretaceous (Late Cenomanian–Coniacian) Western Interior Seaway and their reliability in established zonation schemes. *Mar. Micropaleontol.* 109, 30–45.
- Dias-Brito, D., 2000. Global stratigraphy, palaeobiogeography and palaeoecology of Albian–Maastrichtian pithonellid calcispheres: impact on Tethys configuration. *Cretac. Res.* 21, 315–349.
- Dubicka, Z., Peryt, D., 2014. Classification and evolutionary interpretation of late Turonian-Early Campanian Gavelinella and Stensioeina (Gavelinellidae, benthic foraminifera) from western Ukraine. *J. Foraminifer. Res.* 44, 151–176.
- Eldrett, J.S., Ma, C., Bergman, S.C., Lutz, B., Gregory, F.J., Dodsworth, P., Phipps, M., Hardas, P., Minisini, D., Ozkan, A., Ramerez, J., Bowring, S.A., Kamo, S.L., Ferguson, K., Calum, M., Kelly, A.E., 2015a. An astrochronologically calibrated stratigraphy of the Cenomanian, Turonian and earliest Coniacian from the Cretaceous Western Interior Seaway, USA: implications for global chronostratigraphy. *Cretac. Res.* 56, 316–344.
- Eldrett, J.S., Ma, C., Bergman, S.C., Ozkan, A., Minisini, D., Lutz, B., Jackett, S.-J., Macaulay, C., Kelly, A.E., 2015b. Origin of limestone–marlstone cycles: astronomic forcing of organic-rich sedimentary rocks from the Cenomanian to early Coniacian of the Cretaceous Western Interior Seaway, USA. *Earth Planet. Sci. Lett.* 423, 98–113.
- Falzoni, F., Petrizzi, M.R., MacLeod, K.G., Huber, B.T., 2013. Santonian–Campanian planktonic foraminifera from Tanzania, Shatsky Rise and Exmouth Plateau: species depth ecology and paleoceanographic inferences. *Mar. Micropaleontol.* 103, 15–29.
- Falzoni, F., Petrizzi, M.R., Huber, B.T., MacLeod, K.G., 2014. Insights into the meridional ornamentation of the planktonic foraminiferal genus *Rugoglobigerina* (Late Cretaceous) and implications for taxonomy. *Cretac. Res.* 47, 87–104.
- Fanton, K.C., Holmden, C., 2007. Sea-level forcing of carbon isotope excursions in epeiric seas: implications for chemostratigraphy. *Can. J. Earth Sci.* 44, 807–818.
- Föglöd, S., Wallmann, K., Kuhnt, W., 2011. Cool episodes in the Cretaceous – Exploring the effects of physical forcings on Antarctic snow accumulation. *Earth Planet. Sci. Lett.* 307, 279–288.
- Föllmi, K.B., 2012. Early Cretaceous life, climate and anoxia. *Cretac. Res.* 35, 230–257.
- Friedrich, O., Norris, R.D., Erbacher, J., 2012. Evolution of middle to Late Cretaceous oceans – A 55 my. record of Earth's temperature and carbon cycle. *Geology* <http://dx.doi.org/10.1130/g32701.2>.
- Frijia, G., Parente, M., Di Lucia, M., Mutti, M., 2015. Carbon and strontium isotope stratigraphy of the Upper Cretaceous (Cenomanian–Campanian) shallow-water carbonates of southern Italy: chronostratigraphic calibration of larger foraminifera biostratigraphy. *Cretac. Res.* 53, 110–139.
- Gale, A.S., 1996. Turonian correlation and sequence stratigraphy of the Chalk in southern England. In: Hesselbo, S.P., Parkinson, D.N. (Eds.), *Sequence Stratigraphy in British Geology*. Geological Society of London, Special Publication, pp. 177–195.
- Galeotti, S., Rusciadelli, G., Sprovieri, M., Lanci, L., Gaudio, A., Pekar, S., 2009. Sea-level control on facies architecture in the Cenomanian–Coniacian Apulian margin (Western Tethys): a record of glacio-eustatic fluctuations during the Cretaceous greenhouse? *Palaeogeogr. Palaeoclimatol. Palaeoecol.* 276, 196–205.
- Gradstein, F.M., Ogg, J.G., Smith, A., 2004. *A Geologic Time Scale*. Cambridge University Press, Cambridge.
- Grossman, E.L., Ku, T.-L., 1986. Oxygen and carbon isotope fractionation in biogenic aragonite: temperature effects. *Chem. Geol.* 59, 59–74.
- Gustafsson, M., Holbourn, A., Kuhnt, W., 2003. Changes in Northeast Atlantic temperature and carbon flux during the Cenomanian / Turonian paleoceanographic event: the Goban Spur stable isotope record. *Palaeogeogr. Palaeoclimatol. Palaeoecol.* 201, 51–66.
- Haq, B.U., 2014. *Cretaceous eustasy revisited*. *Glob. Planet. Chang.* 113, 44–58.
- Haq, B.U., Hardenbol, J., Vail, P.R., 1987. Chronology of fluctuating sea levels since the Triassic. *Science* 235, 1156–1167.
- Hardenbol, J., Thierry, J., Farlay, M.B., Jacquin, T., De Graciansky, P.-C., Vail, P.R., 1998. Mesozoic and Cenozoic Sequence Chronostratigraphic Framework of European Basins. In: De Graciansky, P.C., Hardenbol, J., Jacquin, T., Vail, P.R. (Eds.), *Special Publication: Mesozoic and Cenozoic sequence stratigraphy of European basins*. Society for Sedimentary Geology, pp. 3–13.
- Hay, W.W., Leslie, M.A., 1990. Could Possible Changes in Global Groundwater Reservoir Cause Eustatic Sea-Level Fluctuations, Sea-Level Change. National Academic Press, Washington, DC, pp. 161–170.
- Haynes, S.J., 2012. Bulk Oxygen and Carbon Isotopic Variation in the Late Cretaceous along with Morphometric Analysis of Bivalve Planktonic Foraminifera. University of Missouri-Columbia, p. 221.
- Haynes, S.J., Huber, B.T., MacLeod, K.G., 2015. Evolution and phylogeny of Mid-Cretaceous (Albian-Coniacian) bivalve planktonic foraminifera. *J. Foraminifer. Res.* 45, 42–81.
- Holbourn, A., Kuhnt, W., 2002. Cenomanian–Turonian palaeoceanographic change on the Kerguelan Plateau: a comparison with Northern Hemisphere records. *Cretac. Res.* 23, 333–349.
- Huber, B.T., Petrizzi, M.R., 2014. Evolution and taxonomic study of the Cretaceous planktonic foraminifer genus *Helvetoglobotruncana* Reiss, 1957. *J. Foraminifer. Res.* 44, 40–57.
- Huber, B.T., Norris, R.D., MacLeod, K.G., 2002. Deep-sea paleotemperature record of extreme warmth during the Cretaceous. *Geology* 30, 123–126.
- Ifrim, C., Stinesbeck, W., 2008. Cenomanian–Turonian high-resolution biostratigraphy of north-eastern Mexico and its correlation with the GSSP and Europe. *Cretac. Res.* 29, 943–956.
- Ifrim, C., Götz, S., Stinesbeck, W., 2011. Fluctuations of the oxygen minimum zone at the end of Oceanic Anoxic Event 2 reflected by benthic and planktic fossils. *Geology* 39, 1043–1046.
- Immenhauser, A., Holmden, C., Patterson, W.P., 2008. Interpreting the carbon isotope record of ancient epeiric seas: lessons from the Recent. In: Pratt, B.R., Holmden, C. (Eds.), *Dynamics of Epeiric Seas*. Geological Association of Canada, Special Paper, pp. 135–174.
- Jacobs, D.K., Sahagian, D.L., 1993. Climate-induced fluctuations in sea level during non-glacial times. *Nature* 361, 710–712.
- Jarvis, I., Gale, A.S., 1984. The late cretaceous transgression in the SW Anglo-Paris Basin: stratigraphy of the Craie de Villedieu Formation. *Cretac. Res.* 5, 195–224.
- Jarvis, I., Mabrouk, A., Moody, R.T.J., De Cabrera, S., 2002. Late Cretaceous (Campanian) carbon isotope events, sea-level change and correlation of the Tethyan and Boreal realms. *Palaeogeogr. Palaeoclimatol. Palaeoecol.* 188, 215–248.
- Jarvis, I., Gale, A., Jenkyns, H.C., Pearce, M.A., 2006. Secular variation in Late Cretaceous carbon isotopes: a new $\delta^{13}\text{C}$ carbonate reference curve for the Cenomanian–Campanian (99.6–70.6 Ma). *Geol. Mag.* 143, 561–608.
- Jenkyns, H.C., 1996. Relative sea-level change and carbon isotopes: data from the Upper Jurassic (Oxfordian) of central and Southern Europe. *Terra Nova* 8, 75–85.
- Jiménez Berrocoso, Á., MacLeod, K.G., Huber, B.T., Lees, J.A., Wendler, I., Bown, P.R., Mweneinda, A.K., Isaza Londoño, C., Singano, J.M., 2010. Lithostratigraphy, biostratigraphy and chemostratigraphy of Upper Cretaceous sediments from southern Tanzania: Tanzania drilling project sites 21–26. *J. Afr. Earth Sci.* 57, 47–69.
- Jiménez Berrocoso, Á., Huber, B.T., MacLeod, K.G., Petrizzi, M.R., Lees, J.A., Wendler, I., Coxall, H., Mweneinda, A.K., Falzoni, F., Birch, H., Singano, J.M., Haynes, S., Cotton, L., Wendler, J., Bown, P.R., Robinson, S.A., Gould, J., 2012. Lithostratigraphy, biostratigraphy and chemostratigraphy of Upper Cretaceous and Paleogene sediments from southern Tanzania: Tanzania Drilling Project Sites 27–35. *J. Afr. Earth Sci.* 70, 36–57.
- Jiménez Berrocoso, Á., Huber, B.T., MacLeod, K.G., Petrizzi, M.R., Lees, J.A., Wendler, I., Coxall, H., Mweneinda, A.K., Falzoni, F., Birch, H., Haynes, S.J., Bown, P.R., Robinson, S.A., Singano, J.M., 2015. The Lindi Formation (upper Albian-Coniacian) and Tanzania Drilling Project Sites 36–40 (Lower Cretaceous to Paleogene): lithostratigraphy, biostratigraphy and chemostratigraphy. *J. Afr. Earth Sci.* 101, 282–308.
- Joo, Y.J., Sageman, B.B., 2014. Cenomanian To Campanian Carbon Isotope Chemostratigraphy from the Western Interior Basin, U.S.A. *J. Sediment. Res.* 84, 529–542.
- Koch, W., 1977. Biostratigraphie in der Oberkreide und Taxonomie von Foraminiferen. *Geol. Jahrb.* A38, 11–123.
- Kuhnt, W., Wiedmann, J., 1995. Cenomanian–Turonian source rocks: paleobiogeographic and paleoenvironmental aspects. In: Huc, A.Y. (Ed.), *Paleogeography, Paleoclimate, and Source Rocks*. American Association of Petroleum Geologists, Studies in Geology, pp. 213–231.
- Lamolda, M., Paul, C., Peryt, D., Pons, J., 2014. The Global Boundary Stratotype and Section Point (GSSP) for the base of the Santonian Stage, “Cantera de Margas”, Olazagutia, northern Spain. *Episodes* 37, 2–13.
- Laurin, J., Sageman, B.B., 2007. Cenomanian–Turonian coastal record in SW Utah, USA: orbital-scale transgressive-regressive events during Oceanic Anoxic Event II. *J. Sediment. Res.* 77, 731–756.
- Laurin, J., Čech, S., Uličný, D., Štaffen, Z., Svobodová, M., 2014. Astrochronology of the Late Turonian: implications for the behavior of the carbon cycle at the demise of peak greenhouse. *Earth Planet. Sci. Lett.* 394, 254–269.
- Laurin, J., Meyers, S.R., Uličný, D., Jarvis, I., Sageman, B.B., 2015. Axial obliquity control on the greenhouse carbon budget through middle- to high-latitude reservoirs. *Paleoceanography* 30, 133–149. <http://dx.doi.org/10.1002/2014PA002736>.

- Leckie, R.M., 1987. Paleoecology of Mid-Cretaceous Planktonic Foraminifera: A Comparison of Open Ocean and Epicontinental Sea Assemblages. *Micropaleontology* 33, 164–176.
- Lees, J.A., 2008. The calcareous nannofossil record next term across the Late Cretaceous Turonian/Coniacian boundary, including new data from Germany, Poland, the Czech Republic and England. *Cretac. Res.* 29, 40–64.
- Lowery, C.M., Corbett, M.J., Leckie, R.M., Watkins, D., Miceli Romero, A., Pramudito, A., 2014. Foraminiferal and nannofossil paleoecology and paleoceanography of the Cenomanian–Turonian Eagle Ford Shale of southern Texas. *Palaeogeogr. Palaeoclimatol. Palaeoecol.* 413, 49–65.
- Lüning, S., Marzouk, A.M., Morsi, A.M., Kuss, J., 1998. Sequence stratigraphy of the Upper Cretaceous of central-east Sinai, Egypt. *Cretac. Res.* 19, 153–196.
- MacLeod, K.G., Huber, B.T., Pletsch, T., Röhl, U., Kucera, M., 2001. Maastrichtian foraminiferal and paleoceanographic changes on Milankovitch time scales. *Paleoceanography* 16, 133–155.
- MacLeod, K.G., Huber, B.T., Jiménez Berrocoso, Á., Wendler, I., 2013. A stable and hot Turonian without glacial $\delta^{18}\text{O}$ excursions is indicated by exquisitely preserved Tanzanian foraminifera. *Geology* 41, 1083–1086.
- Meyers, S.R., Sageman, B.B., Arthur, M.A., 2012. Obliquity forcing of organic matter accumulation during Oceanic Anoxic Event 2. *Paleoceanography* 27, PA3212.
- Miller, K.G., Sugarman, P.J., Browning, J.V., Kominz, M.A., Hernández, J.C., Olsson, R.K., Wright, J.D., Feigenson, M.D., van Sickel, W., 2003. Late Cretaceous chronology of large, rapid sea-level changes; glacioeustasy during the greenhouse world. *Geology* 31, 585–588.
- Miller, K.G., Sugarman, P.J., Browning, J.V., Kominz, M.A., Olsson, R.K., Feigenson, M.D., Hernández, J.C., 2004. Upper Cretaceous sequences and sea-level history, New Jersey coastal plain. *Geol. Soc. Am. Bull.* 116, 368–393.
- Mitchell, S.F., Paul, C.R.C., Gale, A.S., 1996. Carbon isotopes and sequence stratigraphy. In: Howell, J.A., Aiken, J.F. (Eds.), *High Resolution Sequence Stratigraphy: Innovations and Applications*. Geological Society Special Publication, London, pp. 11–24.
- Moriya, K., Wilson, P.A., Friedrich, O., Erbacher, J., Kawahata, H., 2007. Testing for ice sheets during the mid-Cretaceous greenhouse using glassy foraminiferal calcite from the mid-Cenomanian tropics on Demerara Rise. *Geology* 35, 615–618.
- Niebuhr, B., Baldschuh, R., Ernst, G., Walaszczyk, I., Weiss, W., Wood, C.J., 1999. The Upper Cretaceous succession (Cenomanian/Santonian) of the Staffhorst Shaft, Lower Saxony, northern Germany: integrated biostratigraphic, lithostratigraphic and downhole geophysical log data. *Acta Geol. Pol.* 49, 175–213.
- Niebuhr, B., Wilmsen, M., Chellouche, P., Richardt, N., Pürner, T., 2011. Stratigraphy and facies of the Turonian (Upper Cretaceous) Roding Formation at the southwestern margin of the Bohemian Massif (southern Germany, Bavaria). *Z. Dtsch. Ges. Geowiss.* 62, 295–316.
- Niebuhr, B., Wilmsen, M., Janetschke, N., 2014. Cenomanian–Turonian sequence stratigraphy and facies development of the Danubian Cretaceous Group (Bavaria, Southern Germany). *Z. Dtsch. Ges. Geowiss.* 165, 621–640.
- Ogg, J.G., Hinnov, L.A., Huang, C., 2012. Chapter 27 – Cretaceous. In: Gradstein, F., Ogg, J., Schmitz, M., Ogg, G. (Eds.), *The Geologic Time Scale 2012*. Elsevier, Boston, pp. 793–853.
- Petrizzi, M.R., 2000. Upper Turonian-lower Campanian planktonic foraminifera from southern mid-high latitudes (Exmouth Plateau, NW Australia): biostratigraphy and taxonomic notes. *Cretac. Res.* 21, 479–505.
- Petrizzi, M.R., 2002. Palaeoceanographic and palaeoclimatic inferences from Late Cretaceous planktonic foraminiferal assemblages from the Exmouth Plateau (ODP sites 762 and 763, eastern Indian Ocean). *Mar. Micropaleontol.* 45, 117–150.
- Petrizzi, M.R., 2003. Late Cretaceous planktonic foraminiferal bioevents in the Tethys and in the Southern Ocean record: an overview. *J. Foraminifer. Res.* 33, 330–337.
- Petrizzi, M.R., Falzoni, F., Premoli Silva, I., 2011. Identification of the base of the lower-to-middle Campanian *Globotruncana ventricosa* Zone: comments on reliability and global correlations. *Cretac. Res.* 32, 387–405.
- Posamentier, H.W., Vail, P.R., 1988. Eustatic controls on clastic deposition II – Sequence and systems tract models, Sea-level changes – An integrated approach. *SEPM Spec. Publ.* 125–154.
- Richardt, N., Wilmsen, M., 2012. Lower Upper Cretaceous standard section of the southern Münsterland (NW Germany): carbon stable-isotopes and sequence stratigraphy. *Newsl. Stratigr.* 45, 1–24.
- Richardt, N., Wilmsen, M., Niebuhr, B., 2013. Late Cenomanian–Early Turonian facies development and sea-level changes in the Bodenwöhrener Senke (Danubian Cretaceous Group, Bavaria, Germany). *Facies* 59, 803–827.
- Ripperdan, R.L., Magaritz, M., Nicoll, R.S., Shergold, J.H., 1992. Simultaneous changes in carbon isotopes, sea level, and conodont biozones within the Cambrian-Ordovician boundary interval at Black Mountain, Australia. *Geology* 20, 1039–1042.
- Robaszynski, F., Caron, M., Dupuis, C., Amedeo, F., Gonzalez-Donoso, J.M., Linares, D., Hardenbol, J., Gartner, S., Calandra, F., Deloffre, R., 1990. A tentative integrated stratigraphy in the Turonian of central Tunisia; formations, zones and sequential stratigraphy in the Kalaat Senan area. *Bull. Centres Rech. Explor. Prod. Elf-Aquitaine* 14, 213–284.
- Sageman, B.B., 1996. Lowstand tempestites: depositional model for Cretaceous skeletal limestones, Western Interior basin. *Geology* 24, 888–892.
- Sageman, B.B., Rich, J., Arthur, M.A., Birchfield, G.E., Dean, W.E., 1997. Evidence for Milankovitch periodicities in Cenomanian–Turonian lithologic and geochemical cycles, western interior U.S.A. *J. Sediment. Res.* 67, 286–302.
- Sageman, B.B., Meyers, S.R., Arthur, M.A., 2006. Orbital time scale and new C-isotope record for Cenomanian–Turonian boundary stratotype. *Geology* 34, 125–128.
- Sageman, B.B., Singer, B.S., Meyers, S.R., Siewert, S.E., Walaszczyk, I., Condon, D.J., Jicha, B.R., Obradovich, J.D., Sawyer, D.A., 2014. Integrating 40Ar/39Ar, U-Pb, and astronomical clocks in the Cretaceous Niobrara Formation, Western Interior Basin, USA. *Geol. Soc. Am. Bull.* 126, 956–973.
- Saltzman, M.R., Thomas, E., 2012. Chapter 11 – Carbon Isotope Stratigraphy. In: Gradstein, F., Ogg, J., Schmitz, M., Ogg, G. (Eds.), *The Geologic Time Scale 2012*. Elsevier, Boston, pp. 207–232.
- Scholle, P.A., Arthur, M.A., 1980. Carbon isotope fluctuations in Cretaceous pelagic limestones: potential stratigraphic and petroleum exploration tool. *AAPG Bull.* 64, 67–87.
- Schulze, F., Lewy, Z., Kuss, J., Gharaibeh, A., 2003. Cenomanian–Turonian carbonate platform deposits in west-central Jordan. *Int. J. Earth Sci.* 92, 641–660.
- Schulze, F., Kuss, J., Marzouk, A.M., 2005. Platform configuration, microfacies and cyclicity of the upper Albian to Turonian of west-central Jordan. *Facies* 50, 505–527.
- Sliter, W.V., Baker, R.A., 1972. Cretaceous bathymetric distribution of benthic foraminifers. *J. Foraminifer. Res.* 2, 167–183.
- Sobek, S., Durisch-Kaiser, E., Zurbrügg, R., Wongfun, N., Wessels, M., Pasche, N., Wehrli, B., 2009. Organic carbon burial efficiency in lake sediments controlled by oxygen exposure time and sediment source. *Limnol. Oceanogr.* 54, 2243–2254.
- Sømme, T.O., Helland-Hansen, W., Granjeon, D., 2009. Impact of eustatic amplitude variations on shelf morphology, sediment dispersal, and sequence stratigraphic interpretation: icehouse versus greenhouse systems. *Geology* 37, 587–590.
- Takashima, R., Nishi, H., Yamanaka, T., Hayashi, K., Waseda, A., Obuse, A., Tomosugi, T., Deguchi, N., Mochizuki, S., 2010. High-resolution terrestrial carbon isotope and planktic foraminiferal records of the Upper Cenomanian to the Lower Campanian in the Northwest Pacific. *Earth Planet. Sci. Lett.* 289, 570–582.
- Tronchetti, G., Groscheny, D., 1991. Les assemblages de foraminifères benthiques au passage Cénomanien–Turonien à Vergons, S-E France. *Geobios* 24, 13–31.
- Uličný, D., Jarvis, I., Gröcke, D.R., Čech, S., Laurin, J., Olde, K., Trabucho-Alexandre, J., Švábenická, L., Pedentchouk, N., 2014. A high-resolution carbon-isotope record of the Turonian stage correlated to a siliciclastic basin fill: implications for mid-Cretaceous sea-level change. *Palaeogeogr. Palaeoclimatol. Palaeoecol.* 405, 42–58.
- Voigt, S., Hilbrecht, H., 1997. Late Cretaceous carbon isotope stratigraphy in Europe: correlation and relations with sea level and sediment stability. *Palaeogeogr. Palaeoclimatol. Palaeoecol.* 134, 39–59.
- Voigt, S., Wiese, F., 2000. Evidence for Late Cretaceous (Late Turonian) climate cooling from oxygen-isotope variations and paleobiogeographic changes in Western and Central Europe. *J. Geol. Soc. Lond.* 157, 737–743.
- Voigt, S., Gale, A.S., Jung, C., Jenkyns, H.C., 2012. Global correlation of Upper Campanian–Maastrichtian successions using carbon-isotope stratigraphy: development of a new Maastrichtian timescale. *Newsl. Stratigr.* 45, 25–53.
- Wagreich, M., Lein, R., Sames, B., 2014. Eustasy, its controlling factors, and the limno-eustatic hypothesis – concepts inspired by Eduard Suess. *Aust. J. Earth Sci.* 107, 115–131.
- Walaszczyk, I., Kopaevich, L.F., Olferiev, A.G., 2004. Inoceramid/foraminiferal succession of the Turonian and Coniacian (Upper Cretaceous) of the Briansk region (Central European Russia). *Acta Geol. Pol.* 54, 597–609.
- Walaszczyk, I., Wood, C.J., Lees, J.A., Peryt, D., Voigt, S., Wiese, F., 2010. The Salzgitter-Salder Quarry (Lower Saxony, Germany) and Ślipia Nadbrzeżna river cliff section (central Poland): a proposed candidate composite Global Boundary Stratotype Section and Point for the base of the Coniacian Stage (Upper Cretaceous). *Acta Geol. Pol.* 60, 445–477.
- Walaszczyk, I., Kopaevich, L.F., Beniamovski, V.N., 2013. Inoceramid and foraminiferal record and biozonation of the Turonian and Coniacian (Upper Cretaceous) of the Mangyshlak Mts., western Kazakhstan. *Acta Geol. Pol.* 63, 469–487.
- Walaszczyk, I., Shank, J.A., Plint, A.G., Cobban, W.A., 2014. Interregional correlation of disconformities in Upper Cretaceous strata, Western Interior Seaway: biostratigraphic and sequence-stratigraphic evidence for eustatic change. *Geol. Soc. Am. Bull.* 126, 307–316.
- Weissert, H., Lini, A., Föllmi, K.B., Kuhn, O., 1998. Correlation of Early Cretaceous carbon isotope stratigraphy and platform drowning events: a possible link? *Palaeogeogr. Palaeoclimatol. Palaeoecol.* 137, 189–203.
- Wendler, I., 2013. A critical evaluation of carbon isotope stratigraphy and biostratigraphic implications for Late Cretaceous global correlation. *Earth Sci. Rev.* 126, 116–146.
- Wendler, J.E., Bown, P., 2013. Exceptionally well-preserved Cretaceous microfossils reveal new biomineralization styles. *Nat. Commun.* 4, 2052.
- Wendler, J.E., Wendler, I., 2016. What drove sea-level fluctuations during the mid-Cretaceous greenhouse climate? *Palaeogeogr. Palaeoclimatol. Palaeoecol.* 441, 412–419.
- Wendler, I., Zonneveld, K.A.F., Willems, H., 2002a. Oxygen availability effects on early diagenetic calcite dissolution in the Arabian Sea as inferred from calcareous dinoflagellate cysts. *Glob. Planet. Chang.* 34, 219–239.
- Wendler, I., Gräfe, K.-U., Willems, H., 2002b. Palaeoecology of calcareous dinoflagellate cysts in the mid-Cenomanian Boreal Realm: implications for the reconstruction of palaeoceanography of the NW European shelf sea. *Cretac. Res.* 23, 213–229.
- Wendler, I., Gräfe, K.-U., Willems, H., 2002c. Reconstruction of mid-Cenomanian orbitally forced palaeoenvironmental changes based on calcareous dinoflagellate cysts. *Palaeogeogr. Palaeoclimatol. Palaeoecol.* 179, 19–41.
- Wendler, I., Wendler, J.E., Neuhuber, S., Wagreich, M., 2009. Productivity fluctuations and orbital cyclicity during onset of Early to Middle Turonian marine red-bed formation (Austrian Eastern Alps). In: Hu, X., Wang, C., Scott, R., Wagreich, M., Jansa, L. (Eds.), *Cretaceous Oceanic Red Beds: Stratigraphy, Composition, Origins, and Paleoclimatic Significance*. SEPM Special Publication, pp. 209–221.
- Wendler, J.E., Lehmann, J., Kuss, H.-J., 2010. Orbital time scale, intra-platform basin correlation, carbon isotope stratigraphy and sea-level history of the Cenomanian Turonian Eastern Levant platform, Jordan. In: Homberg, C., Bachmann, M. (Eds.), *Evolution of the Levant Margin and Western Arabia Platform since the Mesozoic*. Geological Society, London, Special Publications, London, pp. 171–186.
- Wendler, I., Huber, B.T., MacLeod, K.G., Wendler, J.E., 2011a. Early evolutionary history of *Tubulogenerina* and *Colomia*, with new species from the Turonian of East Africa. *J. Foraminifer. Res.* 41, 384–400.

- Wendler, I., Willems, H., Gräfe, K.-U., Ding, L., Luo, H., 2011b. Upper Cretaceous inter-hemispheric correlation between the Southern Tethys and the Boreal: chemo- and biostratigraphy and paleoclimatic reconstructions from a new section in the Tethys Himalaya, S-Tibet. *Newsl. Stratigr.* 44, 137–171.
- Wendler, J.E., Wendler, I., Vogt, C., Kuss, J., 2011c. Drivers of cyclic sea-level change during the Cretaceous greenhouse: a new perspective from the Levant Platform (Jordan). *GSA Annual Meeting, Geological Society of America Abstracts with Programs*, Minneapolis, USA, p. 376.
- Wendler, I., Huber, B.T., MacLeod, K.G., Wendler, J.E., 2013a. Stable oxygen and carbon isotope systematics of exquisitely preserved Turonian foraminifera from Tanzania – Understanding isotopic signatures in fossils. *Mar. Micropaleontol.* 102, 1–33.
- Wendler, J.E., Wendler, I., Huber, B.T., 2013b. Revision and evaluation of the systematic affinity of the calcitarch genus *Pithonella* based on exquisitely preserved turonian material from Tanzania. *J. Paleontol.* 87, 1077–1106.
- Wendler, J.E., Meyers, S.R., Wendler, I., Kuss, J., 2014. A million-year-scale astronomical control on Late Cretaceous sea-level. *Newsl. Stratigr.* 47, 1–19.
- Wendler, J.E., Wendler, I., Vogt, C., Kuss, J., 2016. Link between cyclic eustatic sea-level change and continental weathering: Evidence for aquifer-eustasy in the Cretaceous. *Palaeogeogr. Palaeoclimatol. Palaeoecol.* 441, 430–437.
- White, T., Arthur, M.A., 2006. Organic carbon production and preservation in response to sea-level changes in the Turonian Carlileneck term Formation, U.S. Western Interior Basin. *Palaeogeogr. Palaeoclimatol. Palaeoecol.* 235, 223–244.
- Wiese, F., 2009. The Söhlde Formation (Cenomanian, Turonian) of NW Germany: shallow marine pelagic red beds. *SEPM Spec. Publ.* 91, 153–170.
- Wiese, F., Voigt, S., 2002. Late Turonian (Cretaceous) climate cooling in Europe: faunal response and possible causes. *Geobios* 35, 65–77.
- Wiese, F., Čech, S., Ekrt, B., Košťák, M., Mazuch, M., Voigt, S., 2004. The Upper Turonian of the Bohemian Cretaceous Basin (Czech Republic) exemplified by the Upohlavy working quarry: integrated stratigraphy and palaeoceanography of a gateway to the Tethys. *Cretac. Res.* 25, 329–352.
- Wilmsen, M., Nagm, E., 2013a. Sequence stratigraphy of the lower Upper Cretaceous (Upper Cenomanian – Turonian) of the Eastern Desert, Egypt. *Newsl. Stratigr.* 46, 23–46.
- Wilmsen, M., Nagm, E., 2013b. Upper Cenomanian–Lower Turonian ammonoids from the Saxonian Cretaceous (lower Elbtal Group, Saxony, Germany). *Bull. Geosci.* 88, 647–674.
- Wilmsen, M., Niebuhr, B., Janetschke, N., 2014. Sea-level changes across the Lower–Middle Turonian boundary: evidence from borehole BKS 7/91 (Danubian Cretaceous Group, Bavaria, Germany). *Z. Dtsch. Ges. Geowiss.* 165, 641–654.
- Wilson, L.A., Butterfields, N.J., 2014. Sediment effects on the Preservation of Burgess Shale-Type Compression fossils. *Palaios* 29, 145–153.
- Zügel, P., 1994. Verbreitung kalkiger Dinoflagellaten-Zysten im Cenoman / Turon von Westfrankreich und Norddeutschland. *Senckenbergische Naturforschende Gesellschaft*, Frankfurt, Germany.